ULTRAFAST PHOTOPHYSICS OF π - CONJUGATED POLYMERS FOR ORGANIC PHOTOVOLTAIC APPLICATIONS

by

Bill Pandit Chhetri

A dissertation submitted to the faculty of
The University of Utah
in partial fulfillment of the requirements for the degree of

Doctor of Philosophy

in

Physics

Department of Physics and Astronomy

The University of Utah

August 2012

THE UNIVERSITY OF UTAH GRADUATE SCHOOL

STATEMENT OF DISSERTATION APPROVAL

The dissertation of **Bill Pandit Chhetri**

has been approved by the following supervisory committee members :

Zeev Valy Vardeny	**,** Chair	**04/20/2012**
Yong-Shi Wu	**,** Member	**04/20/2012**
Mikhail Raikh	**,** Member	**04/20/2012**
Clayton Williams	**,** Member	**04/20/2012**
Ajay Nahata	**,** Member	**04/17/2012**

and by **David Kieda** , Chair of

the Department of **Physics and Astronomy**

and by **Charles A. Wight**, Dean of The Graduate School.

ABSTRACT

In this work, we used the pump-probe photomodulation (PM) spectroscopy technique to measure the transient PM spectrum and decay kinetics in various π – conjugated polymers (PCPs) films and blends with appropriate molecular acceptors. Using two ultrafast laser systems, we covered a broad spectral range from 0.25 – 2.5 eV in the time domain from 100 fs to 1 ns with 150 fs time resolution. We also used continuous wave (CW) photomodulation spectroscopy, photoluminescence, electro-absorption, doping-induced absorption, and x-ray diffraction to study the excitations and other optical properties of PCPs and polymer donor-fullerene acceptor blends.

In P3HT/PCBM blend with maximum domain separation we found that although the intrachain excitons in the polymer domains decay within ~ 10 ps, no charge polarons are generated at their expense. Instead, there is a build-up of charge-transfer (CT) excitons at the donor (D) – acceptor (A) interfaces that may dissociate into separated polarons in the D and A domains at a later time. Our results elucidate the charge photogeneration mechanism in polymer/fullerene blends, and unravel the important role of the binding energy in generating free charge polarons.

We also studied the photophysics of a low band gap polymer, namely poly-thienophene-benzodithiophene seven (PTB7) film and its blend with acceptor [6,6] phenyl C_{71} butyric acid methyl ester [$PC_{71}BM$]. In the CW PM spectrum of PTB7/$PC_{71}BM$ blend, clear signatures of polarons are observed. Whereas PA bands of

triplet excitons and trapped polarons are observed in pristine PTB7 film. In the transient ultrafast PA spectrum of PTB7/$PC_{71}BM$ blend, surprisingly, we found singlet exciton, charge transfer exciton and a polaron band that are generated simultaneously; this is different from the transient PM spectrum of P3HT/PCBM blend.

We also focused on the photophysics of DOO-PPV with different isotopes and their blends with PCBM. The transient ultrafast PA spectra of all isotope films are dominated by a singlet exciton. Similar results were observed in the isotope/PCBM blends. As in P3HT/PCBM blend, we do not observe the charge transfer exciton and polaron band immediately after photoexcitation, but they show up in the PM spectrum at a later time.

To my parents and my wife

CONTENTS

LIST OF FIGURES

LIST OF TABLES

ACKNOWLEDGEMENTS

I would like to express my sincere gratitude and heartfelt thanks to my honorable advisor Prof. Z. V. Vardeny for his plentiful suggestions, constant guidance, support and encouragement through all the years of my Ph.D. The research opportunity provided by Prof. Vardeny is invaluable for me. I also express my sincere gratitude to my supervisory committee members, Professors Yong-Shi Wu, Mikhail Raikh, Clayton Williams and Ajay Nahata, for their encouraging discussions and suggestions. I also thank Prof. Sumit Mazumdar from University of Arizona for his theoretical insights.

I would like to thank Dr. Randy Polson, Dr. Mathew Delong and Wayne Wingert for assisting with the technical problems encountered in the lab and Mr. Leonard Wojcik for synthesizing the polymer isotopes. I would like to thank Dr. Josh Holt for introducing me to the ultrafast measurements and Dr. Sanjeev Singh, Dr. ChuanXiang Sheng, Dr. Golda Hukic for their valuable suggestions, support and collaboration.

My sincere thanks is extended to my current group members, Tek Prasad Basel, Ella Olejnik, Bhoj Raj Gautam, Uyen Huynh, Dr. Tho Nguyen, Dr. Maria Navas and Dr. Dali Sun for their collaboration, support and friendly suggestions.

Last but not least, I thank my wife, Emma, and my family in Nepal for their endless support, love, patience, care and encouragement through all these years of my Ph.D.

CHAPTER 1

INTRODUCTION

Polymers are a group of materials made up of long covalent-bonded molecules [1]. For a long time, polymers have been taken as insulators, so that any electrical conductance typically caused by loosely bound ions was considered an undesirable effect [2]. The story of π-conjugated polymers (PCPs) began in the early 1960s, [3] when Hideki Shirakawa was working on his Ph.D at the Tokyo Institute of Technology. At that time, he was attempting to reveal the polymerization process for certain triple-bonded molecules. One day, a visiting Korean scholar added 1000 times more catalyst than Shirakawa specified because of a language barrier miscommunication. Surprisingly, they found a shiny film instead of the brownish polyacetylene powder that was normally produced. Although the shiny surface suggested metallic properties of the film, the conductivity of the new polyacetylene was not improved over its predecessor. Shirakawa then advanced the procedure to synthesize and control the polymerization of trans-and cis-polyacetylene. In the meantime, Alan Heeger and Alan MacDiarmid, both at Penn State, were using polymers in general to represent quasi-one-dimensional systems and had begun collaboration on a new inorganic polymer system poly (sulfur nitride), that became metallic at low temperatures. In 1975, MacDiarmid was lecturing in Japan and was introduced to Shirakawa. Both chemists showed off their samples to each other. Shirakawa received the funding from the office of Naval Research to visit Penn and decided to continue the work at Penn State.

MacDiarmid, Shirakawa and Heeger, along with other colleagues, worked together and learned to make very pure polyacetylene. They doped the samples with halogen and tried to measure the conductivity. Unfortunately, their instrument overloaded and burned out. It was an unsuccessful attempt. However, they continued their efforts.

In 1977, Heeger, MacDiarmid and Shirakawa reported that they had oxidized polyacetylene (exposed it to iodine vapor at 1 Torr at room temperature for 10 min) [4] and found an increase in conductivity by seven orders of magnitude; from nanosiemen/cm to 38 siemen/cm. For the discovery of this conducting polymer, they received the Nobel Prize in Chemistry in 2000. Nowadays, the conductivity of best-doped polyacetylene is close to that of copper.

After their colleagues received the Nobel Prize in the field of conducting polymer, many researchers now begin to devote their efforts to various types of research in PCPs. The flexibility, lightweight, relatively low manufacturing cost, and environmental friendliness of the polymers are also the main reasons for attracting the researchers for many applications. In the past 30 years, many significant improvements were achieved in the field of organic photovoltaic (OPV) applications [5-9], organic light emitting diodes (OLEDs) [10], organic field effect transistors [11], organic spin valves [12], biological sensors, etc.

The most advanced organic solar cell is the bulk heterojunction solar cell, in which electron donor and acceptor molecules are blended together in a film to capture the sun's incident photon flux. Although this configuration has so far yielded the highest power conversion efficiency in OPVs of about 6 % [13], significant improvement is necessary to compete with traditional amorphous hydrogenated silicon solar cell devices with efficiencies better than 12 % [14]. To improve the device performance, it is essential to understand how light interacts with the material and charge transports through it. One way to probe the electronic and optical properties of conjugated polymers is to use spectroscopy [15]. In this chapter, we will describe electronic and optical processes in PCPs, and then will introduce its application mainly in the OPV solar cell. The active

layer used in solar cell device is the blend of electron donor and acceptor materials. Here, the main focus of this work is to understand how the charge transports in the active layer after photoexcitation. To understand this, we use steady state and transient photoinduced absorption spectroscopy measurements. In addition, we also use other techniques such as electro absorption (EA), doping-induced absorption (DIA), etc. We also compare several donor and acceptor materials to understand how the morphology and the chemical structure play a role in their optical properties. Ultimately, all of these studies will provide a better understanding of why the organic materials are still not appropriate to compete with inorganic materials for photovoltaic applications.

1.1 π - Conjugated Polymers

A conjugated polymer is a carbon-based macromolecule, which consists of many repeated units typically connected by covalent chemical bonds. The bond between carbon atoms may be single, double, or triple, depending upon the type of hybridization. The hybridization may be of three types, namely Sp^3 Sp^2 and Sp. In Sp^3 hybridization, the bond between carbon atoms is single: one σ bond [Figure 1.1 (a)] and other valence electrons make single σ bond with side group atoms. In this condition, all valence electrons of carbon atoms are engaged to form σ bonds lacking π electrons. Therefore, a large gap (> 6 eV) exists between σ bonding and σ^*anti- bonding and polymers behave as insulators. In Sp^2 hybridization, the bond between carbon atoms is double: one σ bond and the other π bond [Figure 1.1 (b)]. The other two valence electrons from each carbon atom make σ bonds with side groups. The σ bonds lie in the same plane and π bond is perpendicular to that plane. The σ bonds are strong and determine the shape of the backbone, whereas π- electrons of $2p_z$ orbitals are loosely bound, delocalized over a number of intrachain carbon atoms, and primarily responsible for the electronic and optical properties of the polymers. These hybrids π-bonds form molecular orbitals, which are filled according to the Pauli exclusion principle up to the highest occupied molecular

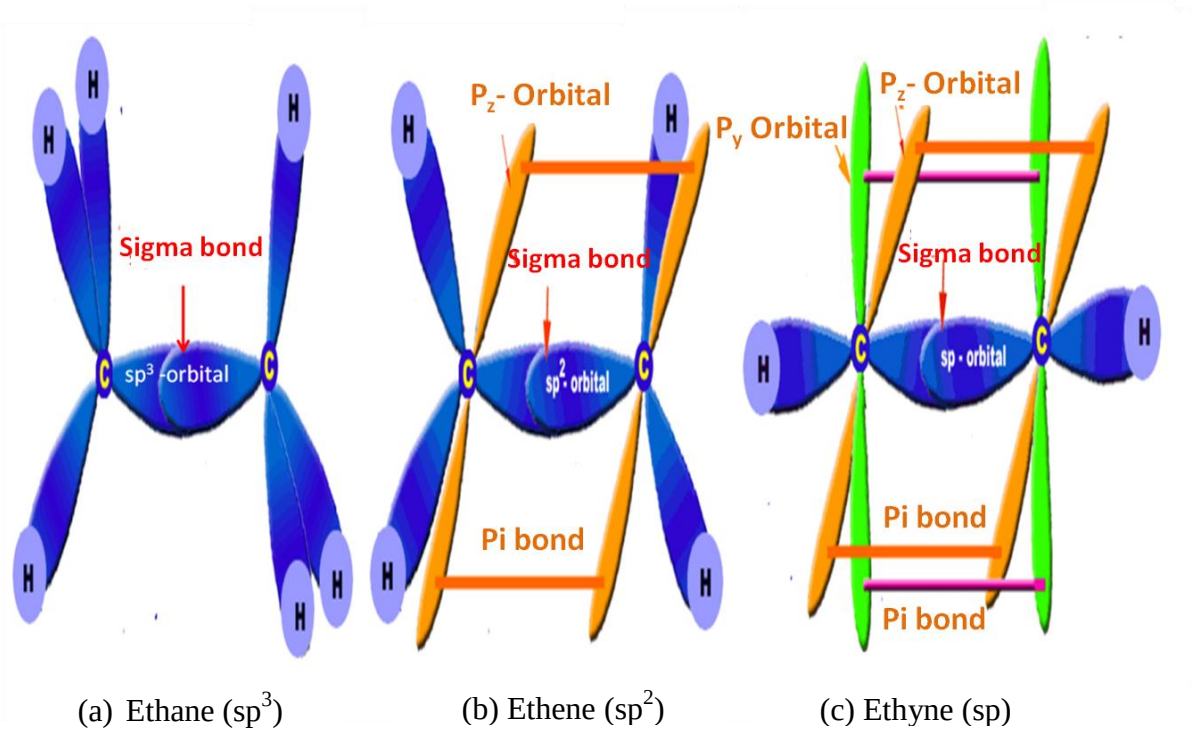

(a) Ethane (sp^3) (b) Ethene (sp^2) (c) Ethyne (sp)

Figure 1.1: Examples of different types of hybridizations (a) ethane (sp^3), (b) ethene (sp^2), and (c) ethyne (sp) showing σ-bonds (blue) and π- bonds (orange and green). Diagrams adapted from (www.collegiate.com)

orbital (HOMO). The next molecular orbital above HOMO is called the lowest unoccupied molecular orbital (LUMO). The gap between HOMO and LUMO is comparable with the band gap of most of the semiconductors (~ 2 eV). Therefore, PCPs also behave as semiconductors.

Similarly in Sp hybridization, the hybridized orbital electrons make σ bonds with each other and with a side group. The other remaining $2p_y$ and $2p_z$ orbitals electrons make π-bonds with neighboring carbon atoms [Figure 1 (c)]. Although the number of π electrons is more in Sp hybridized polymer, it is not appropriate in practical applications because of stability and other issues.

1.2 Symmetry and Excited-State Ordering

The symmetry of the molecular wave functions of the polymer is important when explaining the optical properties of PCPs. The symmetry might be either C_{2h} or C_{2v}. Polyenes ($C_{2n}H_{2n+2}$) are linear chains of CH units with sp^2 hybridization of p_z atomic orbitals. For this type of polymer, symmetry is described by point group C_{2h}[16], and electronic wave functions are classified according to their inversion and rotation properties. It is essential that for each symmetry operation belonging to the point group symmetry, the wave functions have to change within their degeneracy. If the orbital wave functions change (do not change) sign under inversion at the symmetry center, then they are denoted as u (g) and symbolized by b (a) if they change (do not change) sign under 180^0 rotation around the symmetry axis. The atomic 2p-orbitals change sign under reflection in the symmetry plane, so p-electron orbitals are only a_u or b_g.

The wave function describing the electronic states along the polymer chain is still distinguished by its g and u character, but now the inversion properties are denoted by capital letters A or B. The π-electron states in polymers can then have either A_g or B_u symmetry according to:

$$a_u \otimes a_u = b_g \otimes b_g = A_g \tag{1.1}$$

$$a_u \otimes b_g = b_g \otimes a_u = B_u \tag{1.2}$$

In PCPs, all π - orbitals in the HOMO are doubly occupied, so the ground state has always A_g character. The first excited state (LUMO) has B_u character and then other excited states take alternative characters A_g, B_u, A_g, and so on. The excited states can be written in more conventional way as n^pX, where n is the overall quantum number, p is the spin degeneracy of the quantum state; 1 for singlet and 3 for triplet; and X is the electronic wave function symmetry either A_g or B_u.

The ordering of the first two excited states plays a crucial role on luminescent properties of PCPs. If the electron-electron correlation is neglected, then the excited states order can be written as:

$$1^1A_g < 1^1B_u < 2^1A_g \tag{1.3}$$

In this approximation, the energies of the first few configurations are approximately equal to the sum of the orbital energies. However, the electron-electron correlation changes the order of energy states as written below:

$$1^1A_g < 2^1A_g < 1^1B_u \tag{1.4}$$

From Equations (1.3) and (1.4) two possible cases can be explained. When the energy of $1B_u$ state is lower than $2A_g$ [Figure 1.2(a)], the material is expected to show strong fluorescence because the transition $B_u \rightarrow A_g$ is allowed in dipole approximation. This type of property is observed in polythiophene and poly (p-phenylenevenylene)s. However, if the energy of $1B_u$ state is higher than $2A_g$ state, then material decays nonradiatively from the first excited state to ground state and no fluorescence occurs. Although the transition from $A_g \rightarrow A_g$ is forbidden in dipole moment approximation, very little fluorescence might occur mainly during the thermalization process (~1 ps or less). This happens, for instance, in the case of trans-polyacetylene and polydiacetylene.

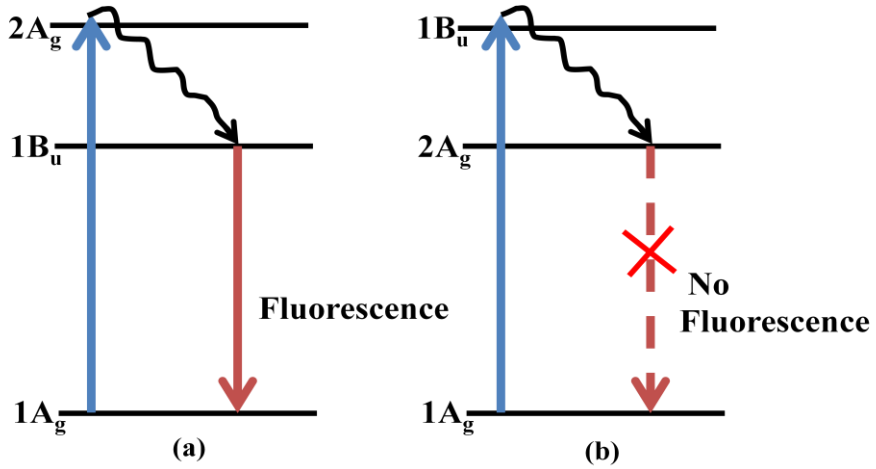

Figure 1.2: The different ordering of the first two excited states shows two different optical properties. (a) The polymer gives fluorescence for $1A_g < 1B_u < 2A_g$, and (b) no fluorescence for $1A_g < 2A_g < 1B_u$.

The detailed information about the role of electron-electron and electron-phonon coupling on energy state ordering is presented in reference [17].

1.3 Selection Rules for Optical Transitions

Selection rules are used to identify whether the transition between two energy states is allowed or not. The selection rules are in fact the conditions constraining the physical properties of the initial and the final systems necessary for a process to occur with a nonzero probability. In general, a transition involves either emission or absorption of photon radiation in spectroscopy. The probability of a transition depends on three quantum states: the photon, the initial state, and the final state. Parity also plays the vital role in selection rule. The symmetry of a wave function with regard to the reflection of all coordinates through the origin is called parity. If a wave function changes (does not change) sign with this operation, parity is odd (even). Photon parity cannot be intuitively assigned because it is never at rest. However, relativistic quantum field theory [18, page 445-449] explains that photons have odd intrinsic parity; this is also in line with the dipole interaction approximation, where the dipole matrix element is odd under inversion or reflection operation. Thus, after absorption or emission of a photon, the parity of the final state must be different from the initial state.

A photon is a boson and carries intrinsic spin angular momentum $\pm\hbar$. The total angular momentum (spin and orbital) must be conserved in the photon-dipole interaction. This condition introduces a rule called electric dipole selection rules [19]

$$\Delta l = \pm 1 \tag{1.5}$$

$$\Delta m_l = 0, \pm 1, \tag{1.6}$$

where l is the angular momentum quantum number and m_l is the magnetic moment quantum number (projection of angular momentum). $\Delta l = 0$ is forbidden in dipole moment approximation because parity remains the same.

The oscillating electric field associated with a transition between an initial and final state can be seen as an electric dipole, and the transition probability is given by the matrix element between them. The transition probability of a dipole is described by D^2 where the transition moment is given by

$$D = \langle i|\hat{\mu}_e|j\rangle \tag{1.7}$$

where $\hat{\mu}_e = e\hat{r}$ is the dipole moment operator. Equation (1.7) shows that the transition probability is related to how well the dipole moment between two energy states can couple to the electric field of a photon, which is *Fermi's Golden Rule*. The nature of the dipole operator now follows:

∗ Total spin is conserved in electric dipole operator, so transitions are possible only in the same spin manifold states. This confirms that the transitions between singlet and triplet states are completely forbidden. Note that this rule may be overcome by spin-orbit coupling.

∗ The electric dipole operator is antisymmetric with respect to the inversion operator, and thus connects the states of opposite parity. This means that transitions are possible between gerade (g) and ungerade (u) states. This is a restatement of *Laport's rule* [20].

∗ In case of particle-hole operator the electric dipole operator is antisymmetric so it connects the states of opposite e-h symmetry. This means the dipole moment direction will reverse if negative electron and positive hole are exchanged.

These are the selection rules for optical transition. We should keep in mind, however, that these rules do not completely prohibit the transitions that violate them. The term forbidden signifies that these transitions are only electric-dipole forbidden and might be allowed due to other reasons such as oscillating magnetic dipole moments, higher-order electric pole moments, etc.

1.4 Photoexcitation Models in π - Conjugated Polymers

The photoexcitations in PCPs are described using different models. The popular models for this purpose are the Hückel model, Su, Schrieffer, and Heeger (SSH) model, Hubbard model, and Pariser-Parr-Pople (PPP) model. Here, we first start with the Hückel model, in which the interaction between the nearest neighbors is considered important and other electronic correlations are neglected. Next, the SSH model is used to add to the effect of electron-phonon interactions. The Hubbard model then introduces the effect of electron-electron repulsion at the same atom. Finally, the PPP model is used to extend the Hückel and Hubbard restrictions from short range potentials to include intersite interactions. Before going into individual models as mentioned before, it is necessary to construct a primitive Hamiltonian to describe the interactions in PCP systems.

In simplest form, a polymer chain can be assumed as an infinite periodic structure, and each atomic site is associated with a wave function. The wave function contains spin and spatial coordinates. For simplicity, the spin coordinate is neglected. The spatial part of the molecular wave function now satisfies the $Schrödinger$ equation,

$$H\psi(r,R) = E\psi(r,R) \tag{1.8}$$

where r and R stand for electronic and nuclear coordinates respectively. E is the energy eigen value of the Hamiltonian. The Hamiltonian is multifaceted and can be separated into its electronic (e-e), electronic-nuclear (e-n) and nuclear (n-n) contributions,

$$H = H_{e-e}(r) + H_{e-n}(r,R) + H_{n-n}(R) \tag{1.9}$$

Here the electronic part Hamiltonian is the sum of electronic kinetic energy and Coulomb potential energy,

$$H_{e-e}(r) = \sum_i \frac{p_i^2}{2m_i} + \frac{1}{2}\sum_{i\neq j}\frac{e^2}{|r_i - r_j|}\,; \tag{1.10}$$

The nuclear component also contains both its kinetic and potential energies,

$$H_{n-n}(R) = \sum_\alpha \frac{P_i^2}{2M_\alpha} + \frac{1}{2}\sum_{\alpha\neq\beta}\frac{Z_\alpha Z_\beta e^2}{|R_\alpha - R_\beta|} \tag{1.11}$$

and the coulomb interactions between protons and electrons contribute the potential energy

$$H_{e-n}(r,R) = -\frac{1}{2}\sum_{i,\alpha}\frac{Z_\alpha e^2}{|R_\alpha - r_i|} \tag{1.12}$$

It is impossible to solve the full Hamiltonian exactly (except for the hydrogen atom) and so several simplifications and approximations have to be made. The nucleon's mass is large compared to electronic mass so that its acceleration is expected to be much smaller than electronic dynamics. In this assumption, the nuclear kinetic energy is negligible and can be eliminated from the Hamiltonian Equation (1.11) and takes the new form

$$H_{n-n}(R) \to \frac{1}{2}\sum_{\alpha\neq\beta}\frac{Z_\alpha Z_\beta e^2}{|R_\alpha - R_\beta|} = V_{n-n}(R) \tag{1.13}$$

Equation (1.13) shows that the effective potential experienced by the nuclei only depends on the nuclear coordinate R. Using these approximations we still have a very complicated Hamiltonian, which needs to be simplified again. These simplifications can be done by neglecting certain interactions. The easiest way is to write the Born-Oppenheimer Hamiltonian in second quantization [17].

$$H_{BO} = \sum_{i,j}\tilde{t}_{ij}\left(c_i^\dagger c_j + c_j^\dagger c_i\right) + \frac{1}{2}\sum_{ijkl}\tilde{V}_{ijkl}\, c_i^\dagger c_k^\dagger c_l c_j + V_{n-n} \tag{1.14}$$

where, $$\tilde{t}_{ij} = \int \psi_i^*(r)\left[\frac{P^2}{2m} - \sum_\alpha \frac{Z_\alpha e^2}{|R_\alpha - r|}\right]\psi_j(r)dr^3 \tag{1.15}$$

is the transfer integral of an electron from the ψ_j orbital to the ψ_i orbital. The second term in Equation (1.14) is a two-electron integral and represents the electron-electron interaction:

$$\tilde{V}_{ijkl} = \iint \psi_i^*(r)\psi_k^*(r')\frac{e^2}{|r-r'|}\psi_l^*(r)\psi_j^*(r')dr^3dr'^3 \tag{1.16}$$

Equation (1.14) can be further simplified: it describes the electronic degree of freedom by considering only the π-electrons. The transitions from $\sigma\ to\ \sigma^*$ always require more energy than $\pi\ to\ \pi^*$ transition so that it does not participate in optical or electronic

operation. Therefore, the effect of σ- electrons can be safely eliminated in the calculations.

1.4.1 Hückel Model

The Hückel model is very simple and useful for understanding the electronic nature of the polymers and the concept of bonding and anti-bonding molecular orbitals built up from atomic orbitals [15]. The simplest way of explaining the electronic properties of π- conjugated system is a tight binding approximation, which takes only nearest-neighbor interactions into account. In this case, the π- electron wave function is written in Bloch representation as

$$\psi_k(x) = \sum_n e^{ikia}\ \phi(x - ia) \qquad (1.17)$$

where a is the lattice constant and $\phi(x - ia)$ is a carbon $2p_z$ orbital wave function on the i-th atomic site. For electrons on the same or neighboring orbital, we assume that the transfer integral is nonzero,

$$\tilde{t}_{ii} = \langle\phi_i|H|\phi_i\rangle = \epsilon \text{ and } \tilde{t}_{i,i+1} = \langle\phi_i|H|\phi_{i\pm1}\rangle = t \qquad (1.18)$$

where ϵ is the energy of the single site and t is the interaction energy of two neighboring sites. Neglecting electron-electron $(V_{ijkl} = 0)$ and electron-phonon interactions, and setting nuclear coordinates to zero $(V_{n-n} = 0)$, Hückel Hamiltonian in second quantization can be obtained from Equation (1.14) as

$$H_{H\ddot{u}} = \sum_i t_{i+1,\ i}\ \left(c_{i+1}^{\dagger}c_i + c_i^{\dagger}c_{i+1}\right) \qquad (1.19)$$

$$= \epsilon + \sum_i t\ \left(c_{i+1}^{\dagger}c_i + c_i^{\dagger}c_{i+1}\right) \qquad (1.20)$$

Using this Hamiltonian in Schrödinger Equation (1.8), we can calculate the eigenvalue E. The detail calculation can be found in [21] as final result,

$$E\ (k) = \epsilon \pm t\sqrt{2 + 2\cos(ka)} \qquad (1.21)$$

where $\epsilon = \langle\phi_i|H_{H\ddot{u}}|\phi_i\rangle$ and $t = \langle\phi_i|H_{H\ddot{u}}|\phi_{i\pm1}\rangle$ (1.22)

We know that PCPs are sp^2 hybridized and each carbon atom contains only one π-electron. Therefore, π-band is half filled and the Fermi surface lies at $k = \pi/2a$ [Figure 1.3 (a)], half the way of the first Brilliouin zone boundary, which is at $k = \pi/a$ with $E(\pi/a) = \epsilon$.

The lack of energy gap in the half-filled electronic band suggests that there is density of states at the Fermi energy and the material is defined as metal. However, the regularly spaced configuration of the 1D lattice is unstable. If any perturbation comes into play in the atomic lattice then it will lower the energy realignment of the atoms which is called *Peierls instability*. The dislocated atoms form the alternating single (longer) and double (shorter) bonds, and lower the symmetry of the system; this process is called dimerization. For the unit cell doubled from a to $a' = 2a$ it includes now two atoms, while the periodic lattice distortion halves the quasi-momentum at the edge. In this case, the energy takes a new form as

$$E(k) = \epsilon \pm \sqrt{t_1^2 + t_2^2 + 2t_1 t_2 cos2ka} \qquad (1.23)$$

where t_1 and t_2 are the transfer integrals for single and double bond nearest neighbor respectively. For $t_1 = t_2$ and $a \to 2a$, Equation (1.23) reduces exactly to Equation (1.21). At the zone boundary edge, the energy is given as

$$E(\pi/2a) = \epsilon \pm \sqrt{t_1^2 + t_2^2 - 2t_1 t_2} = \epsilon \pm |t_1 - t_2|, \qquad (1.24)$$

with the energy gap $E_g = |t_1 - t_2| = 2\Delta$. Here the lower band is fully occupied with two atoms per unit cell, contributing one π - electron from each atom and the upper band is empty. Therefore, the gap created at the Fermi surface by the Peierls distortion results in a semiconductor instead of a metal.

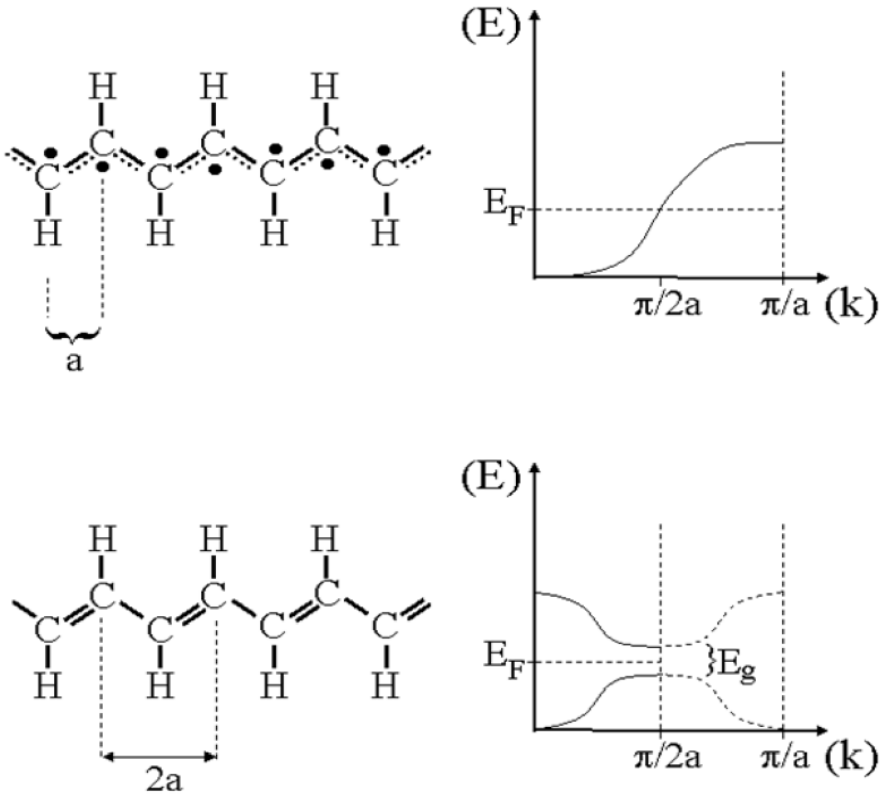

Figure 1.3: Electronic properties of polyacetylene (a) without dimerization showing the properties of a metal; (b) with dimerization showing the properties of a semiconductor. Diagrams adapted from Ref. [22]

1.4.2 Su, Schrieffer, and Heeger (SSH) Model

Su, Schrieffer, and Heeger introduced a model, named the SSH model, for t-$(CH)_x$ considering the role of electron-phonon interaction to the Hückel model but ignoring the electron-electron interaction [23]. Basically, they have used semiclassical Hückel Hamiltonian, which has two parts: lattice kinetic energy and electron-phonon interaction. The lattice kinetic energy is treated classically, and the electron-phonon interaction is treated quantum mechanically as written, in the Hamiltonian.

$$H_{SSH} = \frac{K}{2}\sum_n (u_n - u_{n-1})^2 + \frac{M}{2}\sum_n \left(\frac{du_n}{dt}\right)^2 - \sum_{n,s}\left(t_0 + \alpha(u_{n+1} - u_n)\right)$$
$$\left(C^{\dagger}_{n+1,s}C_{n,s} + C^{\dagger}_{n,s}C_{n+1,s}\right) \quad (1.25)$$

where t_0 is the hopping integral between the nearest neighbors for an undistorted chain, α is the electron lattice coupling constant, and $C^{\dagger}_{n,s}$ and $C_{n,s}$ are the creation and annihilation operators of an electron on site n with spin s, K is the spring constant due to π- electrons and u_n is the deviation of the nth site from the equilibrium position in an undistorted chain with equal distance between sites.

According to this SSH model, the dimerization caused by strong electron-phonon interaction lowers the energy of the system and then creates an energy gap $E_g = 2\Delta$, where $\Delta = 4\alpha u$. In this case, the occupied electronic states in equilibrium are lowered and become more stable. Therefore the system no longer acts as a one-dimensional metal, but instead behaves as a semiconductor.

1.4.3 Hubbard Model

In the previous two models (Hückel and SSH), the repulsion between two electrons on the same site was ignored. This model assumes that the most important repulsion occurs between two electrons on the same site and this has to be included in the Hamiltonian. The on-site Hubbard contribution to the Hamiltonian is

$$H_{Hub} = U\sum_i n_{i,\uparrow}n_{i,\downarrow} \quad (1.26)$$

where U is the Coulomb repulsion between two electrons on the same site, $n_{i,\uparrow}$ and $n_{i,\downarrow}$ are the density operators for electron with spin up and spin down, respectively.

Although the Hubbard model introduced the new idea in the Hamiltonian about the significant role of coulomb repulsion of two electrons on the same site, it neglects the electron-phonon interaction, which is quite strong in the polymer system. From both the SSH and the Hubbard models, we see that the combination of these two models will be more realistic, as suggested by Mazumdar and Dixit [24, 25] to explain the energy levels

of excitations in PCPs. The combination of these two models is the-Pariser-Parr-Pople (PPP) model.

1.4.4 Pariser–Parr–Pople (PPP) Model

The Hubbard model assumes that repulsion between two electrons is important on the same site in PCPs, but neglects all electron-electron interactions beyond the nearest-neighbors. The PPP model takes into account most electronic correlations. Thus PPP model Hamiltonian is the sum of Hückel Hamiltonian (Equation 1.20), Hubbard repulsion (1.26), and an intersite contribution given by

$$V = \frac{1}{2}\sum_{i,j} V_{ij}\,(n_i - 1)\big(n_j - 1\big) \tag{1.27}$$

where V_{ij} is the Coulomb intersite interactions and is given by

$$V_{ij} = \big\langle \phi_i(1)\phi_j(2)\big|\, e^2/r_{12}\,\big|\phi_i(1)\phi_j(2)\big\rangle \tag{1.28}$$

This PPP model is used to analyze the excitons in PCPs in the weak coupling as well as strong coupling limit.

1.5 Major Photoexcitations in π-Conjugated Polymers

π-conjugated polymers are disordered materials in which both types of photoexcitations (charged and neutral) can be created using above-gap photon energy. First, the applied pump beam photon is used to generate the photoexcitations, and then the induced optical absorption due to the presence of photoexctied species is subsequently monitored by the probe beam photon in the broad spectral range from mid-IR to visible using different probe sources. This technique is common in both transient and CW spectroscopy. However, the probe beam is delayed in transient PA measurement whereas there is no delay between pump and probe beam photon in CW PA. Before and after photoexcitation of the polymer, the optical absorption of the polymer is different and this difference is measured as the PM spectrum.

1.5.1 Singlet and Triplet Excitons

The primary photoexcitations in PCPs are mainly the bound electron hole pairs called singlet excitons. When the polymer is excited, absorption of a single photon promotes the electron from lower energy level to a higher energy level and creates exciton in a spinless singlet configuration. This excitation causes structural and polarization relaxation of the surrounding geometry that leads to the exciton binding energy E_b. Using scanning tunneling spectroscopy the intrachain E_b of most of the PCPs is measured to be at least 0.3 - 0.5 eV [26].

Although a singlet exciton is formed immediately after photoexcitation in PCPs, triplet exciton also can be generated via intersystem crossing from singlet. Both singlet and triple excitons are neutral species with different spin alignments: 0 for singlet and 1 for triplet, respectively. The total wavefunction of an exciton must be antisymmetric in spin and electronic coordinate. To construct antisymmetric wavefunction we use a Slater determinant as written below:

$$\psi = \begin{vmatrix} \psi_i(r)\chi_i(\sigma) & \psi_i(r')\chi_i(\sigma') \\ \psi_j(r)\chi_j(\sigma) & \psi_j(r')\chi_j(\sigma') \end{vmatrix} \tag{1.29}$$

where $\psi_i(r)$ is the electronic part of the wavefunction and $\chi_i(\sigma)$ is the spin part. The spin can be either up ↑ or down ↓, and then we can construct wave functions for singlet Equation (1.30), and for triplet Equations (1.31) - (1.33), respectively.

$$\psi^{S=0} = \frac{1}{2}[\psi_1(1)\psi_2(2) + \psi_2(1)\psi_1(2)][\uparrow(1)\downarrow(2) - \uparrow(2)\downarrow(1)] \tag{1.30}$$

$$\psi^{S=1} = \frac{1}{2}[\psi_1(1)\psi_2(2) - \psi_2(1)\psi_1(2)][\uparrow(1)\downarrow(2) + \uparrow(2)\downarrow(1)] \tag{1.31}$$

$$\psi^{S=1} = \frac{1}{2}[\psi_1(1)\psi_2(2) + \psi_2(1)\psi_1(2)][\uparrow(1)\uparrow(2)] \tag{1.32}$$

$$\psi^{S=1} = \frac{1}{2}[\psi_1(1)\psi_2(2) + \psi_2(1)\psi_1(2)][\downarrow(1)\downarrow(2)] \tag{1.33}$$

In the noninteracting case the singlet and triplet energy levels are degenerate, but electron-electron correlation splits the energy level with triplet and lowers the energy.

The singlet exciton bands are shown in Figure 1.4 (a). In the energy band diagram, $1A_g$ is the ground state and $1B_u$, mA_g, kA_g are three singlet-excited states. The excited state mA_g is strongly coupled with the first excited state $1B_u$, and the transition between these two states is well defined as a singlet exciton. However, the excited state kA_g may be due to a biexciton state, i.e., a bound state of two $1B_u$ excitons. Two strong dipole-coupled transitions from $1B_u$ to mA_g and kA_g were expected to form the transitions PA_1 and PA_2, as shown in Figure 1.4 (a). In most of the PCPs the PA_1 band is observed around 1 eV and PA_2 is in the visible/near-IR region.

The other possibility following photogeneration in PCPs is the relaxation process. The photogenerated singlet exciton may relax, emitting either photons (radiatively), phonons (nonradiatively), or combination of both processes. In general, exciton may relax nonradiatively to the lowest excited state within subpicoseconds, which is also called internal conversion in molecular spectroscopy. From the lowest excited state the radiative recombination or photoluminescence (PL) occurs within 100 ps in most of the PCPs. In principle, the photogenerated species present in the lowest excited state must decay to the ground state through radiative channel, but in most of the PCPs this is not a straightforward process. There are other processes that may interfere and compete with the internal conversion in which singlet exciton converts into triplet exciton. The process of converting singlet to triplet excitons is the intersystem crossing, which is more likely to happen when the energy difference between the singlet and triplet states is small, and this process completes within ~10 ns. Like singlet excitons, the energy states of triplet excitons are also defined in Figure 1.4 (b). A triplet has no ground state because it forms from a singlet; however, the ground state of singlet is taken as a common ground state to explain the phosphorescence (PH) process. In some PCPs, PH is sometimes observed and the transition is long-lived on the order of several milliseconds [27]. The triplet energy levels are assigned as 1^3B_u, m^3A_g, and k^3A_g, which have a strong dipole moment

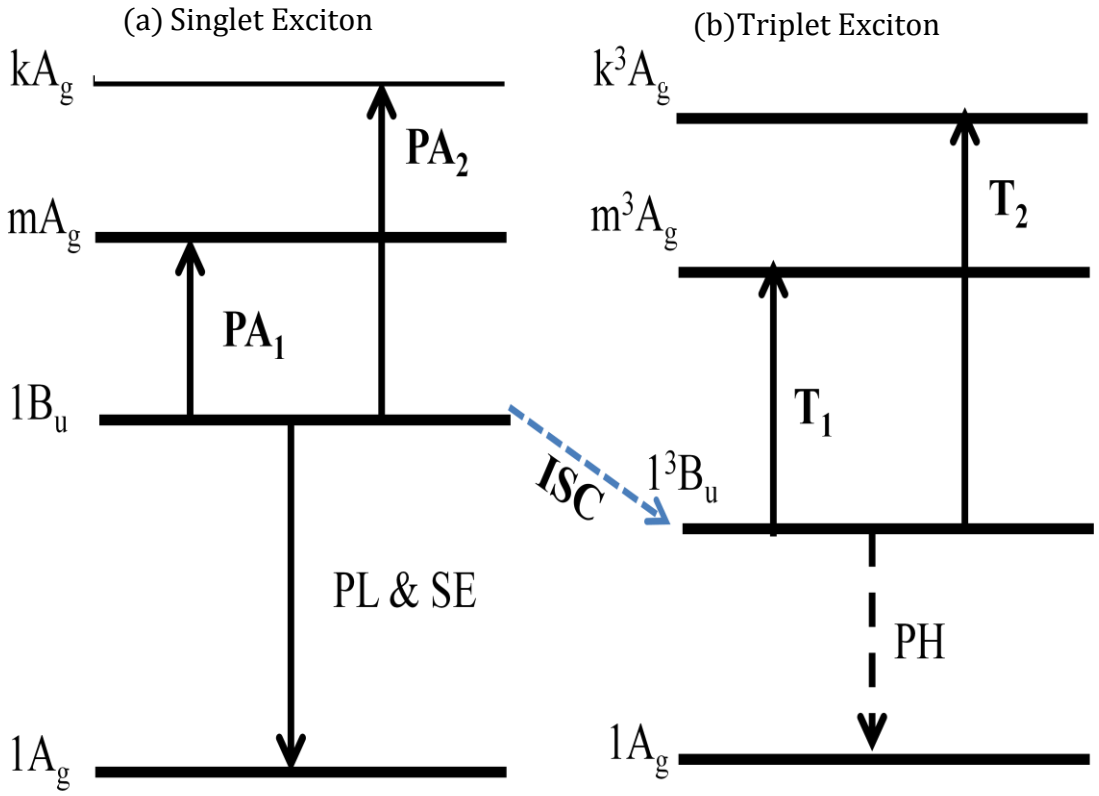

Figure 1.4: Neutral photoexcitations in conjugated polymers with nondegenerate ground state.

coupling and play important roles in optical transitions. Like singlet excitons, there are also two strong transitions, T_1 and T_2, for triplet excitons.

The offset between lowest triplet level 1^3B_u and lowest singlet excited state $1B_u$ is governed by singlet-triplet energy splitting energy Δ_{ST}, which is possible to calculate using following relation:

$$\Delta_{ST} = T_1 - PA_1 \tag{1.34}$$

The value of Δ_{ST} has been recently measured in π – conjugated polymers from phosphorescence emission involving heavy atoms and other techniques [28], and Equation (1.34) has been confirmed.

1.5.2 Polarons

One of the most important charged secondary photoexcitations in nondegenerate PCPs is the polaron. A polaron is a spin 1/2 quasi-particle composed of a unit charge (e) and a polarizing field created due to deformation of the lattice. The charge may be positive or negative. The energy of the polaron is always less than the free electron (or hole) because of lattice distortion. The energy diagrams and the possible optical transitions for both positive polaron (P^+) and negative polaron (P^-) excitations are presented in Figures 1.5 (a) and (b), respectively. Three optical transitions P_1, P_2, and P_3 are possible in both types of polarons, but transition P_3 is not allowed in dipole moment approximation due to having same symmetry states. Therefore, the allowed transitions are only P_1 and P_2. There are several methods for creating the polarons such as doping, charge injection through metallic electrodes, or photogeneration. After creation of polarons in the polymers, their absorption spectrum shows two absorption bands. In the photogeneration process these bands are called photoinduced absorption (PA). In the case of PPV types polymers, P_1 and P_2 bands were observed in mid IR (~ 0.35 eV) and in near IR (~ 1.4 eV) spectral range, respectively [29]. The signature of the polaron P_1 (rise in background < 0.35 eV) is observed in transient PA measurement of polymer/fullerene blend system. However, the P_1 band is not observed recently in the polymers. The reason for not getting P_1 band in mid-IR (~ 0.35 eV) is a big mystery in the photophysics community.

1.5.3 Bipolarons

Bipolarons are formed when two same charge polarons come together with opposite spins on the same chain of a nondegenerate ground state conjugated polymer. At the time of formation, elastic lattice energy is reduced; therefore bipolarons are more stable charged excitation species. The energy level diagrams and possible optical transitions in bipolarons are shown in Figure 1.6.

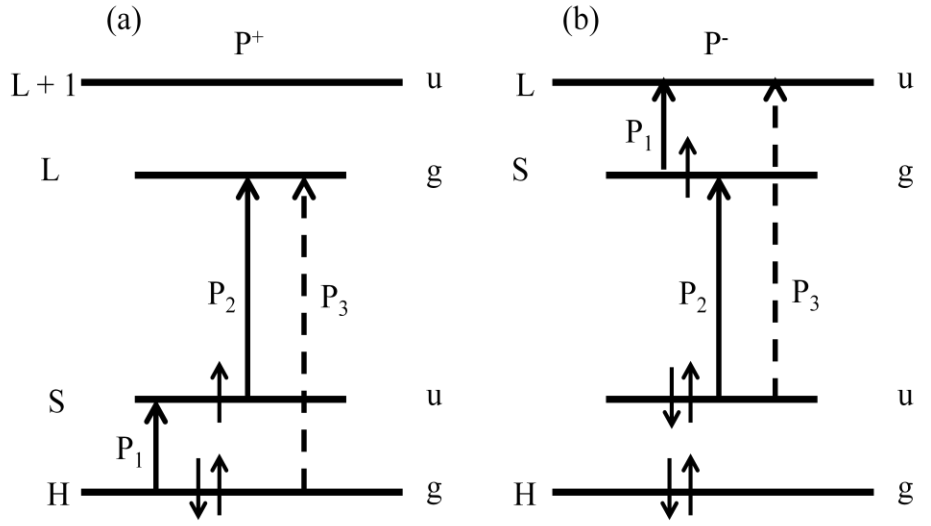

Figure 1.5: Energy level diagrams and possible optical transitions in (a) positive, and (b) negative polarons.

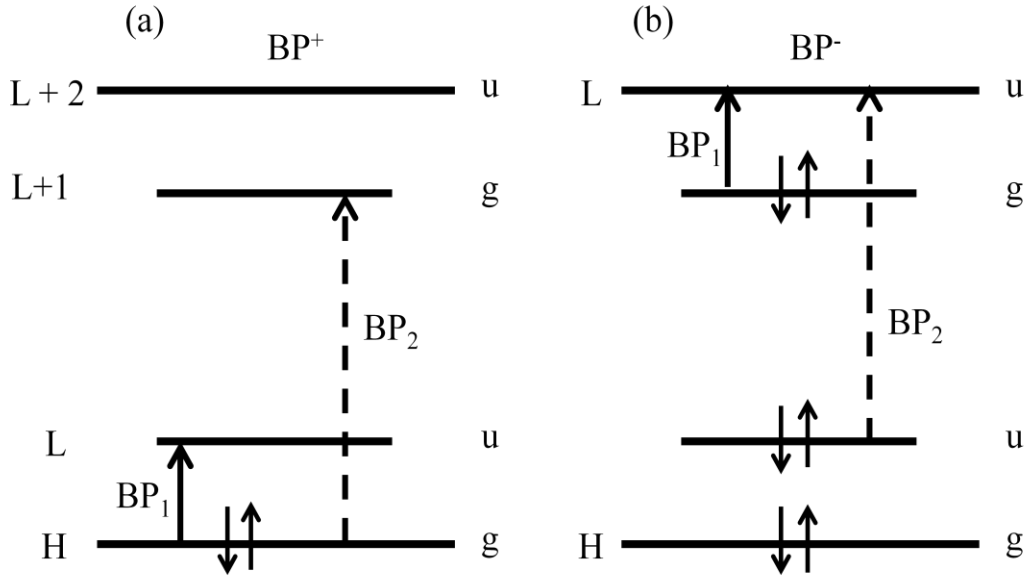

Figure 1.6: Energy level diagrams and possible optical transitions in (a) positive, and (b) negative bipolarons.

Like polarons, bipolarons also may be positively (BP^{2+}) or negatively (BP^{2-}) charged. In the positive bipolarons, there are two unoccupied energy states separated by $2\omega_0$ (BP): the LUMO and LUMO + 1, which are deeper in the gap than corresponding states of positive polaron (P^+).

In both types of bipolarons, two optical transitions BP_1 and BP_2 are possible. However, in short oligomers, BP_1 is allowed and BP_2 is forbidden because of same parity states. However, the forbidden transition BP_2 might gain intensity, especially in the polymers, due to electron correlation and disorder induced relaxation, and then could be observed in real films. BP_1 and BP_2 were observed in polythiophene thin films.

1.5.4 Polaron Pairs

Polaron pairs (PPs) are neutral secondary photoexcitations in which two oppositely charged polarons P^+ and P^- are coulombically bound on two neighboring chains. The binding energy of polaron pair is always less than exciton. Before the formation of the polaron pair, P^+ and P^- have individual energy levels, but when they interact with each other sitting on adjacent chain the stronger overlap leads to larger splitting of their energy levels as shown in Figure 1.7. There are three possible transitions PP_1, PP_2, and PP_3; however, for a tightly bound PP excitation we expect a single transition PP_2 to dominate the spectrum.

Generally, PPs are the intermediate step between excitons and pair of free polarons, and, therefore, this step is prerequisite to the formation of triplet and singlet excitons in OLEDs; thus, their associated physics is very important for device applications.

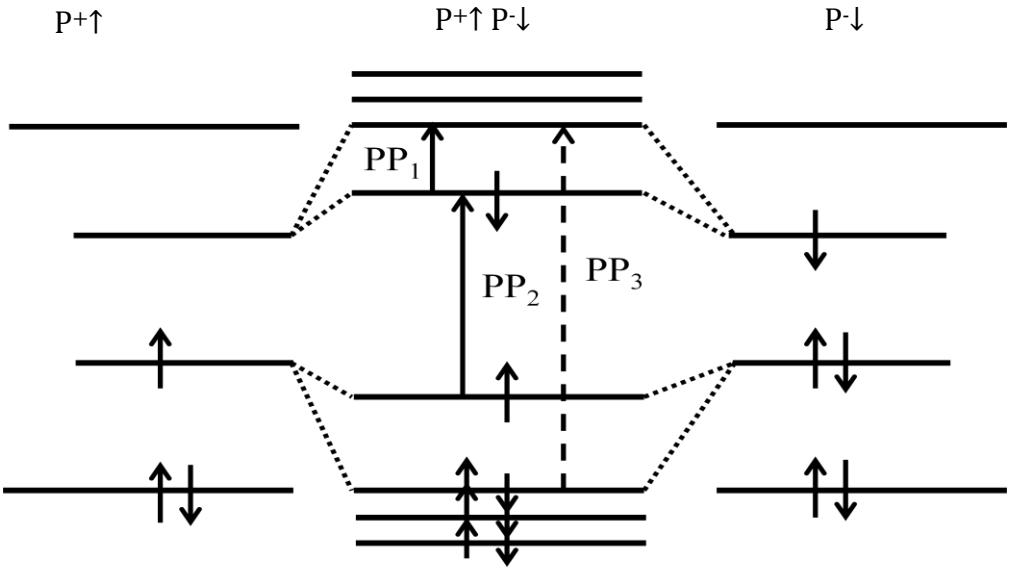

Figure 1.7: Energy level diagrams and possible optical transitions in Polaron-pairs.

1.5.5 Excimers, Dimmers and Exciplexes

Excimers, dimmers, and exciplexes are interchain species, which are generated due to the interaction of two adjacent chains in PCPs. Excimers and dimmers exist only in the excited state. They are formed when two neighboring polymers share their π-electrons equally in the excited state but not in the ground state [30-32]. These are emissive excited state complexes and have a dissociative ground state; that is, the dimmer spontaneously dissociates into two ground state molecules. Furthermore, the excimer cannot be directly excited optically. Instead, an intramolecular singlet exciton is photoexctied that later delocalizes over two molecules, forming the excimer. The formation of the excimer is accompanied by a strong geometric distortion along the intermolecular axis that, when combined with the dissociative nature of the ground state, leads to a featureless, strongly Stokes-shifted emission of the films in comparison to the dilute solution. Excimer formation was observed in PPV- based films [33], leading to quenching of luminescence due to their large nonradiative decay in this polymer.

An interchain excited state, called an exciplex, can also be formed when an unequal sharing of π- electron density between chains or a partial degree of charge transfer occurs [30, 32].

While excimers exist only in the excited state, interchain interaction may also lead to the ground-state interactions, with the formation of aggregate states [34, 31]. Upon aggregation, both the ground-and excited-state wave functions are delocalized over several polymer chains. The aggregate is therefore directly accessible by spectroscopic means. The existence of these species was suggested in the ladder-type polymers [35] and later conclusively disproved [36]) and poly-pyridine films [37], where it appears to quench PL efficiencies in film samples as compare to solution.

1.6 Organic Photovoltaic (OPV) Cell

Harvesting energy directly from sun light using photovoltaic technology is considered one of the most important ways to address growing global energy needs using a renewable source [38]. Polymeric solar cells are a promising alternative for producing clean and renewable energy due to the fact that there is the potential to fabricate them onto large area of lightweight flexible substrates by solution processing at a low cost [39, 40]. In the beginning, organic photovoltaic cells were fabricated using a single component active layer sandwiched between two electrodes with different work functions, and got very low power conversion efficiency due to poor charge carrier mobility and unbalanced charge transport [41].

To eliminate the weaknesses of single layer solar cell devices, Tang implemented a bilayer heterojunction solar cell device in 1986. The device structure was almost the same as a single layer device except the active layer. The P- type and N- type layers were used as an active layer for hole and electron transport respectively. The general working principle in such solar cells is simple and starts with photoexcitation of donor material upon absorption of photon energy, and creates excitons. The coulombically bound

electron-hole pair, known as exciton, diffuses to the donor-acceptor (D-A) interface via an electron-transfer process. The internal electric field drives the fully separated charges to the respective electrodes, which in turn generates photocurrent and photovolatge. Due to the fact that their limited lifetimes only allow excitons to diffuse the short distance between 5 – 14 nm [42, 43], the excitons created far away from the interface decay to the ground state without the chance to reach the acceptor. This phenomenon leads to the loss of absorbed photons and quantum efficiency. Consequently, the performance of the bilayer devices is greatly limited by the small area of charge-generating interface between donor and acceptor.

To overcome this difficulty, the concept of a bulk heterojunction (BHJ) was introduced by the pioneering work of Yu et al. [44]. In this device donor and acceptor materials are blended together and interpenetrating network with a large D-A interfacial area is achieved through controlling the phase separation between two components in the bulk. In this way, any absorbing site in the composite is within a few nanometers from the interface, leading to much enhanced quantum efficiency of charge separation.

The major breakthrough and rapid development of BHJ solar cells arose from the discovery of efficient photoinduced electron transfer in conjugated polymer-fullerene composites as reported by Sariciftci and co-workers [45]. The device architecture and I–V characteristics of BHJ solar cell device are shown in Figures 1.8 and 1.9, respectively. The power conversion efficiency (η) of an OPV cell can be calculated from I–V characteristics (Figure 1.9) curve using following equation (1.35).

$$\eta = FF\,\frac{J_{SC}V_{OC}}{PS} \tag{1.35}$$

where J_{SC} is the short circuit current density, V_{OC} is the open circuit voltage, FF is the fill factor (ratio of maximum power delivered by the solar cell represented by rectangular area in Figure (1.9) divide by the product of J_{SC} and and V_{OC}), and PS is the optical irradiance of the incident light from the sun, 100mW/cm^2. Equation (1.35) shows that the

power conversion efficiency of a solar cell can be improved if we can increase the values of FF, J_{SC} and V_{OC}. In this thesis, we will present I–V characteristics of some solar cell devices and calculate power conversion efficiency using Equation (1.35).

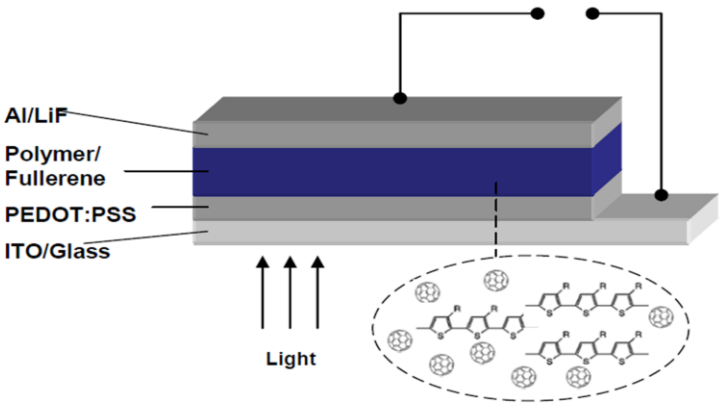

Figure 1.8: Bulk heterojunction solar cell device structure.

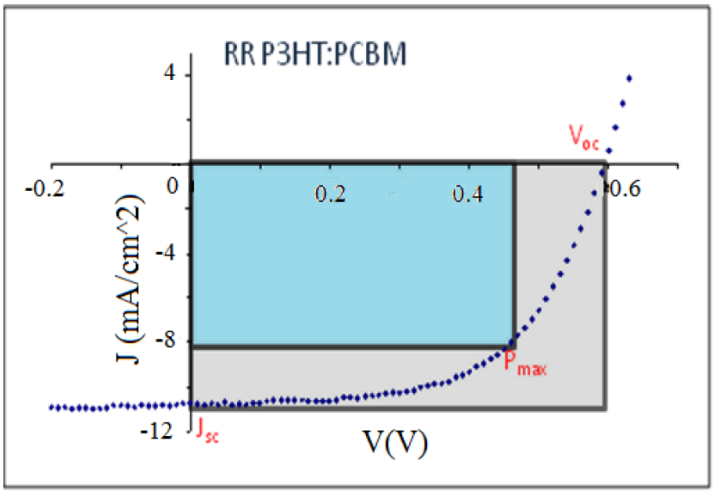

Figure.1.9: I-V characteristics of organic solar cell fabricated using RR-P3HT/PCBM as active layer. Adapted from Ref. [46]

CHAPTER 2

EXPERIMENTAL TECHNIQUES

In this chapter, the experimental techniques that we used to characterize the polymer solutions, films, and their blends with fullerene derivatives are discussed in detail. The polymer solutions were prepared by dissolving the appropriate amounts of polymer powder in suitable solvent. Polymer films were then prepared either by drop casting or spin casting the solution on sapphire or calcium fluoride (CaF_2) substrates. To prevent oxidation and other possible polymer contaminations, all handling processes were done in an inert nitrogen (N_2) atmosphere inside a glove box with oxygen level less than 0.75 ppm. The polymers used in this thesis are isotopes of DOO-PPV, RR P3HT, RRa P3HT, and PTB7 as donor, and $PC_{61}BM$, $PC_{71}BM$ as acceptor; these materials are tabulated below in Figures 2.1(a) – (h) along with their chemical structures.

2.1 Laser Sources for Photoexcitation

2.1.1 Femtosecond Optical Parameter Oscillator (OPO) System

The optical parameter oscillator (OPO) laser system used in this work consists of a continuous wave (CW) solid state laser (Millennia Xs, Spectra–Physics) with average power of ten watts operating at 532 nm; a 100 fs titanium-sapphire pulsed laser with a repetition rate of about 80 MHz (Tsunami, Spectra Physics); and a frequency converter system OPO (Opal, Spectra-Physics). The schematic diagram of this system is shown in Figure 2.2. The CW laser pumps the Ti-sapphire pulse laser.

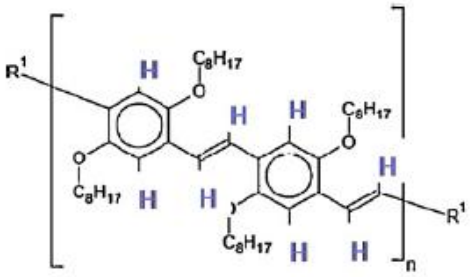

(a) Protonated Poly(dioctyloxy) phenylenevinylene (H-DOO-PPV)

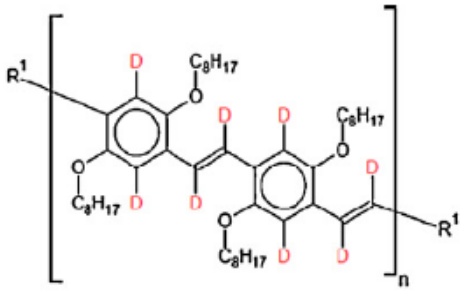

(b) Deuterated Poly(dioctyloxy) phenylenevinylene (D-DOO-PPV)

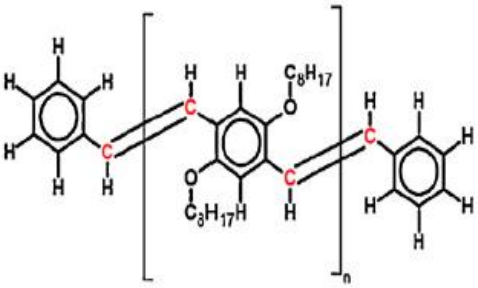

(c) C13-rich Poly(dioctyloxy) phenylenevinylene (C13-DOO-PPV)

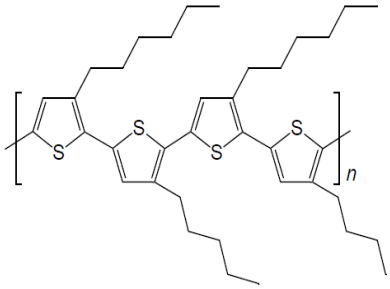

(d) Regio-Regular-poly (3-hexylthiophene) RR-P3HT

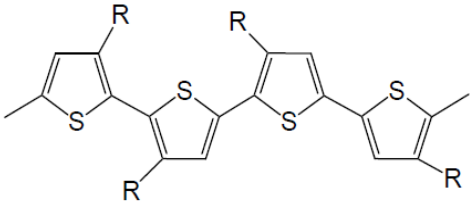

(e) Regio-Random –poly (3-hexylthiophene) RRa-P3HT

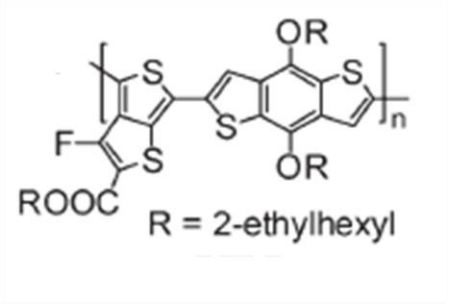

(f) Poly-thienothiophene-benzodithiophene 7 (PTB7)

Figure 2.1: Chemical structures of (a) H-DOO-PPV, (b) D-DOO-PPV, (c) C-13-DOO-PPV, (d) RR-P3HT, (e) RRa-P3HT, (f) PTBT, (g) $PC_{61}BM$, and (h) $PC_{71}BM$.

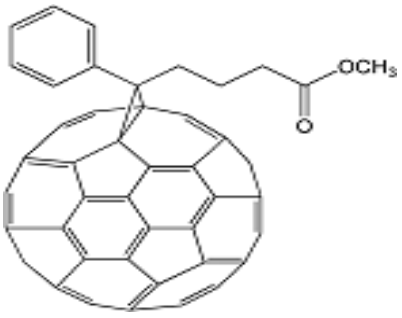

(g) [6,6]-Phenyl C61 butyric acid methyl ester ($PC_{61}BM$)

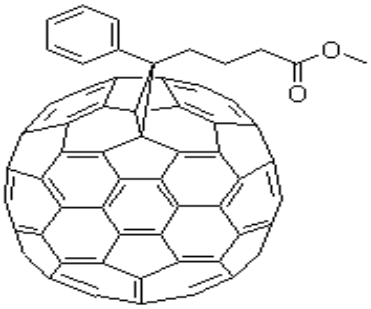

(h) [6,6]-Phenyl C71 butyric acid methyl ester($PC_{71}BM$)

Figure 2.1: Continued.

Subsequently, the Ti-sapphire laser beam ~ 2.2 watts pumps the OPO, which generates two beams: signal and idler (Figure 2.2).

2.1.1.1 Down Conversion and Difference Frequency Generation Using the OPO System

An OPO is not really a laser but a frequency converter. It works on the principle of 'parametric down conversion' (PDC), an optical nonlinear phenomenon, in which three photons interact in a noncentrosymmetric crystal (Brewster-cut lithium triborate, LiB_3O_5 or LBO) via their electric field components: E_1, E_2 and E_3*. In this process, an input or fundamental photon transfers its energy and momentum into two output photons. These are an output photon with higher energy "signal," and a lower energy "idler". The signal and idler wavelengths are tunable, and can be controlled by changing the crystal temperature and the angle of the diffraction grating. In the PDC process, energy and momentum are conserved and satisfy the following conditions:

$$\omega_f = \omega_s + \omega_i \tag{2.1}$$

$$\overrightarrow{k_f} = \overrightarrow{k_s} + \overrightarrow{k_i} \tag{2.2}$$

where the subscripts f, s, and i are used here to denote the fundamental, signal and idler photons, respectively.

In an OPO system, the nonlinear crystal is placed in an optical resonator cavity. This cavity must have exactly the same length as the Ti-sapphire cavity in order to keep the same pulse duration at the OPO crystal as it is in the Ti-sapphire intermediate laser. In OPO two cavities are used, which we call '1.3 μm' and '1.5 μm'. They are used for two spectral ranges. The output of the Tsunami is tuned to 775 nm and is used to pump the '1.3 μm' spectral range, whereas the '1.5 μm range' is pumped by the fundamental at 810 nm from the same Tsunami.

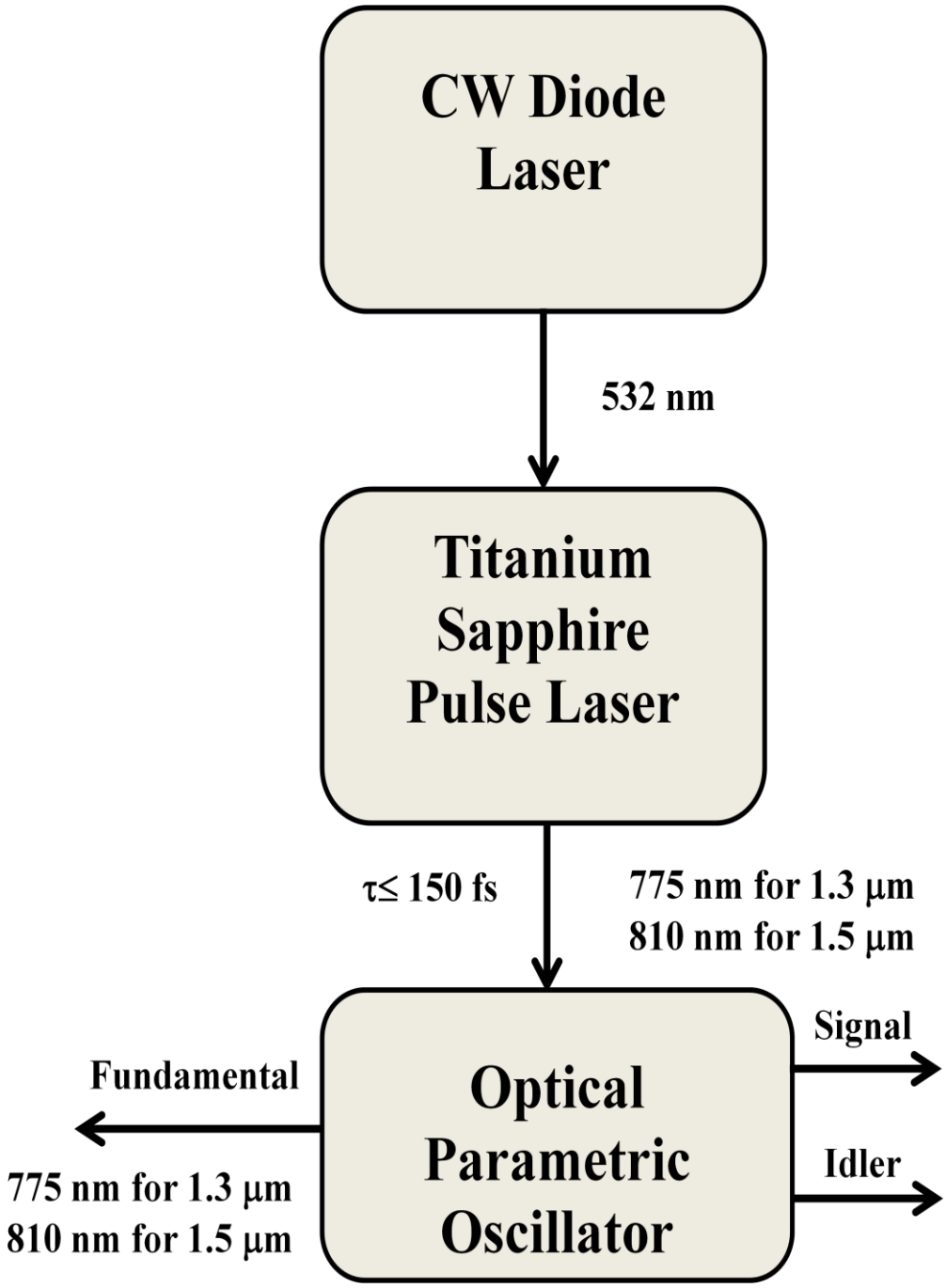

Figure 2.2: Schematic diagram of the OPO femtosecond pulse laser system.

Using both spectral ranges with the appropriate tuning of the OPO crystal temperature and diffraction grating angle, we can span the probe spectral range from 0.53 eV (2.33 μm) to 1.05 eV (1.18 μm) with 150 fs time resolution (see Figure 2.3). In order to extend the probe spectral range from 0.25 to 0.43 eV (2.66 - 4.9 μm), we use a difference frequency generation (DFG) crystal ($AgGaS_2$) [47] outside the OPO, along the path of signal and idler beams. Similar to the PDC above, DFG is also a second order nonlinear optical process. By carefully focusing the collinear 'signal' and 'idler' beams onto the crystal, we generate a difference frequency pulse beam when the incoming signal and idler pulses overlap spatially, temporally and phase matched to the proper rotational angle of the crystal. The photon energy of the generated new DFG frequency is given by the relation:

$$\omega_{df} = \omega_s - \omega_i \tag{2.3}$$

By using the OPO and DFG, the probe spectral range may be tuned from 0.25 to 1.05 eV (see Figure 2.3) in the mid-IR spectral range at low intensity, high repetition rate with ~ 150 fs pulse duration.

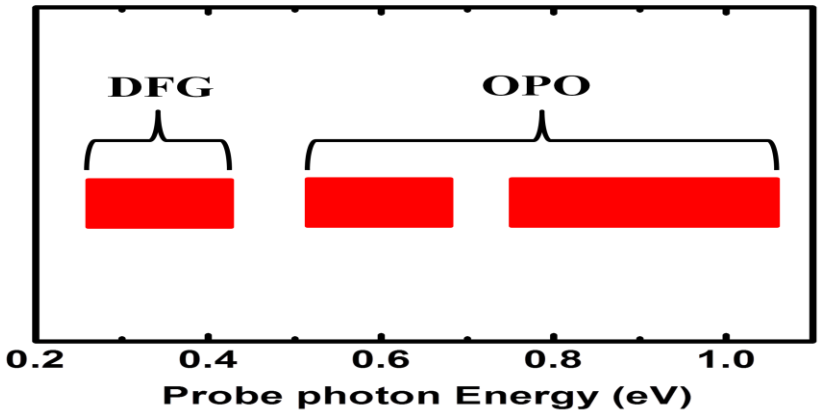

Figure 2.3: The probe spectral range in the mid-IR.

2.1.1.2 Pump/Probe Apparatus

The transient photoinduced absorption (PA) measurements of polymer films and blends are performed utilizing the OPO system using a two-color pump-probe technique with linearly polarized pulsed light beams. Inside the OPO the nonlinear crystal LBO reflects a part of the incident beam that comes out of the opal. This is called 'residual beam'; it is at 775 nm for the '1.3 μm' system and 810 nm for the '1.5 μm' set up. An acousto-optic modulator (AOM) is used to modulate the residual beam, which is then used as a pump that excites the sample with fundamental photon energy of 1.55 eV (below the optical gap) or, alternatively is focused onto a second harmonic generation (SHG) crystal to generate ~ 3.1 eV photon energy for 'above gap' excitation of the polymers. The typical pump energy/pulse is about 0.1 nJ, and the intensity is kept below $5\mu J/cm^2$ per pulse, which corresponds to 10^{13} cm^{-2} initial photoexcitations areal density per pulse on the illuminated sample. To avoid possible complications from exciton-exciton annihilation, polymer films degradation and nonlinear effects, such as two-photon absorption, the pump beam intensity is kept low, and generates low-exciton density of the order of $10^{16}/cm^3$ in the sample film.

In the 'pump-probe' experiment, the relative delay between the 'pump' and 'probe' pulses is obtained by translating the motorized translation stage in the path of the probe beam. The probe beam is then focused on the sample thin film (with a diameter of 20-50 μm) and kept inside the larger pump beam diameter on the film (100-500 μm) depending on the signal/noise ratio (SNR) that we need to obtain during the measurement. A constant photoexcitation density is maintained during the measurement by gently maximizing the spatial overlap of pump and probe beam on the sample, for each probe photon energy. In the measurement, sometimes an out-of-phase signal shows a step-like response at 't = 0'. This indicates that the lock-in is not properly phased with the pump beam modulation. In this case, a small portion of the pump beam is scattered into the detector, and a proper phase lock is established. The out-of-phase signal should

be zero in order to get the best in-phase signal. The misalignment of the probe beam shows a linearly increased or decreased out-of-phase signal (also called ‘beam-walk’), when the probe beam is delayed using the translation stage. In that sense, the delayed probe beam should be realigned, or at least the in-phase signal response should be divided by the ‘beam-walk’ time response (Quadrature signal) in order to get the true ultrafast sample response.

In our set up, we use two modulations scheme for the probe and pump beams respectively. A mechanical chopper is used to modulate the probe beam and isolate it from the near infra-red IR laser source; it operates at ~ 300 Hz and is used to measure the transmission T through the sample. Instead of the mechanical chopper, an acousto-optic-modulator (AOM) that runs at 40 kHz is used to modulate the pump beam when measuring the change, ΔT in transmission, T. The advantage of using AOM is that it helps to improve the signal-to-noise noise ratio (SNR) for low ΔT measurements.

Two optical filters are used in the measurements: one before the sample to block the fundamental and allow the desired probe beam to pass through, and the other filter placed very close to the detector, to avoid the unwanted scattered pump light to influence the probe signal.

A liquid nitrogen (LN)-cooled indium antimonite (InSb) detector in photovoltaic (PV) unbiased mode is used in the spectral range 1.18 to 4.9 μm. The PV mode provides optimum SNR for our modulation frequency.

2.1.2 High Intensity, Low Repetition Rate Ultrafast Laser System

In addition to the low-energy (0.1 nJ/pulse), high repetition rate (80 MHz) ultrafast laser system, we also used a high-energy (mJ/pulse), low repetition rate (1 kHz) femto-second laser system to conduct the transient PA measurement in the visible/near-IR spectral range. A home-built, passively mode-locked titanium-sapphire laser, based on a published design [48], was used as a seed source. It provides a 100 fs laser pulse with a

repetition rate of 76 MHz. This low-intensity pulse train was sent to seed a regenerative amplifier (RGA).

The Q-switched 527 nm YLF pump laser was acquired from Quantronix Inc. About 4 % of the titanium-sapphire amplifier output intensity is used to create white light supercontinuum within the spectral range 1.2 to 2.7 eV by focusing it on to a 1 mm thick sapphire plate. A notch filter is also used after the sapphire plate to remove the residual 800 nm fundamental laser from the white light supercontinnun probe pulses. The reminder of titannium-sapphire (Ti:S) output is fed into an optical parametric amplifier (OPA). The output of the OPA is at 1 kHz repetition rate 800 nm pulses of ~ 150 fs. The pulse energy at the output beam is five orders of magnitude higher than the output intensity from oscillator due to the low repetition rate and amplification that occurs in the system. A SHG crystal (BBO) is used to create 400 nm (3.1 eV) pump from the fundamental 800 nm. The pump beam is modulated mechanically exactly at half the repetition rate of the Ti:S laser system (500 Hz), and the change in transmision ΔT in the probe beam is detected using phase sensitive lock-in amplifier technique, similar as with the high repetition laser set up discussed above. This set-up was earlier operated by Dr. Sanjeev Singh, and is now run by Ms. Ella Olejnik. The details of this aparatus can be found in Ref. [49].

2.2 Transient Pump – Probe Spectroscopy Theory

Transient PA is the time dependent change in the absorption of the material under illumination recorded as a function of wavelength. Two ultrafast pulses are utilized for measuring the PA using pump-probe spectroscopy. Pump pulse is used at time t = 0 to excite the sample and then the probe pulse is subsequently delayed to monitor the excited population dynamics. The change, ΔI in the transmitted intensity of the probe pulse, I, which is induced by the pump pulse is monitored with the help of a detector. The experimental set-up of the transient pump-probe spectroscopy is shown in Figure 2.4.

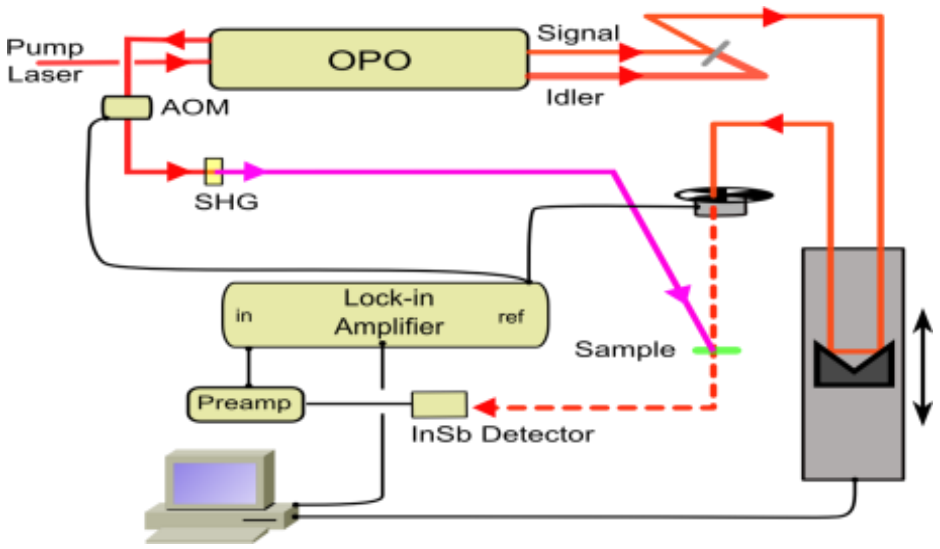

Figure 2.4: Experimental set-up of the transient pump-probe spectroscopy measurement. The transmission of the probe beam is measured using a mechanical chopper. The PM signal, $\frac{\Delta T}{T}$ is measured by modulating the pump beam with an AOM, and perfect spatial and temporal overlap of pump-probe beams is maintained on the sample.

2.2.1 Linear Absorption (Pump)

The absorption of the pump pulse by the π-conjugated polymer is the linear process in which elecrons get excited from the ground state, $S_{0,}$ to a higher singlet electronic state, S_1. This is not the only possible case when light impinges on a material. In addition to absorption the incident light is reflected, scattered, or transmitted. The ratio of reflected and transmitted energy to the amount of incident light energy is defined as reflectance (R), and transmittance (T), so that the total incident intensity (assuming negligible scattering) is conserved: $I_0 = I_r + I_t + I_a$. The reflected intensity is related to the incident intensity by the relation

$$I_r = RI_0 \tag{2.4}$$

Similarly, the absorbance is related with transmittance by the relation

$$A = -\text{Ln } T = -\left(\frac{I_t}{I_0}\right) \tag{2.5}$$

The optical absorption coefficeint (or extinction coefficient) α is defined as the product of density of optical absorbers N and cross-section of those absorbers σ, and both are wavelength-dependent.

$$\alpha(\lambda) = N(\lambda)\,\sigma(\lambda) \tag{2.6}$$

From the Lambert-Beer law,

$$I_t = I_0\,(1-R)e^{-\alpha d} \tag{2.7}$$

where d is the optical thickness of the sample. The absorbance can be derived by using Equations (2.4) and (2.7) as follows:

$$I_a = I_0 - I_r - I_t \tag{2.8}$$

$$= I_0\,(1-R)[1 - e^{-\alpha d}] \tag{2.9}$$

$$= \begin{cases} 0, & if\ \alpha d \approx 0 \quad (2.10) \\ I_0(1-R)\alpha d, & if\ \alpha d \ll 1 \quad (2.11) \end{cases}$$

Again, Equations (2.5) and (2.7) can be used to to find the following result

$$A = \alpha d - \ln(1-R) \tag{2.12}$$

If the reflectance is negligible while αd<<1, then the absorbance relation reduces to

$$A = ln\left(\frac{I_a}{I_0}\right) = \alpha d \tag{2.13}$$

so that absorbance is proportional to the sample thickness while the transmittance varies logarithmically with thickness

$$T = e^{-\alpha d} \tag{2.14}$$

Optical density (OD) is a dimensionless measure of absorption: absorbance per unit length (i.e., divided by the thickness of the sample).

The energy per pulse also can be calculated by using following relation;

$$\epsilon_{pulse} = \int_0^{\tau} p(t)dt = N\hbar\omega \tag{2.15}$$

where p(t) is the instantaneous power, τ is the pulse duration and N is the number of photons per pulse. One repetition rate r creates a single pulse so 1/τ can be replaced by r. The average power which can be measured directly using a power meter then can be expressed as

$$\bar{p} = \frac{1}{\tau}\int_0^{\tau} p(t)\,dt = \frac{\epsilon_{pulse}}{\tau} = r\epsilon_{pulse} \tag{2.16}$$

and the number of photons per pulse is given by

$$N = \frac{\bar{p}}{r\hbar\omega} \tag{2.17}$$

2.2.2 Photoinduced Absorption (Probe)

The transmission of the probe beam decreases after the sample illumination by the pump beam. The difference in transmission, ΔT between transmission before illumination T_D (dark) and after illumination T_L (light) is given by

$$\Delta T = T_L - T_D \tag{2.18}$$

Considering that the change in transmission is related with light induced change in absorption coefficient α,

$$T_L = T_D\, e^{-\Delta\alpha d} \tag{2.19}$$

$$1 + \frac{\Delta T}{T_D} = e^{-\Delta\alpha d} \tag{2.20}$$

$$\Delta\alpha d = -\ln\left(1 + \frac{\Delta T}{T_D}\right) \tag{2.21}$$

$$\Delta T \ll T_D \Longrightarrow \Delta\alpha d \approx -\frac{\Delta T}{T_D} \tag{2.22}$$

Here, we recognize two types of signals as photoinduced absorption (PA, $\Delta\alpha > 0$) and photoinduced bleaching (PB, $\Delta\alpha < 0$). In the case of PA signal, new states are created whereas the decrease in the ground state optical tansition by the pump pulse is called PB.

2.2.3 Kinetic Analysis

From Equation (2.6), we clearly see that the absorption coefficient α, photoexcitation density N, and optical cross-section σ, are wavelength dependent. Assuming that the photoexcitation density N varies with time, a cross-section σ that does not depend on time, then an equation can be rewritten as

$$\Delta\alpha(t) = \Delta N(t)\sigma \tag{2.23}$$

Again, from Equation (2.22), we have

$$\Delta\alpha(t)d = \frac{\Delta T}{T_D} \tag{2.24}$$

Comapring Equations (2.23) and (2.24), we get

$$\Delta\alpha(t)d = \Delta N(t)\sigma d = \frac{\Delta T}{T_D} \tag{2.25}$$

Here, we want to understand the mechanism of the photoexcitation dynamics in the time domain. For this purpose, we use a simple model that distinguishes between generation and recombination processes. These processes are described by a single rate equation for the photoexcitation density

$$\frac{dN}{dt} = G(t)S(N_0) - R\,(N) \tag{2.26}$$

where N is the photoexcitation density, σ is the optical cross-section of the sample, and d is the optical thickness, or the optimum distance light can penetrate in the sample. G is the photoexcitation generation rate and R is the recombination. S (N_0) is a saturated term due to defect limited case, which is assumed 1 for simplicity in this work.

For steady-state conditions (i.e., CW spectroscopy), Equation (2.26) reduces to

$$\frac{dN}{dt}|_{ss} = G - R = 0 \tag{2.27}$$

so that G = R. In transient spectroscopy, however, the photoexcitation density changes with time, N = N (t) and the generation rate is given by

$$G = \frac{\alpha\eta}{\hbar\omega V} I_L = aI_L \tag{2.28}$$

where I_L is the excitation laser intensity that is absorbed by the sample, α is the extinction coefficient corresponding to pump photon energy, η is the quantum efficiency, $\hbar\omega$ is the photon excitation energy, V is the volume of the excitation and a is a coefficient. G(t) is propotional to genaration rate g, and it is proportional to the pump intensity I_L.

2.2.3.1 Dispersive Kinetics

Because polymers are disordered materials most of the processes are temporally dispersed. In this condition, Equation (2.26) appears in more general form as

$$N\,(t) = \int_{t_1}^{t_2} R(\tau) e^{-\frac{t}{\tau}} d\tau \qquad (2.29)$$

where t_1 is the temporal resolution of the measurement and t_2 is the pulse repetition time, and $R(\tau)$ is the distribution of lifetimes in the sample. The distribution of life-times can be several types, as discussed below.

Case One. The simplest possible case is biexponential decay, which explains the interaction of two species.

$$R\,(\tau) = N_1\delta(t - \tau_1) + N_2\,\delta(t - \tau_2) \qquad (2.30)$$

where N_i is the respective state populations, τ_i is the lifetimes and δ is the kronecker delta function. In this case, final solution of Equation (2.29) becomes

$$N(t) = N_1 e^{-\frac{t}{\tau_1}} + N_2 e^{-\frac{t}{\tau_2}} \qquad (2.31)$$

Case Two. Another possibility is power law decay for which the recombination rate is

$$R(\tau) = \left(\frac{t}{\tau_1}\right)^{-(1+\alpha)} \qquad (2.32)$$

In this condition, the integral is evaluated using saddle-point technique and the solution is

$$N(\tau) \propto \left(\frac{t}{\tau_1}\right)^{-\alpha} \qquad (2.33)$$

Case Three. There is also possibilty of stretched exponential when lifetimes are dispersed with a profile of lifetimes. The recombination rate for this case is of the form,

$$R(\tau) \propto e^{-\left(\frac{\tau}{\tau_0}\right)^{\nu}} \qquad (2.34)$$

and the solution is

$$N(t) \propto (\frac{t\tau_0^{\nu}}{\nu})^{\frac{1}{1+\nu}} \exp\left[-(\nu+1)(\frac{t}{\nu t_0})^{\beta}\right] \qquad (2.35)$$

where the stretch coefficient $\beta = \frac{\nu}{\nu+1}$

2.2.3.2 Monomolecular and Bimolecular Recombinations

For understanding the recombination processes in π – conjugated polymers following photoexcitation it is important to know what kind of species are generated at the time of photoexcitation. The recombination is monitored using transient PA dynamics, which depend on various generation and recombination conditions. The simplest possible channel of recombination is *monomolecular*, in which only one kind of excited species is involved in the process. In this circumstance, the recombination rate depends directly on the excited state population N, and inversely with the state lifetime τ, or $R = -\frac{N}{\tau}$. In transient spectroscopy, there is no possibility of generation after the excitation pulse ends, so G is zero in Equation (2.26), which then takes a new form

$$\frac{dN}{dt} = -\frac{N}{\tau} \qquad (2.36)$$

This is a first order differential equation with straightforward solution,

$$N(t) = N(0)e^{-\frac{t}{\tau}} \qquad (2.37)$$

Therefore, a single exponential fit decay dynamics verifies MR process in transient PA measurement.

In the steady state, Equation (2.26) reduces to

$$\frac{dN}{dt}|_{ss} = G - \frac{N_{SS}}{\tau} = 0 \qquad (2.38)$$

and solution is

$$N_{ss} = G\tau = aI_L\tau \qquad (2.39)$$

From the above equation, the PA signal $\frac{\Delta T}{T}$ depends linearly with the excitation laser intensity in CW spectroscopy if there is MR process.

The other possibility of recombination is *bimolecular*, in which two excited-state species are involved in the process. In this condition, R is proportional to the square of the excited state population N, i.e., $R = -bN^2$, where b is the proportionality constant. For this process, Equation (2.26) reduces to

$$\frac{dN}{dt} = -bN^2, \tag{2.40}$$

and solution is

$$N(t) = \frac{N(0)}{1+tbN(0)} \tag{2.41}$$

In steady state condition, Equation (2.26) becomes

$$\frac{dN}{dt}|_{ss} = G - bN_{ss}^2 = 0 \tag{2.42}$$

so that solution is

$$N_{ss} = \sqrt{G/b} = (\frac{aI_L}{b})^{1/2} \tag{2.43}$$

This result shows that BR in CW spectroscopy shows a PA sublinear power law dependence with the excitation laser intensity with an exponent of 0.5.

2.2.4 Background in the Ultrafast Spectroscopy Measurements

At high repetition rate (80 MHz) in the low intensity laser system, the time between two consecutive pulses is about 12.5 ns. In this case, there may not be sufficient time for all photoexcited states from a single pulse to completely relax back to the ground state until the next pulse arrives at the sample. The photoexcited species linger long enough to create what we call a transient "background" PA. In fact, it is the accumulated steady-state background of the 'left-over' transient populations in between successive pulses. If the pump beam in the CW PA measurement is modulated with the same frequency as the pump beam of the transient PA measurement, the background PA

observed in transient PA spectroscopy corresponds to the CW PA in-phase signal. The in-phase signal in CW PA measurement always gives information about long-lived photoexcited species, having life-time of the order of 1/f, where f is the pump beam modulation. Therefore the transient background PA is also an alternative way to obtain information about such type of long-lived photoexcited species. The background PA masks the true PA dynamics in the ps time domain, because it appears as a base signal independent of the usual 'step' at ~ t = 0. While we perform the measurement in polymer films, the transient background signal is mostly small, and does not affect the PA dynamics significantly. However, the background PA is large in polymer blends, especially at < 0.5 eV, and thus the decay dynamics may be difficult to obtain. In this case the transient dynamics of long-lived photoexcited species in the ultrafast regime can be analyzed only qualitatively.

2.3 Other Systems and Techniques

2.3.1 Linear Absorption Measurement

Linear absorpton is the basic measurement to identify the band gap of conjugated polymers, and it guides us to choose the appropriate pump excitation energy in both CW and transient PA spectroscopy measurements. When a polymer absorbs light, it promotes electrons form the ground state to any higher excited state that is optically coupled to the ground state. The transition from the ground state to higher states S_n can happen (where n denotes any higher electronic state) if these states have appropriate parity, angular momentum, and enough oscillatory strength with respect to the ground state. The optical transition from lower to higher energy states is the manifestation of absorption. The absorption strength depends on incident radiation flux, optical cross-section of the material from initial to final states, and the sample thickness. The wavefunction overlap of the upper and lower enegry states determines how strong the transition between these states will be; this is also called the Frank Condon principle. Whether or not the transition

is allowed is determined using the dipole selection rule, which is described in detail in Section 1.3.

The absorption of various polymers films in the visible, ultraviolet, and near infrared range is measured using the CARY-17 spectrometer. The glass substrate is cleaned nicely with toluene, and the film is then deposited by dropcasting the polymer solution onto it. Substrate effects and system response are eliminated by substracting the transmission spectrum of a blank substrate from the transmission spectrum of the sample during the measurement. No further corrections are done for scattering and reflection from the sample, assuming that these effects are negligible small. Absorption is measured in units of optical density (OD), which is related with the transmission T by $T = T_0 10^{-OD}$, where T_0 is the transmission of the system without the film and OD = αd, α is the absorption coefficient, and d is the sample thickness. Typically for π – conjugated polymers there are three absorption bands marked I, III, and IV, as observed in poly (para-phenylenevinylene) PPV [50] (Figure 2.5).

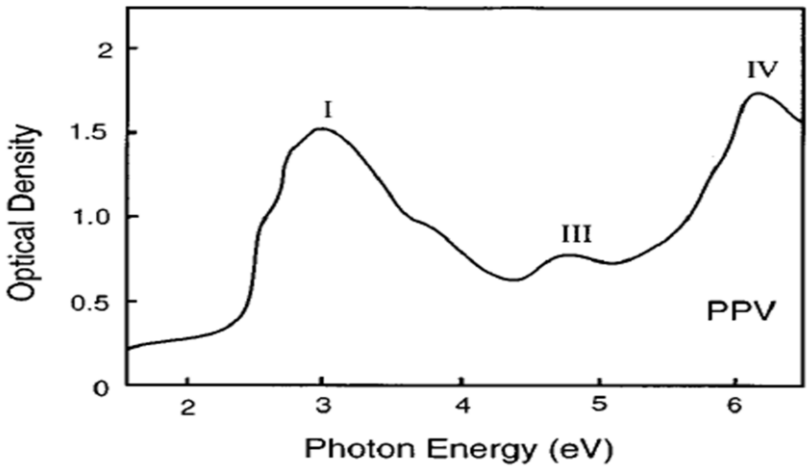

Figure 2.5 : Absorption spectrum of unsubstituted PPV Film. The absorption bands centered at 2.4, 4.7 and 6.0 eV are labeled I, III and IV, respectively. Adapted from Ref.[50]

In addition to these bands, a weak shoulder ~ 3.7 eV is also seen. These bands have been identified as optical transitions between π (occupied) and π^* (unoccupied) molecular orbitals [51]. Calculations show that bands I and II originate from d-d* transitions, polarized parallel to the chains [50, 52] and band III involves degenerate transitions d-1* and 1-d*, and perpendicular to the chain [52]; where d stands for delocalized and l for localized states. The band IV is due to l-l* and lacks prefered polarization.

2.3.2 CW Photoinduced Absorption Measurement

The continuous wave (CW) photoinduced absorption is the experimental technique to monitor the long lived photoexcited species, such as triplet and polarons. In this measurement, the sample is constantly illuminated by a CW laser pump source (mostly Ar+) modulated at ~ 300 Hz, and the steady-state change in the transmission is detected (Figure 2.6). The probe source is white light coming from either a tungsten or Xe lamp, which can can probe the broad spectral range from 0.4 to 3 eV. First, the pump-beam is blocked and probe beam is modulated at 300 Hz, using optical chopper and transmission of the probe beam through the sample is measured after a monochromator using a suitable detector of either silicon or LN-cooled Ge or InSb, depending on the desired probe spectral range. After the transmission measurement, the pump beam is modulated using the same optical chopper with the same frequency, and used to excite the sample. The pump and probe beam are ovelapped spatially on the sample to maximize the signal and then measured as described before. A phase sensitive (Lock-in) detection technique is used to measure the ΔT signal. Typically, the $\Delta T/T$ signal sensitivity is of the order of 10^{-5}. The CW photo-modulation spectra measured in RR-P3HT/PCBM film using above gap (2.5 eV) and below gap (1.55 eV) pump excitations are shown in Figure 2.7. For both excitation energies, two clear signatures of polarons P_1, P_2 and IRAV bands are observed.

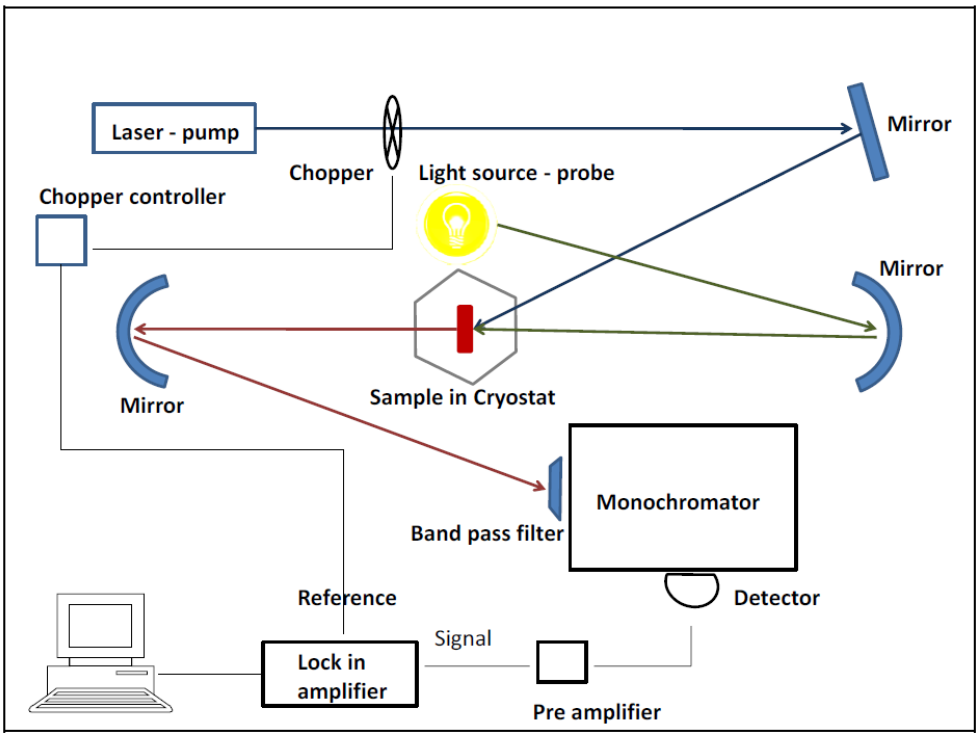

Figure 2.6: The CW photoinduced absorption experimental setup.

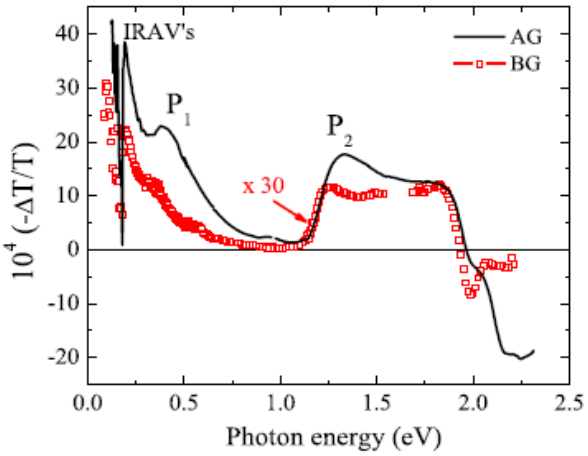

Figure 2.7: CW PA spectra of RR-P3HT/PCBM film using above gap ($\hbar\omega$ = 2.5 ev black solid line) and below gap ($\hbar\omega$ = 1.55 eV-red square) pump excitation. Both spectra show the known PA signatures of polarons P_1 and P_2 bands and IRAV, as denoted. Adapted from Ref. [53].

2.3.3 Photolumiscence (PL) Measurement

One of the possible excited state decay channels in the polymer films and blends is the radiative decay or photolumiscence (PL), where the excited state species relaxes to the ground state by emitting a photon with energy equal to the the optical transition. By using the same set-up as the CW spectroscopy (Figure 2.6), we can measure the PL of any sample if it is luminescent. In this measurement, we simply excite the sample by a modulated pump beam and collect the emission using a parabolic mirror. Then the collected emission from the sample is fed into a monochromator and detected using a suitable detector either Ge ($\hbar\omega > 0.8\,eV$ or Si ($\hbar\omega > 1.1\,eV$). Before the monochromator we always use an appropriate filter to block the unwanted scattered pump beam. The PL spetrum of D-DOO-PPV film is shown in Figure 2.8. Since all the electronic states of the polymer are coupled to the vibational modes, phonon modes coupled to dipole-allowed transitions, increase the transition oscillator length. The transitions involving the creation of vibrational quanta in the ground state are assigned as 0-0, 0-1 and 0-2 in the PL spectrum.

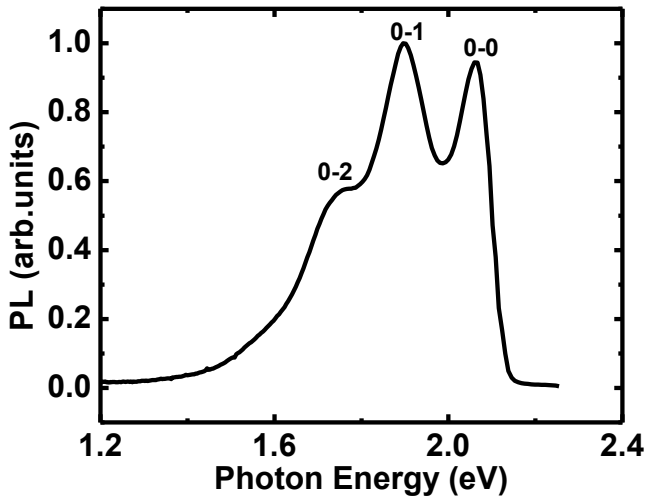

Figure 2.8: Photoluminescence (PL) spectrum of D-DOO-PPV Film. The phonon side bands 0-0 to 0-2 are assigned.

2.3.4 Doping Induced Absorption (DIA) Measurement

One of the most reliable techniques to identify the presence of long-lived photoexcitations in conjugated polymer films is to compare the PA spectrum with the doping-induced absorption (DIA) spectrum. In the DIA measurement, the films are doped by exposure to iodine (I_2) vapor for ~ 20 s. First, the transmission of the undoped sample, $T_{u,}$ is obtained. Then the transmission of the doped sample T_D is measured. The DIA spectrum, $\Delta T/T$, is obtained by taking the difference of transmission before and after doping, and then normalizing by transmission before doping the sample. The doping induced absorption (DIA) spectrum of PTB7 film is depicted in Figure 2.9. Here, the doping was done using Iodine vapor for two minutes, and the measurement was carried out using a FTIR spectrometer. The DIA spectrum consists of bands P_1, P_2 and IRAV due to charge polarons on the polymer chains.

Polymers are one-dimensional, and in this model the added charge carrier to the polymer chain forms a spin ½ polaron with two localized states in the energy gap. So, polarons have two allowed optical transitins, P_1 and P_2. In this experiment, one possibility is the isolation of polymer chains by large iodine ions and cause quasi-one dimensional electronic properties or iodine counter ions may localize the induced polarons. Thus, the DIA spectrum consists of two polaron bands in low and high photon energy as P_1 and P_2.

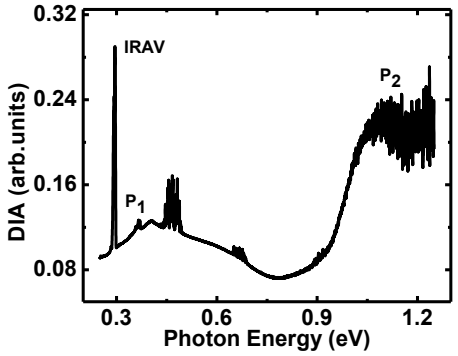

Figure 2.9: Doping induced absorption (DIA) spectrum of PTB7 film, where the polaron bands P_1, P_2 and IRAVs are assigned.

2.3.5 Electroabsorption

The electroabsorption (EA) is a powerful technique to reveal the electronic transitions which are forbidden in other absorptions measurement. It also helps to identify the transitions that are weak and unsolved by other absorption techniques. From this technique, we can get the information for both the even and odd parity of states. This process is third-order nonlinear, so the EA signal is proportional to the imaginary part of a third-order nonlinear susceptibilty $\chi^{(3)}$.

$$\frac{\Delta T}{T} \cong -\Delta\alpha d = \frac{4\pi\omega}{nc} Im[\chi^3(-\omega;\ \omega, 0,0)]F^2 \qquad (2.44)$$

where F is the applied electric field, d is the film thickess, and n is refractive index. In this measurement, the modulation frequency of the applied elecctric field is ~ 500 Hz, $f \ll \omega$, and thus can be assumed zero with respect to the optical frequency of the applied electromagnetic wave.

To perform the EA measurement, we need a special device structure in the form of interdigitated electrode array (Figure 2.10). A sapphire plate with a diameter of 1 inch and thickness of 2 mm is the substrate. A 50 nm titanium film followed by 150 nm of gold was sputtered on the substrate. Then, an interdigitated gold electrode array was photolithographically patterned and etched with a $40\mu m$ gap between the electrode fingers, as shown in Figure 2.10. On such a type of substrate, a sample was deposited with an optical density of 0.2 – 0.4 to get the substantial EA signal even for photon energy above the polymer gap.

The experimental set-up of EA measurement is shown in Figure 2.11. It is the modified set up of the CW PA measurement, in which the sample is excited using a modulated (~ 500 Hz) electric field of ~ 10^5 V/cm and then excited populations are monitored using xenon or tungsten probe photons as a probe beam. The very high electric field is achieved through high AC voltage of 200-300 V applied to the electrodes using a function generator and step-up transformer.

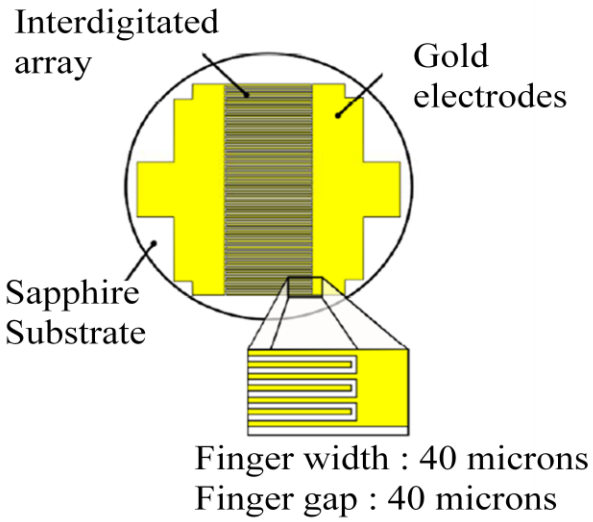

Figure 2.10: Sapphire substrate with interpenetrating finger electrodes used in EA measurement.

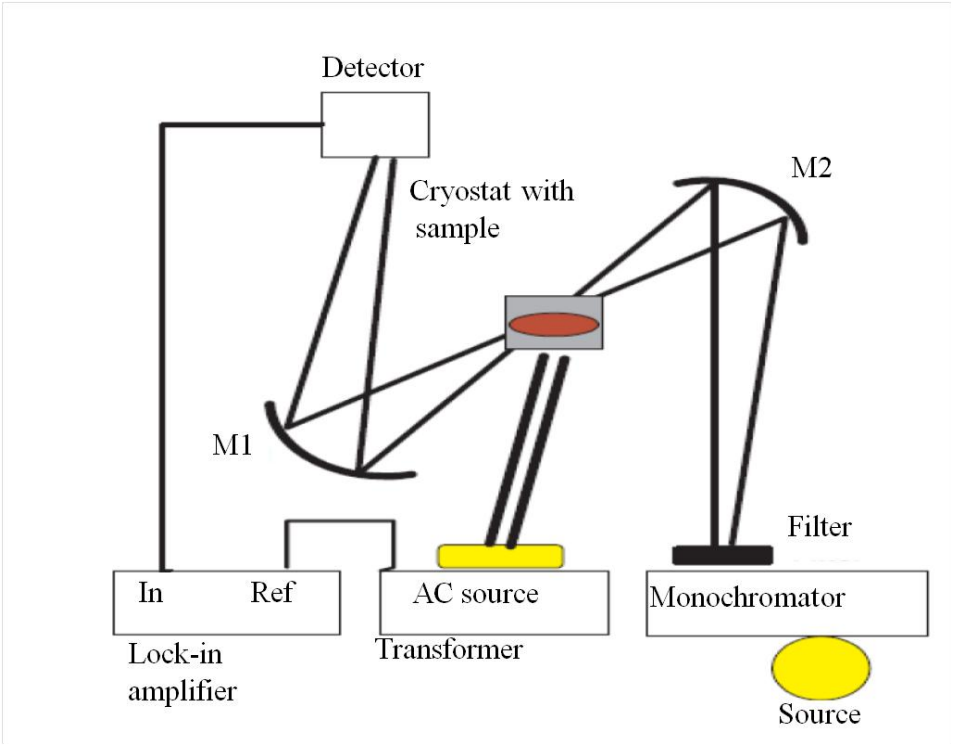

Figure 2.11: Experimental set-up for EA the measurements.

Here, the probe beam is fed through the monochromator and the selected wavelength incidents on the sample. In the presence of an applied modulated electric field and probe beam on the sample, the EA signal is collected by the curved mirror and focused onto a UV- enhanced silicon detector. The signal is then detected at 2f using phase-sensitive lock-in amplifier technique.

The EA spectrum of freshly prepared RR-P3HT film is shown in Figure 2.12. The spectrum comprises of two singlet excited states $1B_u$, mA_g and charge transfer state CT. From this result, we see that the energy difference between $1B_u$ and mA_g excited states is ~ 0.6 eV. In contrast, we always get exciton PA_1 transition that peaks at ~ 0.95 eV in the transient PM spectrum of RR-P3HT. The difference in these two measurements is still unresolved.

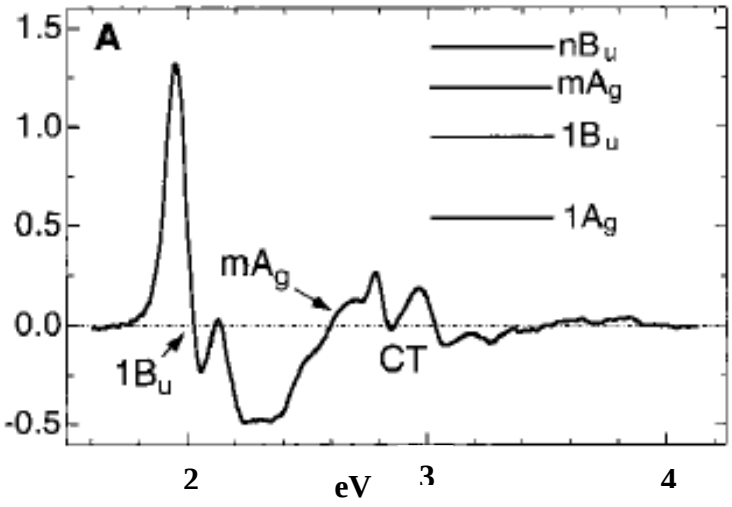

Figure 2.12: The EA spectrum of freshly prepared RR-P3HT Film. The energies of the intrachain excitons $1B_u$, mA_g, and charge transfer (CT) excitons are assigned. Adapted from Ref. [54].

2.3.6 FTIR Infrared Spectroscopy Measurement

The Fourier transform infrared spectroscopy technique is used to measure absorption and CW photo-induced absorption in mid-IR to far-IR photon energy range. The principle used in this technique is based on the Michelson Interferometer where the incident beam I_0 spilts into two beams, I_1 and I_2, after the beam splitter, as shown in Figure 2.13. One of these two beams is reflected from a moving mirror and the other from a stationary mirror. When these two beams pass through the sample, then superposition of the beams generate interferogram. The interference spectrum can be described as

$$I_{out(x)} = \frac{1}{4}\int_{-\infty}^{+\infty} I_0(\overline{\nu})\,[1+\cos(2\pi\bar{\nu}x)]d\bar{\nu} = constant + \frac{1}{4}\int_{-\infty}^{+\infty} I_0(\overline{\nu})\cos(2\pi\overline{\nu})d\bar{\nu} \tag{2.45}$$

where $I_{out}(x)$ is the interferogram spectrum as a function of displacement x.The inverse Fourier transform of the second part of the equation describes the spectrum of the interference as a function of $\bar{\nu}$ given by

$$I_0(\bar{\nu}) = \frac{2}{\pi}\int_{-\infty}^{+\infty} I_{out}(x)\cos(2\pi\bar{\nu}x)dx \tag{2.46}$$

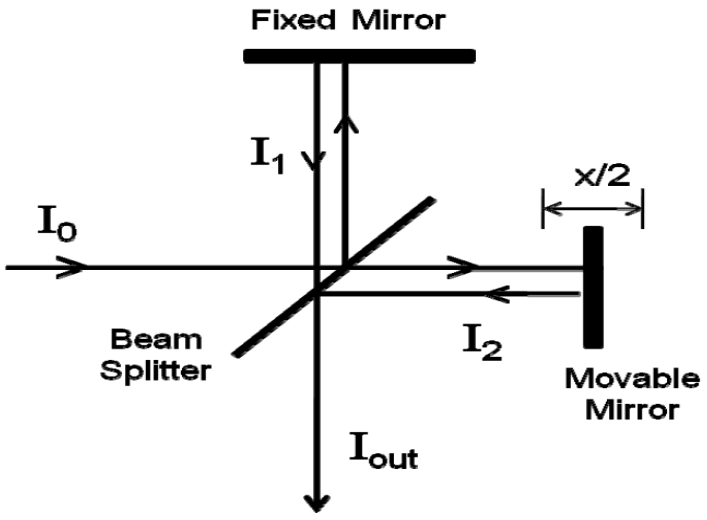

Figure 2.13: Schematic diagram of Michelson interferometer used in FTIR spectroscopy

In this spectroscopy, the infrared light source is the Glow-bar lamp and the beam splitter is KBr crystal. The transmitted intensity of light from the sample is measured using a liquid nitrogen-cooled MCT detector in the range from 400 – 7500 cm^{-1}. Figure 2.14 shows the FTIR spectra of MEH-PPV/C_{60} (10%) measured at 85 K and room temperature (RT). A PA band at 0.4 eV and two IRAV modes below 0.4 eV are observed. The strength of the IRAV modes is comparable to the P_1 band.

2.3.7 Photoluminescence Quantum Efficiency

The photoluminescence quantum efficiency (PLQE) is defined as the ratio of number of emitted photons per absorbed photons. This measurement gives very useful information about the radiative recombination channels in organic materials. The experimental set-up used to measure the PLQE is shown in Figure 2.15. The excitation source is Ar+ ion laser, which is modulated using an optical chopper.

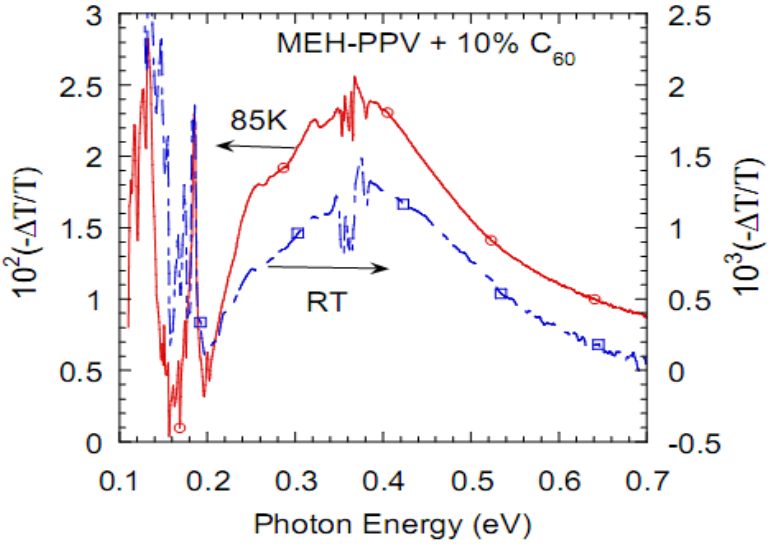

Figure 2.14: CW PM spectra of MEH-PPV/C_{60} (10%) mixture using FTIR spectroscopy at 85 K and room temperature, respectively. Adapated from Ref. [55]

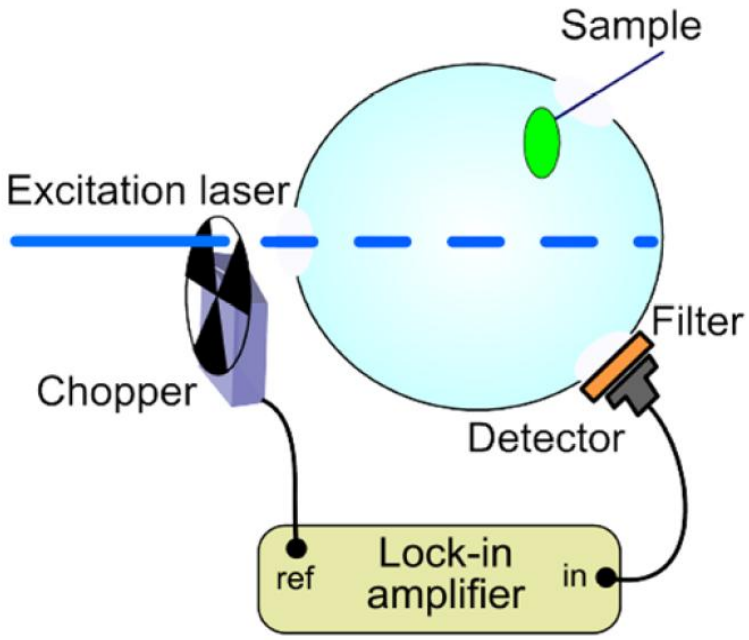

Figure 2.15 : Experimental set-up for PLQE measurement.

Inside the integrated sphere, the sample is placed and the emission is collected with the solid state detector and then measured using the lock-in technique. The optical density of spin coated sample should be less than 1 for PLQE measurement. The basic formula used to calculate PLQE is shown in Equation (2.47).

$$PLQE = \frac{I_{PL}-(R+T)I_{PL,corr}}{(1-R-T)I_L}\,\frac{D_L}{D_{PL}}\,\frac{S_L}{S_{PL}}\,\frac{E_L}{E_{PL}}\,\frac{1}{T_{F(PL)}} \qquad (2.47)$$

In the above Equation (2.47), $I_L, I_{PL}, I_{PL,corr}$ needs to be measured and stands for laser intensity without the sample inside the integrated sphere, the reflected uncorrelated PL intensity with the sample inside the path of laser, and the correlated PL intensity with the sample inside IS but out of the laser path, respectively. Here the correction term $I_{PL,corr}$ is necessary to measure for eliminating the contribution of the reflected photons (from IS walls) to the collected light emission.

R and T are the reflection and transmission coefficients at laser wavelength. D_L , D_{PL} are detector sensitivities, and S_L, S_{PL} are IS sensitivities at laser and the PL wavelengths, respectively. Similary, E_L and E_{PL} are photon energies of laser and PL emission, and $T_F(PL)$ is the transmission of the optical long pass filter used in the experiment at PL wavelength.

If the lifetime of the singlet exciton, τ_{exc} is known (from transient PA decay dynamics of PA_1) along with PLQE, then the radiative life-time of the singlet exciton can be calculated by using following relation

$$\tau_{rad} = \frac{\tau_{exc}}{PLQE} \tag{2.48}$$

and is usually of the order of nanosecond.

CHAPTER 3

ULTRAFAST PHOTOPHYSICS STUDIES OF PRISTINE P3HT FILMS AND BLENDS WITH PCBM

3.1 Introduction

In this chapter, we present the detailed ultrafast photophysics studies of pristine poly(3-hexyl-thiophene) [P3HT] films and blends with [6,6]-phenyl C_{61} butyric acid methyl ester [PCBM] using two pulsed laser systems: a low energy (0.1 nJ/pulse), high repetition rate (~80 MHz) system; and a high energy (10μJ/pulse), low repetition rate (~1kHz) system. The polymer/PCBM blend that we use here to study its photophysics is the most common active layer in organic photovoltaic (OPV) solar cell. The understanding of the photophysics of pristine polymer films and blends with an acceptor is important in order to learn more about the optical phenomenon that happens during the illumination in the active layer of OPV devices. In particular the photophysics of pristine polymer films and blends with PCBM is important for understanding the charge generation and exciton dissociation processes in the active layer of the OPV solar cell. Here, we have used a simple model to explain the charge transfer process in donor/acceptor blends. The schematic diagram is shown in Figure 3.1. First, the polymer absorbs the incident photon and the exciton is generated. The exciton diffuses towards the interface in short time scale and then forms a charge transfer exciton. Finally, a charge transfer exciton dissociates into free polarons in which positive polarons reside in polymer network and negative polarons in acceptor domains.

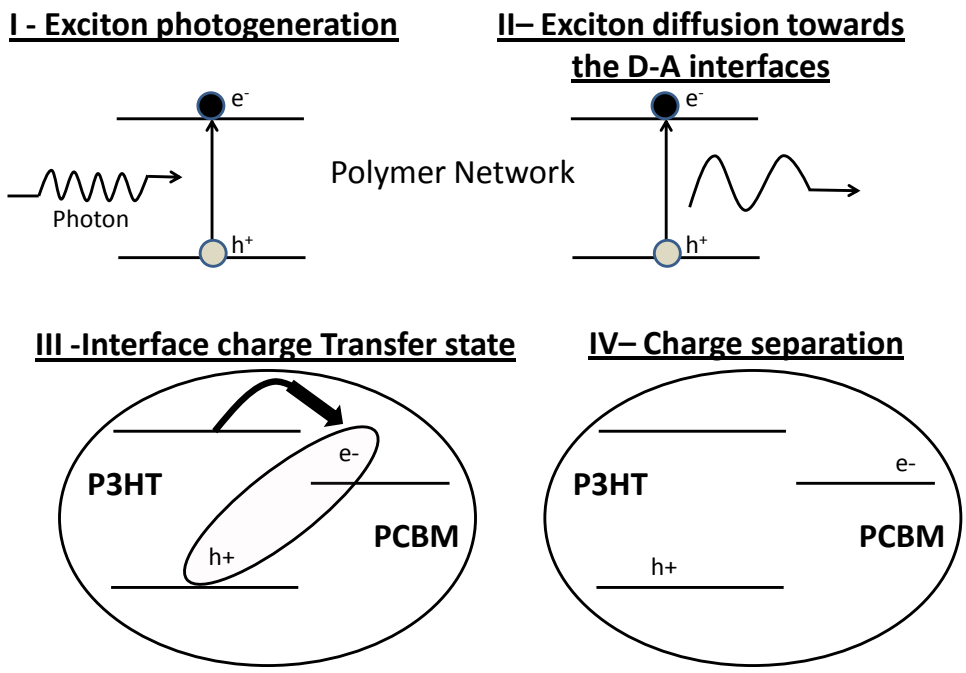

Figure 3.1: Charge transfer process in donor/acceptor blend system upon photoexcitation

One of the most efficient OPV cells is made from the combination of P3HT/PCBM as the active layer; the best power conversion efficiency achieved for this blend based solar cell is 5.2 % [56 – 58]. In our photophysics study, we have used P3HT polymers with different regio-orders, namely regio-regular (RR) and regio- random (RRa) P3HT polymers, for understanding where the large difference in their performance as active layers in OPV cells originates.

For this purpose, we have performed transient photomodulation (PM) measurements of the pristine polymer films and blends with PCBM in an unprecedented broad spectral range from 0.25 to 2.5 eV. We also studied the transient decay dynamics at various probe energies. In addition to the transient ultrafast photophysics results, doping-induced absorption (DIA), X-ray diffraction (XRD), and organic solar cell I-V characteristics and power conversion efficiency results are also presented in this chapter.

3.2 Materials

The materials used here are of two types: donor and acceptor. The donor materials are RR-P3HT, RRa-P3HT, whereas the acceptor is a derivative fullerene molecule, namely PCBM; their chemical structures are shown in Figure 2.1 [(d), (e), and (g), respectively (Chapter-2)]. In P3HT, the hexyl side groups have two types of attachment with the thiophene rings. In the structure of RR-P3HT, the side group is attached in a regular fashion (head to tail) with the main chain; whereas, the side group is in random order (head to head or tail to tail, no specific order) in RRa-P3HT [59 - 61]. The advantage of head to tail attachment of the side group with the main chain is that RR-P3HT forms lamellae, as shown in Figure 3.2, when films are prepared from solutions [57]. The acceptor PCBM is the derivative of C_{60} (fullerene molecule) with one side group attached to it which makes it soluble. The electro negativity of the fullerene molecule is high, so this material is considered a suitable candidate for the acceptor material in OPV devices.

The RR-P3HT, RRa-P3HT and PCBM fullerene were supplied by Plextronics; they have excellent properties compared to other commercial suppliers. The RR-P3HT obtained from Plextronics was of two types: low molecular weight (~15 kDa) and high molecular weight (~50 kDa). In addition to low and high molecular weight RR-P3HT, we also purchased RR-P3HT from the American Dye Source (ADS) Company and the Rieke Company, for comparison.

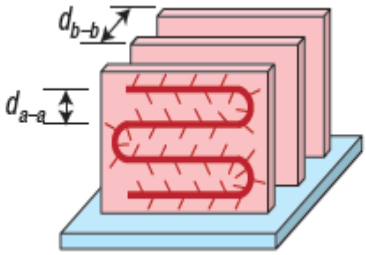

Figure 3.2: Schematic diagram of RR-P3HT lamellae folding and ordering on a substrate. Adapted from Ref. [57]

3.3 Sample Preparation

In order to make films, the following procedures were used. First, 12 mg of RR-P3HT and RRa-P3HT were weighted in separate vials inside a globe box in a nitrogen (N_2) environment. One ml of ortho-dichlobenzene (ODCB) was added in each vial and stirred for 30 minutes, keeping it on a hot plate at a suitable temperature. After 30 minutes, the heat was turned off and the vial was stirred for a long time (>12 hours) to make sure no polymer was left over to dissolve in ODCB. The polymer solution was then ready to drop-cast to make a film. In our measurement, the film was prepared by drop-casting the solution on CaF_2 or sapphire or glass substrates, depending upon the measurement we wanted to do. The procedure for making the blend of RR-P3HT/PCBM or RRa-P3HT/ PCBM, was the same as that used for polymer films. Normally 16 mg of RR-P3HT or RRa-P3HT was mixed with 13.33 mg of PCBM in a vial and 1ml of ODCB was added to prepare the solution. Subsequently the solution was drop-casted on the appropriate substrate to make the blend film.

Similarly, in order to make the PCBM film 18 mg of PCBM powder was dissolved in 1ml of ODCB solvent inside a globe box in a nitrogen environment. The solution was then stirred overnight to make sure no PCBM was left over undissolved in the ODCB solvent. The PCBM dispersed in the polystyrene was prepared as follows: 100 mg of polystyrene and 10 mg of PCBM were dissolved in 10 ml of toluene in separate vials. Then the polystyrene solution was mixed with the PCBM solution in the ratio of 100:1 and stirred for one hour. Films were prepared by drop-casting the proper solution on CaF_2 and sapphire substrates for transient PA measurement in mid-IR and near-IR/visible regions.

3.4 Linear Absorption and Photoluminescence Spectra

Figure 3.3 shows the linear absorption in terms of optical density (O.D.) and photoluminescence (PL) spectra of RR-P3HT and RRa-P3HT film measured under

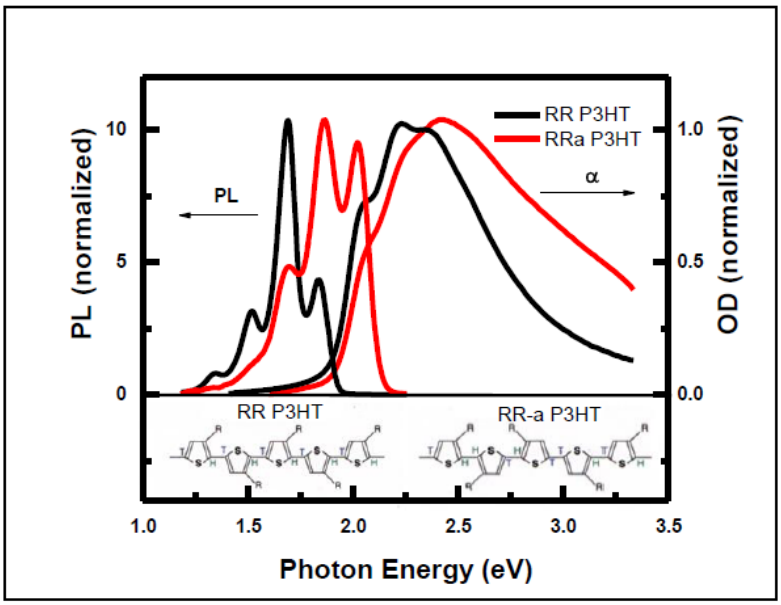

Figure 3.3: Absorption optical density (O.D.) and photoluminescence (PL) spectra of RR-P3HT and RRa-P3HT Films. The absorption was measured at 300 K, whereas the PL was obtained at 80 K.

similar conditions [these measurements were done by Dr. Golda Hukic-Markosian in our group]. The black and red color spectra belong to RR-P3HT and RRa-P3HT, respectively. The absorption band above the optical gap is due to π to π^* transitions' leading to the formation of singlet excitons [62 - 64]; the absorption below the gap is considered to be due to the impurities and/or native defects present in the sample. The normalized absorption spectra of high molecular weight RR-P3HT (50 kDa) and RRa-P3HT clearly show that RR-P3HT has stronger absorption in near-IR and visible regions, and red-shifted as compared to RRa-P3HT. The red shift in the absorption of RR-P3HT may be due to a better order in lamellae and a longer conjugation length [65]. Similarly, the PL spectrum of RR-P3HT is red-shifted with respect to RRa-P3HT, and the reason is the same as in absorption. In RR-P3HT absorption and PL spectra, the pronounced structures due to phonon replica are clearly noticeable and suggest more homogeneity of polymer chains in the film. [66].

The ratio of 0-0 to 0-1 vibronic side bands in PL spectrum of RR-P3HT is smaller than in RRa-P3HT, and implies that the degree of aggregation is higher in RR-P3HT as compared to RRa-P3HT, as reported previously by other groups [67, 68]. The strength of PL intensity is higher in RRa-P3HT than in RR-P3HT. This is consistent with the PL quantum efficiency (PLQE) 13 % for RRa-P3HT and 4 % for RR P3HT, respectively, that we measured using an integrated sphere.

3.5 Ultrafast Photophysics Studies

3.5.1 Ultrafast Photophysics of RR-P3HT Film

RR-P3HT is assumed to be one of the best materials to blend with PCBM and used as active layer for organic photovoltaic application [57]. Here, we have used low molecular weight (~15 kDa) and high molecular weight (~50 kDa) RR-P3HT supplied from Plextronics, and the other two RR-P3HT materials of different molecular weights from ADS and Rieke companies. The various films were prepared separately in the same environment, and ultrafast photophysics measurement was performed to identify which material is the best to use as the active layer in an OPV solar cell.

The transient spectra of all brands of RR-P3HT at t = 0 ps are shown in Figure 3.4 (a). The excitonic band PA_1 of high molecular weight (HMW) and ADS RR-P3HT films are observed at same probe energy 1 eV. In contrast, the PA_1 band of low molecular weight (LMW) and Rieke RR-P3HT films are red- and blue- shifted, respectively, as compared to HMW and ADS RR-P3HT. In addition to the PA_1 band, another band PA* is clearly observed in ADS and Rieke RR-P3HT. This band is more pronounced in LMW RR-P3HT than HMW RR-P3HT. The PA* band is more red-shifted (~ 0.55 eV) in ADS RR-P3HT as compared to other companies' RR-P3HT. The PA* band is more pronounced for those RR-P3HT materials that have less aggregation. Therefore, it is noticeable that the HMW RR-P3HT material has more aggregation than other RR-P3HT

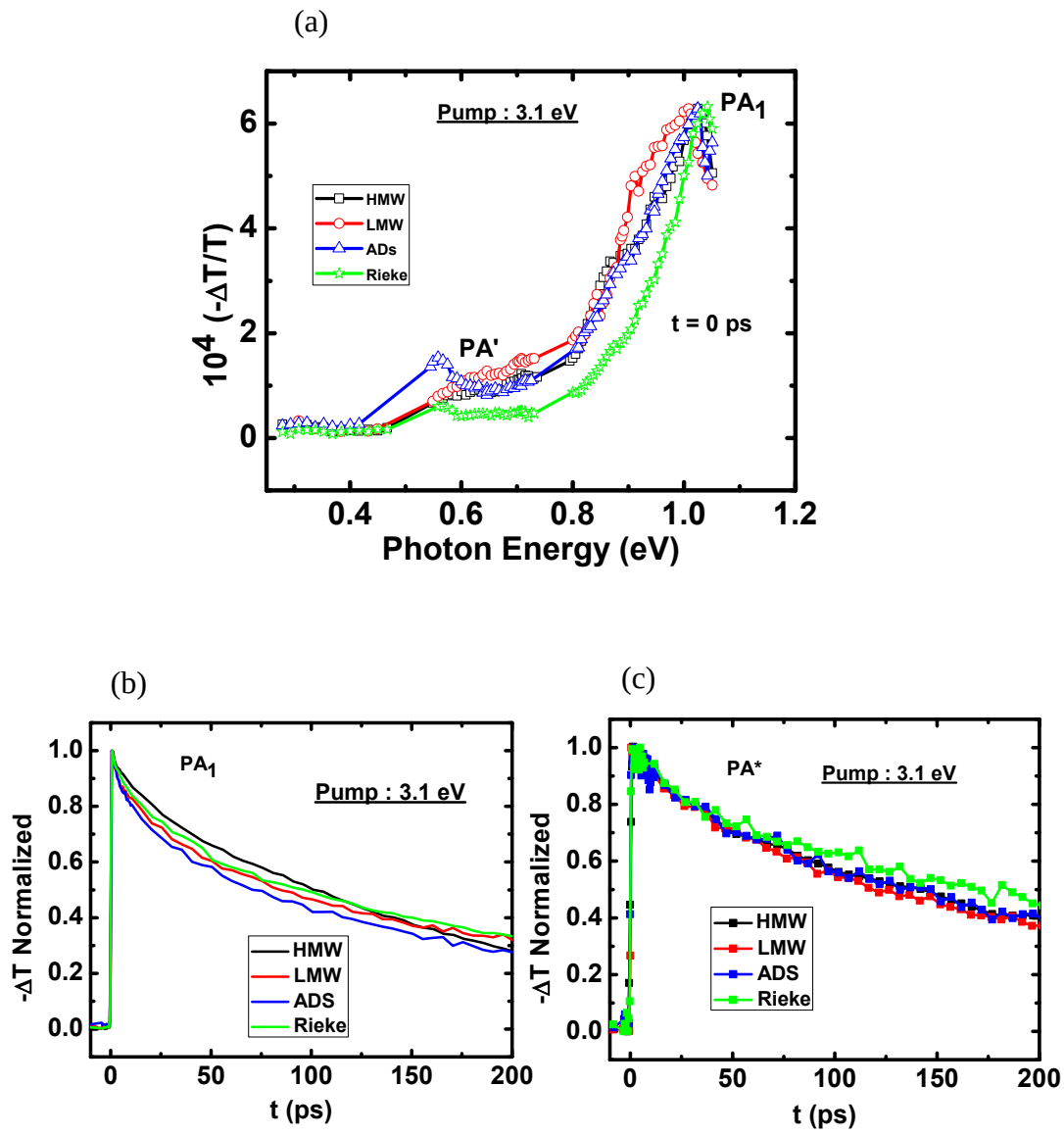

Figure 3.4 : Ps transient of pristine RR-P3HT Film. (a) Transient PM spectra of low molecular weight, high molecular weight, ADS and Rieke at t = 0 ps. The bands PA_1 and PA* are assigned. (b) Transient decay kinetics of PA_1; and (c) transient decay kinetics of PA*.

materials and should be the best material for using the active layer in organic photovoltaic cell application.

We also studied the transient decay kinetics of PA_1 and PA* bands in all types of RR-P3HT films. Figures 3.4 (b) and (c) show the dynamics of the two bands PA_1 and PA* assigned in different colors for different films. Here we see that PA_1 in HMW film decays slower (~ 70 ps) than PA_1 in the others (~ 60 ps); however, PA* decay is almost the same (~ 125 ps) in all films. When we compare the decays of these two bands it is clear that PA_1 decays faster than PA* indicating that two different types of species are generated in these two spectral regions. The band PA_1 is the excitonic band, whereas PA* may be due to trapped excitons. The pronounced band PA* is not good for device application, because the trapped exciton does not easily dissociate into charge carriers. Therefore, we only continued to study in detail the transient PM spectra of HMW RR-P3HT films and blend with PCBM.

Figure 3.5 (a) shows the transient PM spectra of high molecular weight (50 kDa) pristine RR-P3HT film at t = 0 ps, and 100 ps measured using low intensity and high intensity ultrafast laser systems upon excitation at 3.1 eV, above the polymer band gap. The spectra measured using two different laser systems are normalized properly to extend the spectrum in an unprecedented broad spectral range from 0.25 to 2.5 eV. The spectrum at t = 0 ps is dominated by a single PA_1 band at 1 eV followed by photo-bleaching above 1.97 eV and a small stimulated emission band at 1.75 eV, which attests to the excellent quality of the RR-P3HT polymer used here [69]. These three spectral features originate from photogenerated excitons since they decay together [Figure 3.5 (b)], having an exponential time constant, τ_0 = 70 ps. The band PA_1 was previously assigned to optical transitions related to the photogenerated singlet excitons [70], and the other band at 0.34 eV was reported as P_1 due to the lower energy polaron optical transition [66, 69]. The splitting of PA_1 was also reported previously without the clear explanation [69, 71]. In contrast, we do not observe the polaron band (~ 0.3 eV) or the splitting of PA_1 (~ 1 eV) in the transient PM spectrum of RR-P3HT film at t = 0 ps.

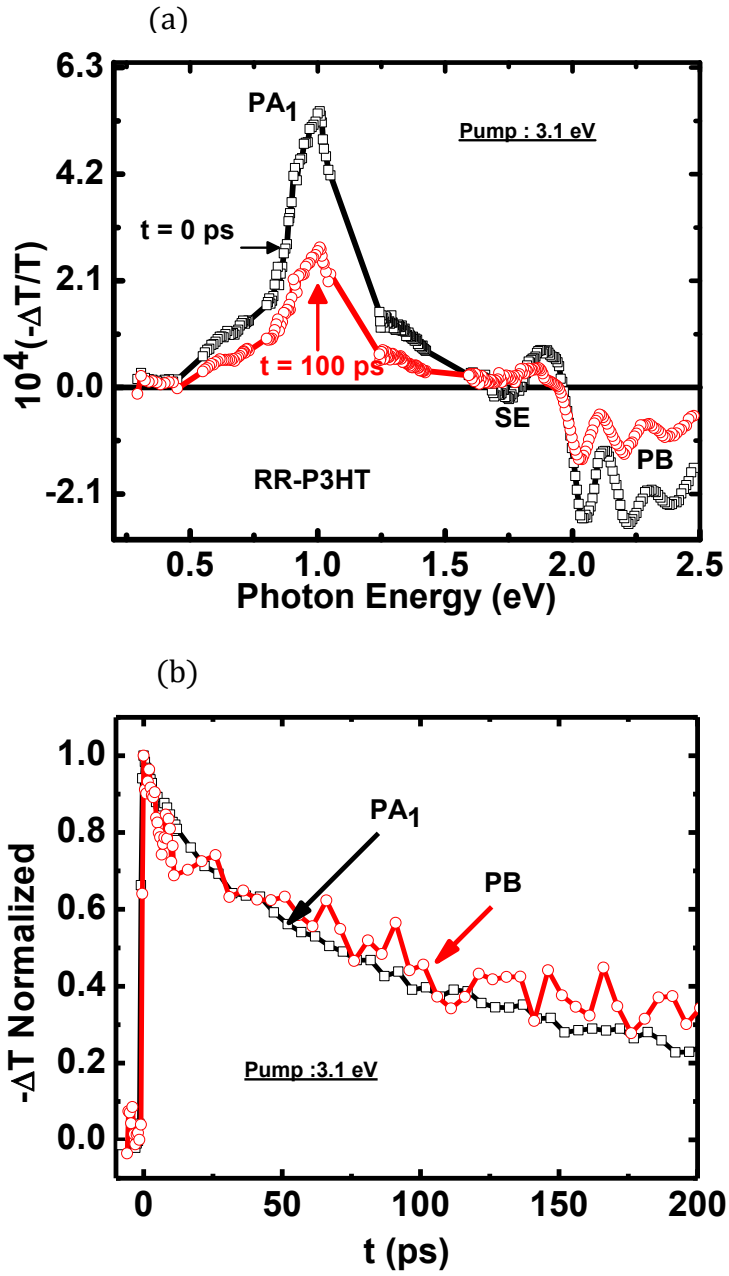

Figure 3.5: Ps transient of pristine RR-P3HT Film, (a) Transient PM spectra at t = 0 ps and 100 ps. The bands PA_1, PB and SE are assigned. (b) Decay kinetics of PA_1 and PB bands.

Again this is due to the superior polymer used in our studies. The PM spectrum at t = 100 ps shows that PA_1 and PB bands decay similarly with time. In contrast, the SE band changes into PA after ~100 ps.

3.5.2 Ultrafast Photophysics of Pristine PCBM Film

Before going to the transient PM measurement of RR-P3HT/PCBM blend, we performed transient PM measurement of a pristine PCBM film. The transient PM spectrum of pristine PCBM film from 0.55 to 2.5 eV measured at t = 0 ps, upon pump excitation at 3.1 eV is shown in Figure 3.6(a). Importantly the PA signal in PCBM is more than one order of magnitude smaller compared to the PA signal in the pristine RR-P3HT film [Figure 3.4(a)]. The spectrum is dominated by two PA bands, EX_1, and EX_2 at 1 and 2.25 eV, respectively, that are due to photogenerated excitons, and a third band, CT at 1.75 eV, that originates from charge-transfer excitons in the fullerene film, since it does not exist in the photomodulation spectrum of isolated PCBM molecules in polystyrene [Figure 3.6 (b)]. No photogenerated polarons that peak at 1.15 eV are discerned [72, 73].

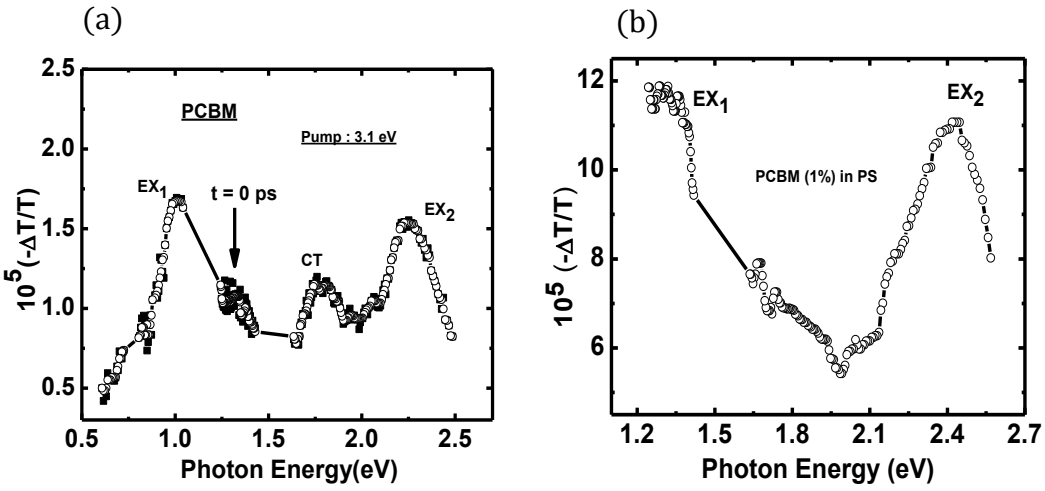

Figure 3.6: Transient PM spectra at t = 0 ps of (a) pristine PCBM film, and (b) PCBM (1%) dispersed in polystyrene matrix.

3.5.3 Ultrafast Photophysics of RR-P3HT/PCBM Blend

The transient PM spectra of the RR-P3HT/PCBM blend (1.2:1) measured at t = 0 and t = 300 ps, and the background (BG) spectrum measured at t = -5 ps are shown in Figure 3.7 (a). The sample was thermally annealed at 150^0C for 30 minutes, as the annealing plays a role in achieving superior efficiency in the solar cell while using this combination as the active layer [74]. The transient PM spectrum of the blend at t = 0 is very similar to that in pristine RR-P3HT film at t = 0 [Figure 3.5 (a)], which indicates that excitons are initially photogenerated in the polymer domains with not much interference from the PCBM matrix in the film. As in the pristine film, the blend PM spectrum at t = 0 ps contains a singlet exciton band at ~ 1 eV and photobleaching band above 1.97 eV, but no SE band is observed. At t > 0 the photogenerated excitons decay; however, no polarons are generated at the expense of the exciton decay up to 300 ps, since there is no PA build-up at low probe energy range, where the polaron P_1 band dominates the absorption spectrum [Figure 3.7 (a), inset]. We thus conclude that the exciton in the polymer domains decay into a new state that is not due to separated polarons. This new state must be related to the Donor (D)-Acceptor (A) interfaces in the film, and we propose that it is a CT exciton at the D-A interface. In contrast, the BG spectrum in the mid-IR [Figure 3.7 (a)] is very similar to the P_1 band in the polaron doping-induced absorption spectrum [Figure 3.7 (a), inset], showing that charge polarons are indeed photogenerated in RR-P3HT/PCBM, in agreement with the solar cell high efficiency based on this blend [69]. We thus conclude that the charge photogeneration process in the blend proceeds in two stages [75]. The first stage is exciton trapping in CT states at the D-A interfaces, followed by the much slower exciton dissociation into free polarons in the D and A domains.

The decay dynamics in the blend [PA_1 decay in Figure 3.7 (b)] is much faster than in the pristine [PA_1 in Figure 3.5 (b)]. The shorter life-time in the blend is related to the exciton dynamics towards the D-A interfaces, and we studied the PA_1 decay kinetics in

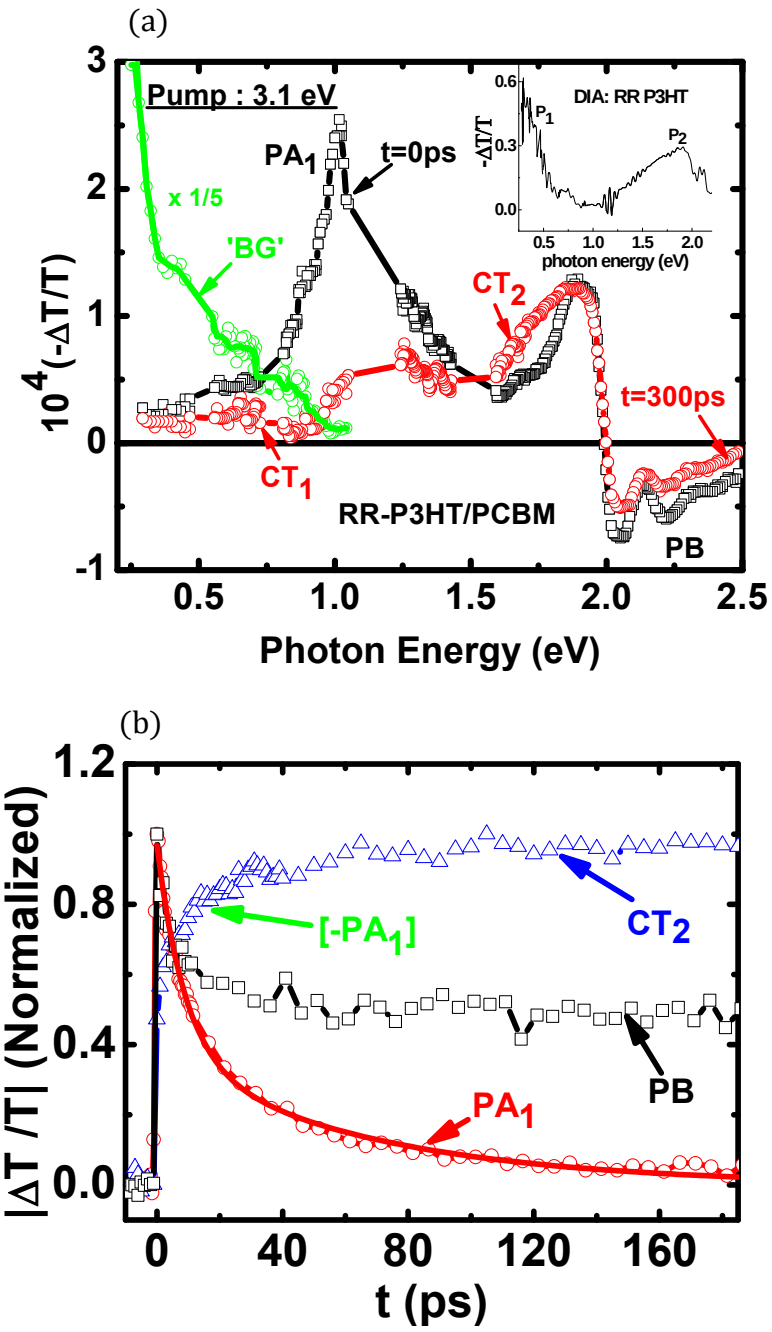

Figure 3.7: Transient PM Measurement of RR-P3HT/PCBM blend. (a) The transient PM spectrum at t = 0 and t = 300 ps, respectively. The green circles and the line represent the background (BG) PA spectrum measured at t = -5 ps. (b) The transient decay of PA_1, buildup dynamics of CT_2, and decay dynamics of PB.

more detail because of this phenomenon. PA_1 decay cannot be fit with a single, or a few exponential decay functions, nor can it be fit using the diffusion model [$\sim (1+t/\tau)^{-1}$]. Alternatively, PA_1 decay can be fit using multiple power-law decays that originate from a F*ö*rster resonant energy transfer (FRET) into the CT exciton [76], averaged over the exciton initial distance from the D-A interface (see in Appendix A). This model yields the following time-dependent surviving exciton density, N(t) in the polymer domains:

$$N(t)/N(0) = \exp(-t/\tau_0)[m_1 + m_2(C_1 t^{1/2} - C_2 t^{1/3} + C_3 t^{1/6})],$$

where τ_0 = 70 ps is the natural exciton life-time in RR-P3HT; m_1 and m_2 are fitting parameters; and the constants are $C_1 = 0.2u^{-3}$, $C_2 = 0.66u^{-2}$, and $C_3 = 0.54/u$, where $u = D/2R_0$ is the ratio of the grain size, D to twice the FRET radius, R_0, measured before to be between 3 and 9 nm [77]. Using R_0 = 6 nm and D = 16 nm, we obtain u = 1.3. The excellent fit to the PA_1 decay seen in Figure 3.7 (b) was obtained using $m_1 = 0.14$ and $m_2 = 7$.

In support of the CT intermediate role in the charge photogeneration process in the blend, Figure 3.7 (a) also shows that PA build-up indeed occurs in both the mid-IR and near-IR [78] spectral ranges. In fact there are two PA bands, namely CT_1 and CT_2 that are generated at a longer time at the expense of the exciton PA_1 decay. Figure 3.7 (b) shows that the CT_2 build-up dynamics in the near-IR closely matches the exciton PA_1 decay, since the same function of time fits both PA_1 decay and CT_2 build-up dynamics (measured at 1.75 eV probe).

In order to obtain the CT spectrum more clearly at the above gap excitation, we subtracted the photomodulation spectrum at t = 30 ps from that at t = 0 ps, after normalizing the two PA bands at 1 eV and 2 eV for the CT_1 and CT_2 bands, respectively [Figure 3.8 (a)]. The CT spectrum clearly shows two prominent PA bands that peak at 0.6 eV (CT_1) and 1.75 eV (CT_2), respectively, which are very different than the bands P_1 and P_2 of polarons [Figure 3.7 (a), inset].

Consequently, we propose that these two PA bands are the results of optical transitions within the CT manifold at the D-A interfaces [79]. To support this assumption, we also measured the transient photomodulation spectrum of the RR-P3HT/PCBM blend using the excitation energy 1.55 eV that is below the band gap of the both polymer and fullerene constituents. Such low excitation pump energy can resonantly excite the CT state at the D-A interface, since its energy was measured to be between 1.2 to 1.6 eV [69], without first generating excitons in the polymer domain. The PM spectrum measured at t = 0 along with the BG spectrum upon excitation at 1.55 eV is shown in Figure 3.8 (b), which clearly shows instantaneously photogenerated two CT bands CT_1 and CT_2. The charge transfer exciton bands observed using the below gap excitation pump energy (1.55 eV) are similar to that obtained after the manipulation of the t = 30 ps spectrum using the above gap excitation pump energy 3.1 eV. Therefore, the manifestation of similar CT_1 and CT_2 bands in below gap excitation is compelling evidence that they originate from CT states at the interface. This supports our assignment of the CT bands in the transient PM spectrum of this blend.

Interestingly, the background PA spectrum excited below-gap pump excitation [Figure 3.8 (b)] is very similar to that generated using above-gap pump excitation [Figure 3.7 (a)], which we identified as due to long-lived charge polarons. This shows that there exists a mechanism where thermalized CT excitons at the D-A interfaces are able to separate into free polarons in the donor and acceptor domains, regardless of the initial pump excitation energy. This finding is very important, since it can refute the notion that the CT state in the blend lies too deep in the gap to have any influence over the charge photogeneration process. Apparently, the exciton kinetic energy when reaching the CT state plays a minor role in the charge photogeneration process; this explains the flat spectral response of the photocurrent action spectrum in organic solar cell [69].

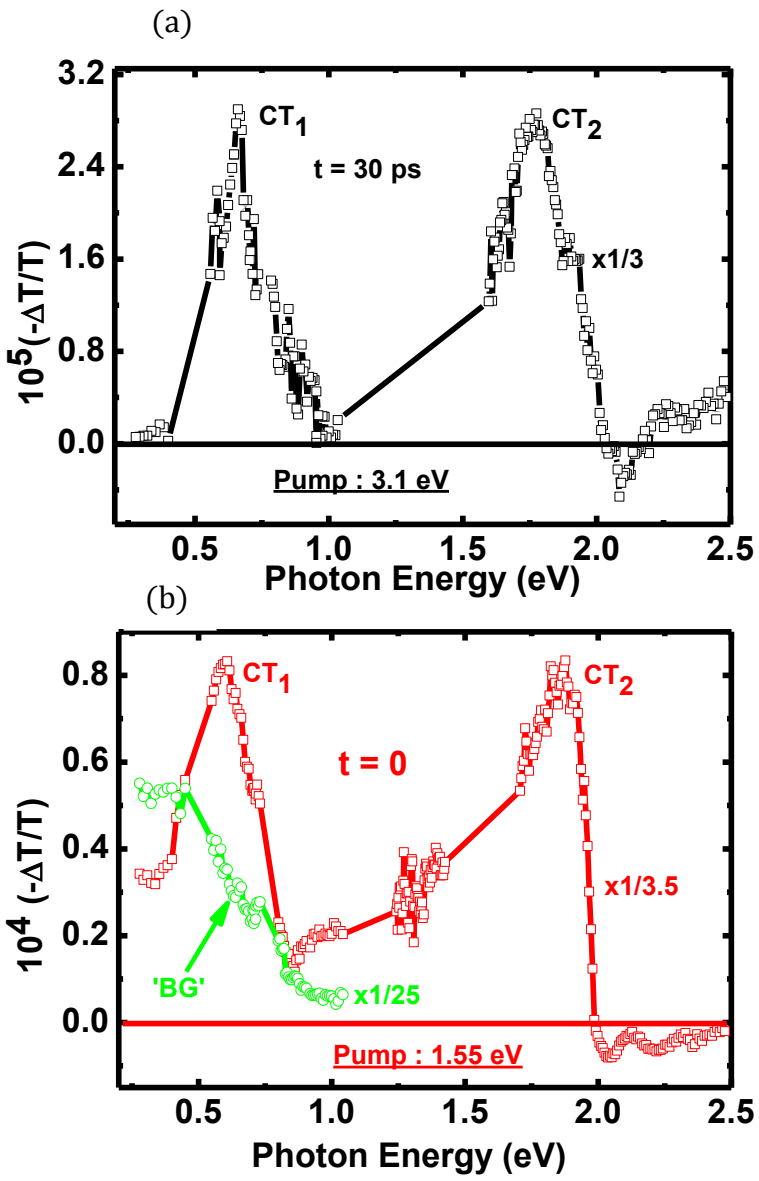

Figure 3.8: Transient PM Measurement of RR-P3HT/PCBM blend. (a) The transient PM spectrum at t = 30 ps excited at 3.1 eV, normalized and subtracted from the PM spectrum at t = 0 ps. (b) Same as in (a) but at t = 0 ps, and excited at 1.55 eV below the optical gap of polymer and fullerene.

3.5.4 Ultrafast Photophysics of Pristine RRa-P3HT Film

The difference in attachment of hexyl side groups with thiophene rings (head to head, tail to tail, or; no specific order) of RRa-P3HT as compared to head to tail or tail to head attachment of RR-P3HT led us to determine how the side group attachment affects the ultrafast photophysics of these polymers. Therefore we prepared films of RRa-P3HT the same way as the RR-P3HT film using same weight and solvent, and then the transient ultrafast PM measurement was performed. Figure 3.9 (a) shows the PM spectra at t = 0 and t = 200 ps in a broad spectral range from 0.25 to 2.2 eV, using low-intensity and high-intensity ultrafast laser systems. In both systems the RRa-P3HT film was excited by the 3.1 eV pump, above the optical band gap of the polymer. The spectrum at t = 0 shows mainly two bands: one in the mid-IR region $PA_{1,}$ which is due to the formation of singlet exciton, and the other SE band in the range from 1.75 to 2.1 eV in near-IR/visible region. The spectral decay shows that even after 200 ps, PA_1 and SE are not completely gone.

To understand how the two bands PA_1 and SE decay over time, we also studied transient decay kinetics up to 200 ps. It is clearly observed that both bands share the same dynamics, which decay at the same rate and fit well with the double exponential function with τ_1 = 7 ps, τ_2 = 78 ps. From this result we can conclude that SE and PA_1 are related to the same kind of photogenerated species. Previous research proposed that PA_1 arises from the formation of singlet exciton [70]. Therefore, SE also corresponds to singlet excitons because it is also sharing the same decay dynamics of PA_1 band.

3.5.5 Ultrafast Photophysics of RRa-P3HT/PCBM Blend

The ultrafast PM spectra of the RRa-P3HT/PCBM blend (1.2:1) at t = 0 and t = 10 ps at 3.1 eV pump excitation, above the band gap of the polymer and fullerene, is shown in Figure 3.10 (a). The PM spectrum is comprised of two clear charge transfer exciton bands CT_1 and CT_2 at 0.7 eV and 1.65 eV, respectively, similar as in RR-P3HT/PCBM

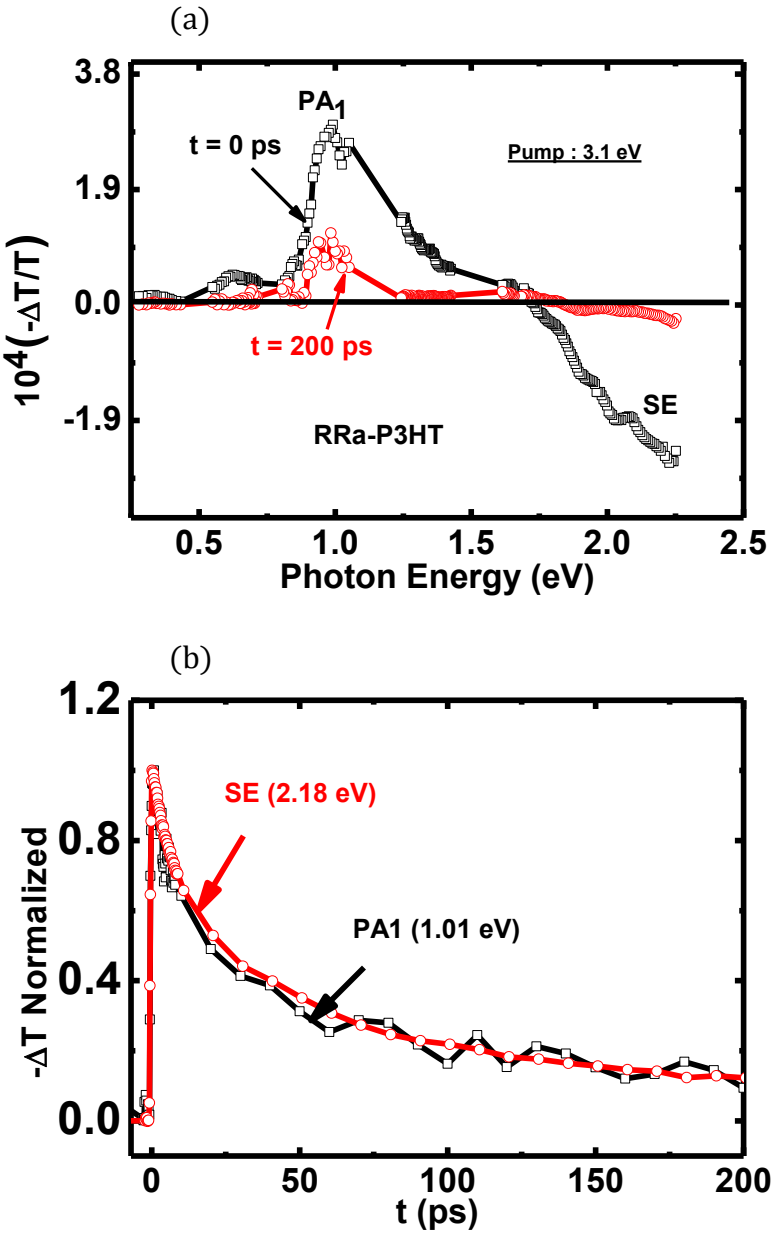

Figure 3.9: Transient PM in pristine RRa-P3HT film: (a) The transient PM spectra at t = 0 and t = 200 ps. PA_1 and SE bands are assigned. (b) Transient decay kinetics of PA_1 and SE bands.

discussed above. In addition to these bands a weak band is also observed at ~ 0.95 eV, which is due to singlet excitons that decay very fast into CT excitons. When we compare the t = 0 spectrum of RRa-P3HT/PCBM [Figure 3.10 (a)] with the spectrum of RRa-P3HT Film [Figure 3.9 (a)], we see that they are completely different, whereas the spectra were very similar in the case of RR-P3HT films [Figure 3.5 (a)] and RR-P3HT/PCBM blend [Figure 3.7 (a)]. This result tells us that RRa-P3HT behaves completely differently than RR-P3HT when mixed with PCBM. From transmission microscopy (TEM) images of the RR-P3HT/PCBM annealed film and RRa-P3HT/PCBM film, it has been shown that there is no phase separation of polymer and PCBM in RRa-P3HT/PCBM blend, whereas nanodomains (~ 20 nm in size) of the PCBM network are observed in the RR-P3HT/PCBM blend [80]. Thus, we propose that the generated exciton reaches at the D-A interface of RRa-P3HT/PCBM within a few tens of femtosecond, and subsequently get trapped forming CT excitons. There is less chance of charge separation after CT formation due to the lack of phase separation between RRa-P3HT and PCBM domains. Therefore the PM spectrum later times remain the same at t = 1 ps.

We also measured the background PA spectrum [Figure 3.10 (a), green color] at t = -5 ps in the mid-IR spectral region, and found that it looks very similar to the PA spectrum measured at t = 0 ps. In contrast, this was not the case in the RR-P3HT film and the RR-P3HT/PCBM blend.

Figure 3.10 (b) shows the decay kinetics of three PA bands PA_1, CT_1, and CT_2. PA_1 decays fast, within 0.5 ps, at the same time as CT_1 and CT_2 buildup. These two bands, CT_1 and CT_2 cannot be singlet excitons because these bands are created at the expense of singlet excitons. Therefore, we assume that these bands are charge transfer excitons, similar as in the case of RR-P3HT/PCBM blend discussed above. The charge transfer excitons formed at the D-A interfaces are long-lived and have very little possibility of separation into free charges due to the lack of phase separation between RRa-P3HT and PCBM domains.

(a)

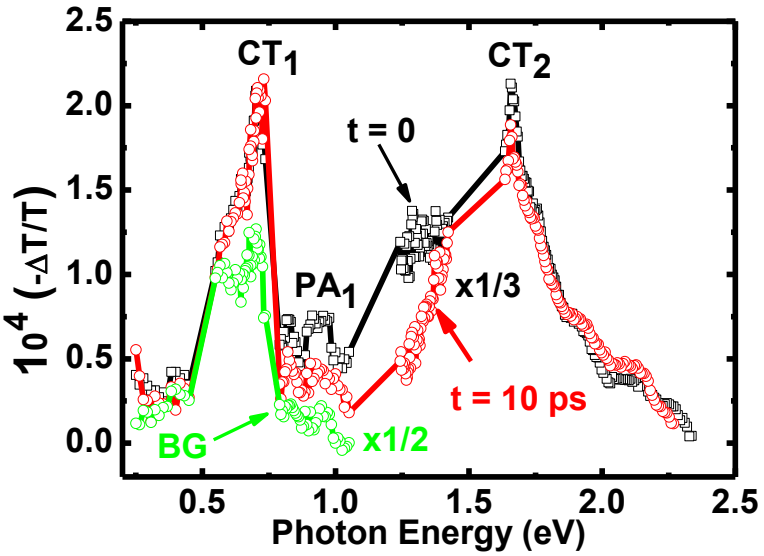

(b)

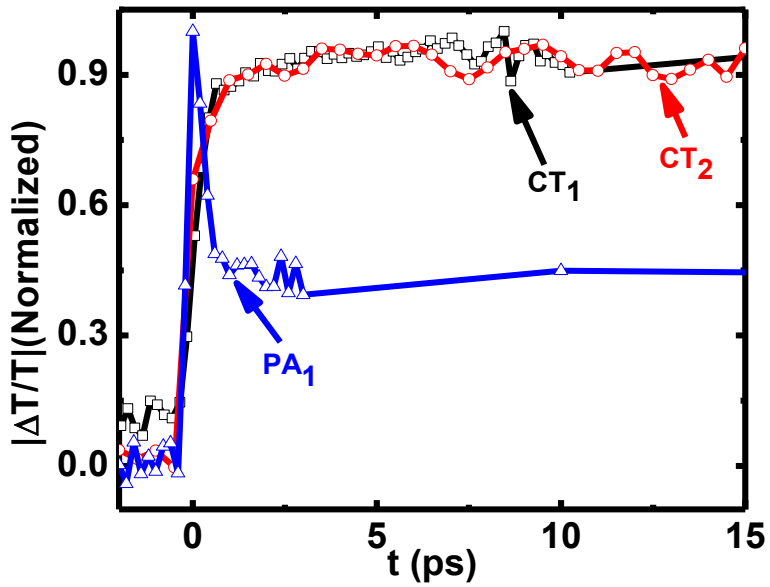

Figure 3.10: Transient PM in RRa-P3HT/PCBM blend. (a) The transient PM spectra at t = 0 and t = 10 ps. PA_1, CT_1 and CT_2 bands are assigned. (b) Transient dynamics of PA_1, CT_1 and CT_2.

This might be the reason for getting low power conversion efficiency in RRa-P3HT/PCBM solar cell device (0.1 %) as compared to RR-P3HT/PCBM device (4 %).

3.5.6 Ultrafast Photophysics of RR-P3HT/PCBM Blend in OPV Devices

The organic solar cell device structure composed of *Glass/ITO/PEDOT/RR-P3HT+PCBM (1.2:1)/Al* having an internal built-in electric field is created from the difference in work functions of the electrodes. In order to understand the role of the built-in electric field of the device on the ultrafast photophysics of an active layer RR-P3HT/PCBM in the device structure, we studied the ultrafast PM spectra of RR-P3HT/PCBM blend in mid-IR spectral range from 0.55 to 1.05 eV using the low intensity ultrafast laser system. The PM spectrum could not be extended below 0.55 eV due to a very low transmission signal from the ITO-coated glass substrate.

Figure 3.11 (a) shows the transient PM spectra at t = 0, 5 ps, 50 ps, and 200 ps, respectively. The PM spectrum at t = 0 looks very similar to the RR-P3HT/PCBM blend spectrum at t = 0 ps [Figure 3.7 (a)] with a single dominant band PA_1. The singlet exciton band PA_1 is red-shifted in the device blend PM spectrum, as compared to the blend film discussed above. The spectral decay shows the existence of a PA_1 band even after 200 ps without any build-up in the spectrum, as we observed in the case of the blend. The decay kinetics [Figure 3. 11 (b)] are also similar to those in the blend.

We conclude that the exciton energy transfer from the RR-P3HT phase to the D-A interfaces is common, and it also happens in the device structure. Therefore, the charge generation and separation in RR-P3HT/PCBM blend is directly related to the same phenomenon that happens in the real solar cell device structure. Thus, the study of photophysics in a D-A blend film without the device structure is justified.

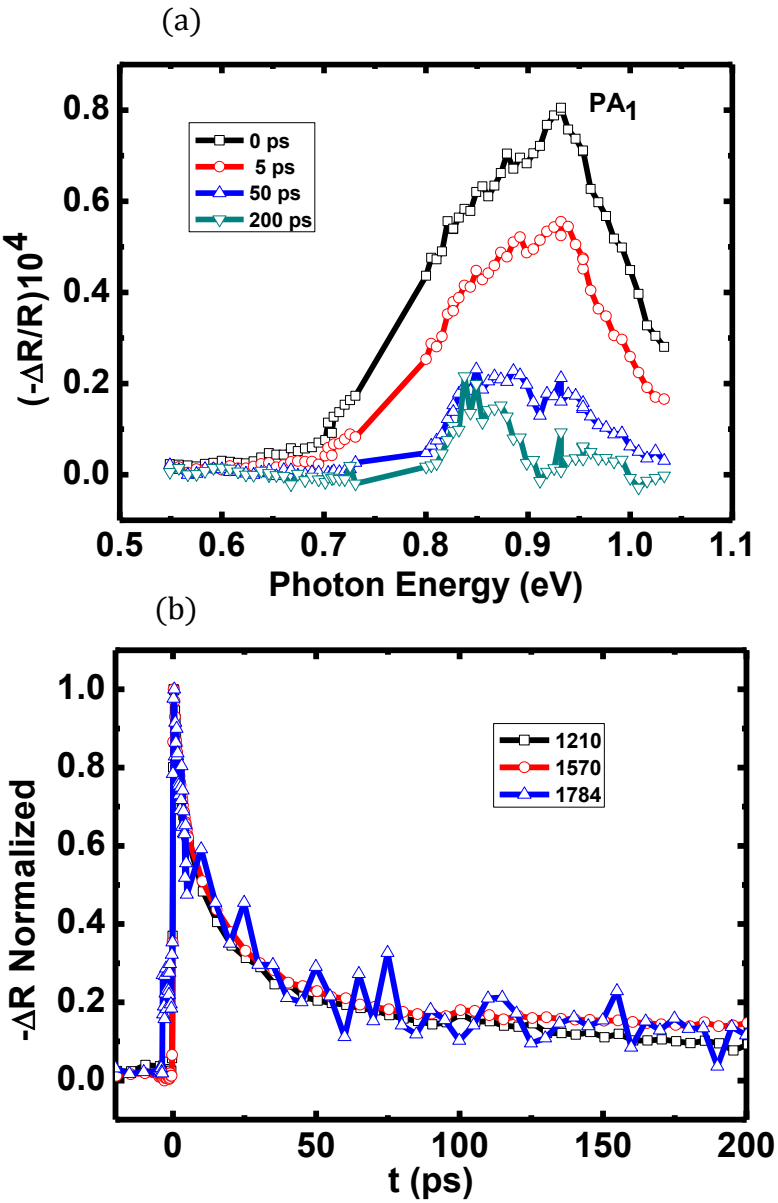

Figure 3.11: Photophysics of the RR-P3HT/PCBM device. The band PA_1 is assigned. (a) Transient PM spectra at t = 0, 5, 50, and 200 ps. (b) Transient decay kinetics at various probe energies.

3.6 Intensity Dependent Measurements of the Transient PM in RR-P3HT and RR-P3HT/PCBM Blend

In order to study whether we have exciton-exciton annihilation in our spectral range of interest, we performed the intensity dependent measurement of photoinduced absorption (PA) band at 1eV in RR-P3HT film and RR-P3HT/PCBM blend. Figures 3.12 (a), and (b) show the variation of the PA signal at 1 eV with the pump excitation laser intensity in RR-P3HT film and RR-P3HT/PCBM blend, respectively. In Figures 3.12 (a) and (b), we clearly see that PA varies linearly with the intensity in both RR-P3HT film and RR-P3HT/PCBM blend and it does not saturate in the intensity range of our measurement. The linear dependence of the prompt PA signal on the pump intensity proves that a single species is generated in the polymer film following pump excitation. These photoexcitations were identified as singlet, intrachain $1B_u$ exciton [81].

For the same excitation intensity range, we also measured the ultrafast PA dynamics in both polymer film and its blend with PCBM. Figures 3.12 (c) and (d) show the decay dynamics of PA band at 1 eV in RR- P3HT film and RR-P3HT/PCBM blend, respectively. In RR-P3HT film, the decay fits well with a single exponential for all excitation intensity with time constant ~ 75 ps and does not show any dependence on pump intensity. The decay dynamics curves are shown without normalization. If we multiply the transient PA decay curves measured at low intensity by the pump intensity ratio, we can easily reproduce the PA measured at a higher intensity. Similarly, the transient decay curves measured in RR-P3HT/PCBM blend at different pump intensity do not show the intensity dependence as in RR-P3HT film. In contrast, the decay curve does not fit with the single exponential but fits well with the double exponential showing fast and slow decay components. The fast and slow components ~ 5 ps and ~ 60 ps also do not show the dependence on pump intensity. If we again multiply the decay curve measured at low intensity by intensity ratio, the higher intensity decay curve is reproducible. Thus, the photogenerated species is a single species that should be singlet

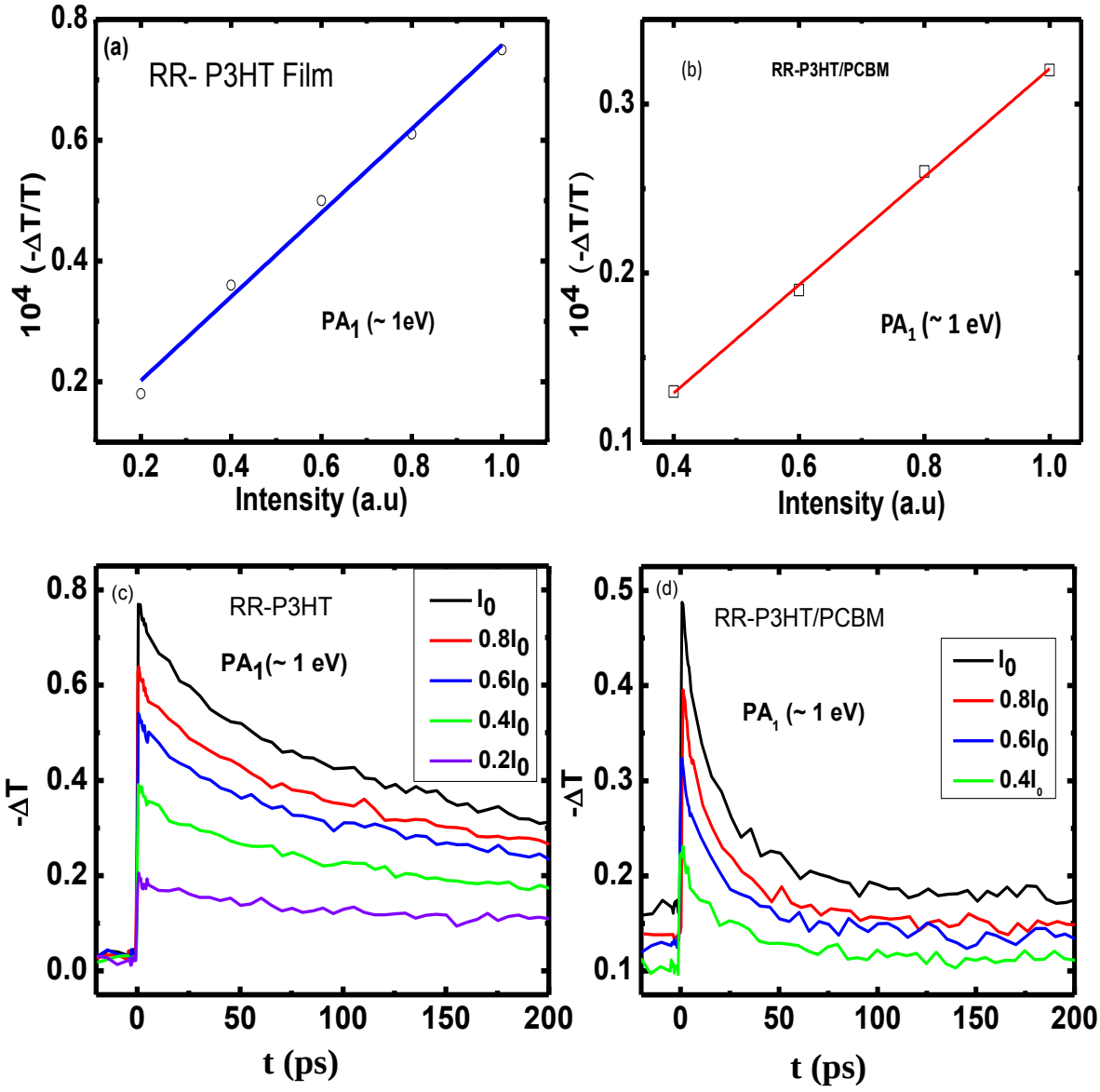

Figure 3.12: PA signal at ~ 1 eV at t = 0 vs. the pump excitation intensity. (a) RR-P3HT (b) RR-P3HT/PCBM. Pump excitation dependent dynamics of PA_1 at 1 eV at various excitation intensity; (c) RR-P3HT, and (d) RR-P3HT/PCBM.

exciton. We do not see the possibilities of exciton-exciton annihilation in RR-P3HT film and RR-P3HT/PCBM blend. However, the singlet exciton decays faster in the blend than film due to the proximity of the acceptor molecule PCBM, as discussed above.

3.7 Study of X-ray Diffraction Pattern of RR- and RRa-P3HT/PCBM Blends

To better understand the transient PA spectra in the polymer/fullerene blends, we measured the x-ray diffraction (XRD) pattern from the RR-P3HT/PCBM and RRa-P3HT/PCBM blend films, using the CuKα X-ray line at λ = 0.154 nm. Figures 3.13 (a) and (b) show the XRD pattern of RR-P3HT/PCBM blend film and RRa-P3HT/PCBM blend film, respectively. The XRD pattern of RR-P3HT/PCBM contains a prominent Bragg band at $2\theta = 5.3^0$, and its harmonics at $2\theta = 10.7^0$ and 16^0, respectively, from the RR-P3HT nanocrystalline domains [82]. The diffraction angle $2\theta = 5.3^0$ corresponds to the diffraction of the crystallographic (100) plane of RR-P3HT, suggesting that the preferred orientation of the crystalline RR-P3HT is parallel to the substrate. In addition to these diffraction bands, we also observe a smaller Bragg band at $2\theta = 19.3^0$ from the PCBM nanocrystalline domains, corresponding to the (311) crystallographic plane [83]. We therefore conclude that the annealed RR-P3HT/PCBM blend film contains separate donor and acceptor crystalline domains. We estimated the average nanocrystalline domain size, D from the full width at half maximum, $\Delta_{2\theta}$ of the respective Bragg bands using the Scherrer relation: $D = 0.9\lambda/\Delta_{2\theta}.\cos\theta$; and obtained D ≈ 16 nm (20 nm) for the RR-P3HT (PCBM) nanodomains.

In contrast, the XRD pattern of the RRa-P3HT/PCBM blend does not show prominent RRa-P3HT band harmonics, and the Bragg band of the PCBM is missing [Figure 3.13 (b)]. This result shows that in the RRa-P3HT/PCBM blend, PCBM

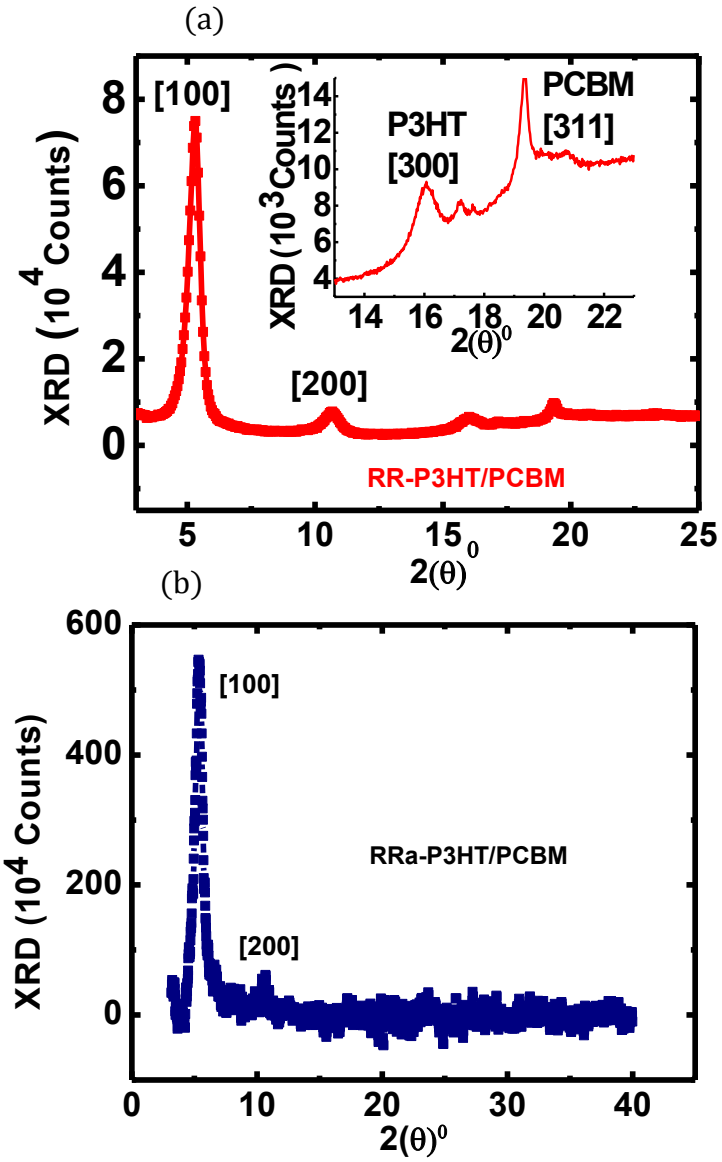

Figure 3.13: XRD pattern of (a) RR-P3HT/PCBM blend and (b) RRa-P3HT/PCBM blend. The inset in (a) focuses on the XRD bands of PCBM domains.

molecules do not form the well-separated domains that they do in the RR-P3HT/PCBM blend. In addition to forming separated nanodomains, PCBM molecules penetrate into the RRa-P3HT lamellae, and, consequently, lie closer on average to the polymer chains.

3.8 Study of I-V Characteristics in RR-P3HT/PCBM and RRa-P3HT/PCBM Solar Cell Devices

From the x-ray diffraction pattern measurement of RR-P3HT/PCBM and RRa-P3HT/PCBM we have seen that RR-P3HT and PCBM molecules form well-separated nanocrystalline domains; however, PCBM molecules do not form nanocrystalline domains in RRa-P3HT/PCBM blend. Similarly, ultrafast photophysics of these two blends are also different. We then make organic solar cell (OPV) devices using RR-P3HT/PCBM and RRa-P3HT/PCBM as the active layer in device configuration *Glass/ITO/PEDOT/RR-P3HT+PCBM (1.2:1)/Al* and estimated the power conversion efficiency (PCE) from the I-V characteristics curve observed under 1.5 AM illumination (these measurements were done by Mr. Tek Basel in our group). We also checked whether high molecular weight or low molecular weight RR-P3HT is better for the OPV device.

Figures 3.14 (a), (b), and (c) show the respective I-V characteristic curves of HMW RR-P3HT/PCBM, LMW RR-P3HT/PCBM, and RRa-P3HT/PCBM devices measured under 1.5 AM irradiation using Xe-light source. The obtained parameters are presented in the inset of each I-V curve. Although the I-V curves of HMW and LMW RR-P3HT/PCBM devices look similar, there is an increase in individual values of field factor (FF), short circuit current (Jsc), and open circuit voltage (Voc) in the HMW RR-P3HT/PCBM device, which increases the power conversion efficiency of this device by 25 % as compared to the LMW RR-P3HT/PCBM device.

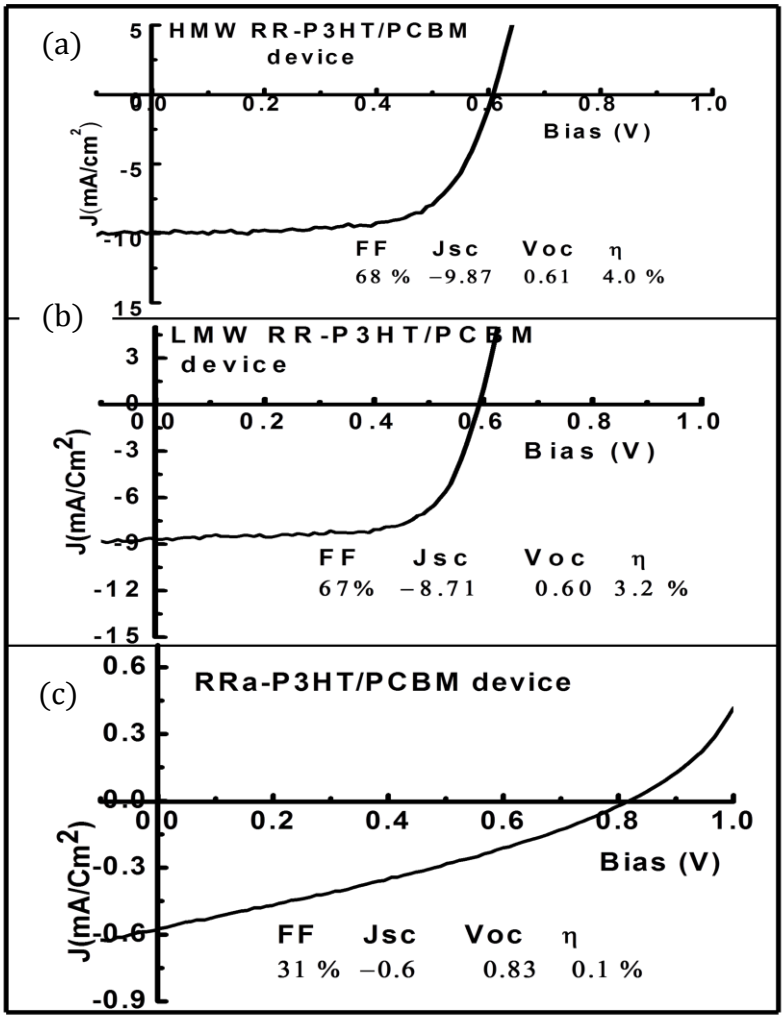

Figure 3.14: I - V characteristic curves of OPV cells under solar illumination conditions. (a) HMW RR-P3HT/PCBM device, (b) LMW RR-P3HT/PCBM device, and (c) RRa-P3HT/PCBM device.

The key variables of the polymer primary structure in P3HT are polydispersity, regioregularity, and molecular weight, [84], which affect the PCE of the OPV device. The effect of each variable on photovoltaic performance was pursued in refs. [57, 85 - 87]. A systematic study of the effect of polydispersity of P3HT has not been reported, although it does appear that a broad mix of high-and low-molecular weight P3HT in a given sample improved the performance of P3HT/PCBM composite solar cells [86]. The regioregularity is the same in HMW and LMW RR-P3HT. Thus the discussion is only focused on the difference in molecular weight. The correlation between molecular weight and P3HT conformation has been investigated in detail in the past. Brinkmann et al. [88] reported that the crystallinity decreases with increasing molecular weight, which was also reported by Schilinsky et al. [85] on a lower threshold for the molecular weight of P3HT to give sufficient device performance. Transport studies have suggested that HMW P3HT should also give the highest mobility [89], and this increases the device performance. Koppe et al. [90] studied the dependence of PCE of a P3HT/PCBM device on molecular weight of P3HT from 26 kDa to 153 kDa and showed that PCE is almost the same from ~ 43 kDa to ~77 kDa and decreases elsewhere. This result is inconsistent with what we observed with PCE on HMW (50 kDa) and LMW (15 kDa) RR-P3HT/PCBM devices. We thus conclude that HMW RR-P3HT polymer is better suited for OPV applications.

The next task is to compare the PCE of HMW RR-P3HT/PCBM device with the RRa-P3HT/PCBM device. In Figures 3.14 (a) and (c) it is clearly seen that FF, J_{SC} are greatly reduced here in (c), whereas V_{oc} increases in the RRa-P3HT/PCBM device as compared to the RR-P3HT device. The PCE of RRa-P3HT/PCBM device (0.1 %) is far less than that of the RR-P3HT/PCBM device (4%). As stated earlier in XRD pattern measurement, PCBM does not form separate nanodomains while mixed with RRa-P3HT to make blend film. The lack of crystallinity decreases the mobility and, finally, the PCE of the OPV device. This result was confirmed by Vakhshouri et al. [91] and tells us that the electron mobility of amorphous mixtures of RRa-P3HT/PCBM decreases

significantly below volume fraction of 0.58, where the components are miscible. *The strong dependence of charge transport on the miscibility of P3HT and PCBM suggests that partial miscibility may be critical for efficient OPV device performance.*

3.9 Discussion

The power conversion efficiency of organic photovoltaic (OPV) cell is still not high enough to compete with the inorganic solar cell due to a lack of understanding of photophysics in the active layer and other limitations in the process of device fabrication. If we could understand the processes of charge generation, recombination, and separation in the polymer/PCBM blend, this would ultimately help to improve the power conversion efficiency of OPV devices. Thus, the potential application of π – conjugated polymers in an OPV cell is the main motivation to study the photophysics of the pristine polymer films and their blends with the acceptor PCBM, specifically to understand the photogeneration and dissociation processes in these materials.

To achieve this goal, we first conducted photophysics measurements of pristine RR-P3HT and RRa- P3HT films, and subsequently moved to their blends with PCBM under similar excitation conditions. From linear absorption and PL measurements we found that RR-P3HT forms a better degree of lamellae in the film and reduces the trapping time of photogenerated species, which might help to improve the mobility of charge carriers in the OPV device based on this polymer blend. The transient PM spectra of RR-P3HT films [Figure 3.4 (a)] show that when the aggregation increases the lamellae order is better. The formation of lamellae is considered to be a good property for charge transport in the polymer matrix. Thus, we believe that HMW RR-P3HT should be better for OPV application.

To understand how RR-P3HT and RRa-P3HT behave with PCBM in the blend, we also studied the ultrafast PM spectra of both polymer blends with PCBM. We clearly observed that these two polymers act in completely different ways in blends [Figures 3.7

(a) and, (b) and 3.10 (a)] even though their PM spectra look very similar in the films [Figures 3.5 (a) and 3.9 (a)]. In the RR-P3HT/PCBM blend, we see the decay of singlet excitons but do not observe a build-up of polarons in the entire spectral range, even though the background PA spectrum below 0.55 eV shows that polaron photogeneration occurs in this blend. Instead, charge transfer excitons are formed on the expense of singlet excitons after a few picoseconds (~ 10 ps), and presumably dissociate very slowly (microsecond time scale) into free polarons. Due to the intermediate charge transfer exciton state, fewer free polarons are photogenerated. In contrast, the formation of the charge transfer exciton state from photogenerated excitons in RRa-P3HT/PCBM is very fast (within 500 fs), but this state is tightly bound in the RRa-P3HT/PCBM blend, and thus does not easily dissociate into free polarons.

To support these results, we also studied XRD of RR-P3HT/PCBM and RRa-P3HT/PCBM blends, and found that RR-P3HT and PCBM form separate nanodomains, but RRa-P3HT and PCBM are homogeneously mixed without phase separation. The lack of phase separation prevents the charge transfer ionization process into the D- and A-domains in the latter blend. This leads to small power conversion efficiency for OPV cell based on RRa-P3HT/PCBM blend.

To verify our claim, we also fabricated OPV devices of HMW, LMW RR-P3HT/PCBM, and RRa-P3HT/PCBM separately, and tested them under the same condition. As expected, we found that HMW RR-P3HT/PCBM has the highest PCE (4%), followed by 3.2 % and 0.1 % in LMW RR-P3HT/PCBM and RRa-P3HT/PCBM respective devices. Finally, we came to the conclusion that RR-P3HT with high molecular weight (~50 KDa) is the best donor material for OPV device application because of its ability to form better order of lamellae and phase separation between the polymer and PCBM domains as compared to RRa-P3HT.

3.10 Conclusion

The main goal of this chapter has been to identify the best polymer among HMW RR-P3HT, LMW RR-P3HT, and RRa-P3HT for organic photovoltaic (OPV) application. For this purpose we have used various experimental tools such as absorption, photoluminescence, transient ultrafast spectroscopy, doping-induced absorption, TEM and x-ray diffraction. In addition to these measurements, we also fabricated OPV devices using these polymers blend with PCBM acceptor active layers and obtained their power conversion efficiency and other electrical parameters. From the absorption and PL spectra, we found a clue that RR-P3HT forms lamellae and this is good for improving the mobility of charge carriers. Our important task was to find out which polymer is better for device application, HMW RR-P3HT or LMW RR-P3HT. From the ultrafast measurement we found that the aggregation is better in HMW than in LMW RR-P3HT and forms lamellae in the film.

In the transient PM spectra we found similar results in RR-P3HT and RRa-P3HT pristine films, in which the entire PM spectrum is dominated by the singlet exciton band, PA_1. So from these ad-hoc measurements it was not clear which polymer is better. However, when we mixed these polymers with the PCBM acceptor in the same weight ratio, the photophysics turns out to be completely different. The RR-P3HT/PCBM blend PM spectrum shows the formation of charge transfer exciton CT_1 and CT_2 at the D-A interface after ~ 20 ps, that later dissociates into free polarons leading to high BG in the mid-IR spectral region, whereas, this is not the case in the RRa-P3HT/PCBM blend. Instead in RRa-P3HT/PCBM the charge transfer excitons CT_1 and CT_2 form in less than 1ps that is trapped at the D-A interface for a long time without dissociation into free polarons, because the charges cannot hop to other polymer chains or fullerene molecules in the CT exciton vicinity since the nearest neighbors are not close enough. This is not the situation in the RR-P3HT/PCBM blend, since the charges in the CT excitons can more easily hop to neighboring molecules in the D- and A-respective domains.

To clearly understand the mixing properties of PCBM with RR-P3HT and RRa-P3HT polymers, we also studied the XRD pattern of RR-P3HT and RRa-P3HT/PCBM blends separately. From the XRD measurements we found that PCBM forms well-separated nanodomains while mixed with RR-P3HT, but it is homogeneously mixed with RRa-P3HT. The lack of a Bragg band for PCBM in RRa-P3HT/PCBM blend points to a small possibility of charge transfer exciton separation into polarons in the respective D- and A-domains.

A similar picture also occurs in the TEM images of RR-P3HT/PCBM and RRa-P3HT/PCBM blends [80]. There were well-separated nanodomains of PCBM in the RR-P3HT/PCBM blend but not in the RRa-P3HT/PCBM blend.

Finally, we fabricated OPV devices of RR-P3HT/PCBM (LMW and HMW), and RRa-P3HT/PCBM under similar conditions and I-V characteristics curves were measured using AM 1.5 sun-like illumination from a Xe-light source. Estimates from I-V characteristics show the highest PCE (4%) in the HMW RR-P3HT/PCBM device, followed by 3.2 % and 0.1 % in the LMW RR-P3HT/PCBM and RRa-P3HT/PCBM devices, respectively. Thus, we believe that HMW RR-P3HT is the best material among these polymers for device application because of its high degree of aggregation in the film that allow lamellae formation that increases the mobility of the charge carriers. Furthermore, PCBM forms separate nanodomains in the blend and this creates a possible mechanism of charge separation into RR-P3HT and PCBM nanodomains, respectively.

CHAPTER 4

PHOTOPHYSICS OF LOW BAND GAP POLYMER PTB7 PRISNTINE AND BLEND WITH $PC_{71}BM$

4.1 Introduction

The photophysics study of π – conjugated polymer pristine films and blends with the acceptor [6, 6]-phenyl-C_{61}-butyric acid methyl ester (PCBM) is common among researchers to better understand the charge generation and recombination and/or dissociation processes in the active layer of an organic photovoltaic (OPV) cell. However, to the best of our knowledge, the photophysics of polymer films and blends with various acceptor molecules is still not clearly understood. The lack of proper understanding of the photophysics in these blends is somehow hindering the material scientists from improving the power conversion efficiency of the OPV cell to compete with the inorganic solar cells. Although many OPV polymer materials have been studied, derivatives of polythiophene, such as poly (3-hexylthiophene) P3HT, are commonly used as the electron donor and PCBM as the electron acceptor. In spite of their intense absorption in the visible region, P3HT derivatives are still not energetically optimized for light harvesting from the solar spectrum, especially in the near IR region [92].

To maximize the light harvesting from the solar spectrum, much effort has been put into lowering the band gap of the photoconducting polymers by chemical modification, such as synthesizing copolymers with alternating electron rich and electron deficient units [93].

A series of low band gap polymers synthesized by Yongye Liang and Luping Yu at the University of Chicago are such examples [94-101]. Liang et al. [102] showed that after an extensive structural optimization of a new polymer from the poly-thienothiophene-benzodithiophene (PTB) family, PTB7 exhibited an excellent photovoltaic effect with power conversion efficiency (PCE) 7.4 % when blended with phenyl-C_{71}-butyric acid methyl ester ($PC_{71}BM$). The first polymer solar cell showing a PCE over 7 % [102] lured us to study the continuous wave (CW) as well as transient ultrafast photophysics of low band gap polymer PTB7 pristine film and blend with $PC_{71}BM$.

In this chapter, we first present the linear absorption in terms of optical density (O. D.) and photoluminescence (PL) and then show the CW and transient photoinduced absorption (PA) spectra of a PTB7 pristine film and blend with $PC_{71}BM$. In order to understand the charge generation and dissociation processes, we also study the transient decay kinetics of photogenerated species at various probe energies.

4.2 Materials

4.2.1 Poly-thienothiophene-benzodithiophene Seven (PTB7)

The copolymer used as a donor material studied in this chapter is PTB7, which was synthesized by Yongye Liang and Luping Yu at the University of Chicago. The chemical structure of this copolymer PTB7 is shown in Figure 2.1 (f). This low band gap polymer PTB7 has essentially the same sequence of alternating thieno [3,4-b] thiophene (TT) and benzo-dithiophene (BDT) monomer units attached with different side groups. Over 10 PTB polymers have been reported to date and differ by their aliphatic pendant side chains and the presence of fluorine on the TT unit [92]. The best PTB polymer reported with power conversion efficiency (PCE) 7.4 % [102] is PTB7. This copolymer was provided by the Chicago group in powder form, and the sample was prepared in an inert nitrogen (N_2) environment inside the globe box using the same technique as described detail in Chapter 3. 10 mg of PTB7 was dissolved in 1 ml of ODCB to prepare

the solution. Similarly, 10 mg of PTB7 and 15 mg of $PC_{71}BM$ in weight ratio (1:1.5) were dissolved in 1 ml of the same solvent ODCB and prepared solution. The solution was either drop-casted or spin-casted on CaF_2 or sapphire substrates to make the film for the measurements.

4.2.2 [6,6]Phenyl-C_{71}-butyric Acid Methyl Ester ($PC_{71}BM$)

Although [6,6]-phenyl-C_{61}-butyric acid methyl ester (PCBM) is considered the best acceptor material for most of the donor materials to make an active layer in organic photovoltaic (OPV) solar cell devices, this is not true for PTB7 donor copolymer. To the best of our understanding from the literature studied, so far, the acceptor material proved most efficient in combination with donor material PTB7 for OPV cell application is $PC_{71}BM$ [92]. The chemical structure of $PC_{71}BM$ is shown in Figure 2.1(h). The structure of $PC_{71}BM$ is very similar to that of $PC_{61}BM$; however, the absorption of the solar spectrum is higher in the former rather than the latter acceptor. As in PCBM, the side group attached in $PC_{71}BM$ improves the solubility of this acceptor molecule.

4.3 Linear Absorption and Photoluminescence Spectra

Before going to perform continuous wave (CW) and transient photomodulation (PM) measurements PTB7 film and PTB7/$PC_{71}BM$ blend, we measured the linear absorption in terms of optical density (O.D.) and photoluminescence (PL) spectra of both samples using a Cary-17 spectrometer and PL set up (Figure 2.4), respectively. Figure 4.1 (a) shows the O.D. and PL of PTB7 in which O.D. was measured at 300 K and PL at 80 K. The polymer PTB7 shows strong absorption from 1.7 to 2.25 eV, which is the same as reported by Liang et al. [102] and the absorption below 1.7 eV and above 2.25 eV is relatively weak. As we know, the absorption above the optical gap of the polymer is due to π - π^* transitions [62-64] related with the singlet excitons, and below the gap is due to impurities, defects, and /or disorders present in the polymers.

The PL spectrum of PTB7 film is red-shifted as compared to absorption spectrum, as is generally observed in many other polymers. In contrast, the phonon side bands are not clearly observed in the PTB7 film, as we obtained before in P3HT films and DOO-PPV isotope films. Instead, the shoulder at low energy region is observed with only one pronounced PL peak ~ 1.54 eV.

As we already mentioned above, the absorption of PTB7 polymer film is relatively weak above 2.25 eV. To compensate the absorption of PTB7 in the visible range, we used $PC_{71}BM$ instead of $PC_{61}BM$ because the absorption of $PC_{71}BM$ is stronger than $PC_{61}BM$ in that spectral region. Figure 4.1 (b) shows the absorption and PL of PTB7/$PC_{71}BM$ blend measured under similar conditions as in the PTB7 film. Here, it is clearly noticeable that the absorption of blend increases above 1.85 eV in the visible range. However, the absorption of PTB7 film is reduced above 2 eV as presented in Figure 4.1 (a). Thus, in the blended system absorption is improved in the visible region due to the contribution of $PC_{71}BM$.

The PL spectrum of the blend system is also red-shifted as compared to the absorption spectrum, which is obvious in all polymer films and blends with any acceptors. The PL is decreased in the blend due the proximity of the acceptor molecule which tries to capture the photogenerated species and reduces the radiative recombination. Although PL is reduced in the blend, any spectral shift of PL peak is not observed. In both pristine film and blend systems the PL is peaked at ~ 1.54 eV. This result illustrates that the C = C bond length in the polymer chain is unaltered due to the effect of the acceptor molecule $PC_{71}BM$. The PL peak is also sharper in the blend than the film, which is not understood at present.

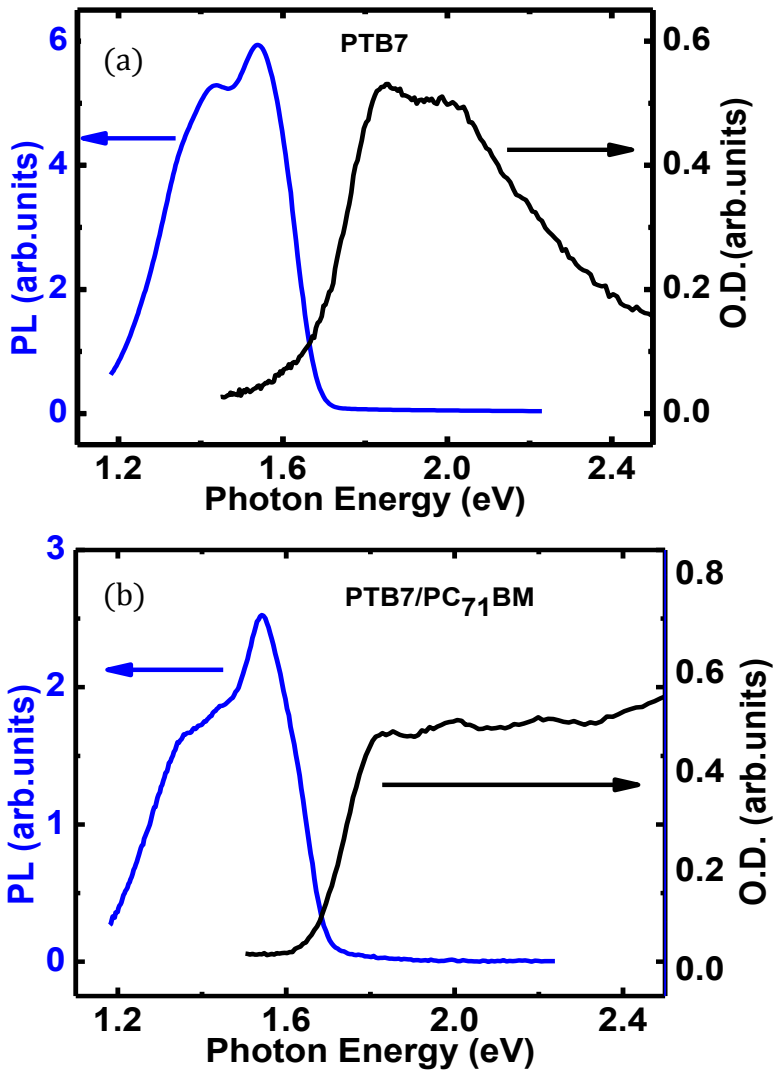

Figure 4.1: Linear absorption in terms of optical density (O.D.), and photoluminescence (PL) spectra of (a) PTB7 film, and (b) PTB7/$PC_{71}BM$ blend. The absorption was measured at 300 K and PL was obtained at 80 K.

4.4 Photophysics Studies

4.4.1 CW Photoinduced Absorption (PA) of PTB7 Film

The copolymer PTB7 was dissolved in ODCB to prepare the solution and then drop-casted on a sapphire substrate for preparing the film. Sample preparation was done inside the globe box in the nitrogen (N_2) environment to avoid any contamination of the films. The CW photoinduced absorption (PA) measurement of the PTB7 film was performed using a pump – probe experiment at 80 K. The sample was photoexcited at 2.54 eV using an Argon laser beam as a pump, and photoinduced absorption was monitored by a tungsten probe beam in the spectral range from 0.3 to 1.8 eV. Figure 4.2 (a) shows the PA spectrum of the PTB7 film in which a broad band peaked at ~ 1.2 eV is observed followed by very weak broad band ~ 0.5 eV. The band at ~ 1.2 eV is assigned as triplet exciton (T) as confirmed by the photoinduced absorption detected magnetic resonance (PADMR) experiment (PADMR result is not shown here but was done by Mr. Tek Basel to identify this band). The doping-induced absorption of PTB7 shows a polaron band at low energy and, thus, we assign the low energy band in PA spectrum as a polaron (P_1) band. In a PA study of high molecular weight RR-P3HT film [103], the polaron band was not observed clearly at low energy, whereas, this band was seen in low molecular weight RR-P3HT film. The power conversion efficiency (PCE) of a high MW RR-P3HT/PCBM active layer solar cell device was higher (4 %) than a low MW RR-P3HT/PCBM active layer device (3.2%). Thus, the absence of a polaron band at low energy in the polymer film is better for OPV application, and this is consistent with PCE 7.4 % observed in the PTB7/PC_{71}BM solar cell device.

4.4.2 CW Photoinduced Absorption (PA) of PTB7/PC_{71}BM Blend

Although [6,6]-phenyl butyric acid methyl ester (PCBM) is the most popular acceptor in blend photophysics study and OPV solar cell applications, we have used

$PC_{71}BM$ acceptor to blend with PTB7 for studying its photophysics because of its high PCE 7.4 % observed in OPV device characterization. The blend of PTB7/$PC_{71}BM$ was prepared in the weight ratio (1:1.5) and PA measurement was conducted as it was performed on the PTB7 film using same experimental technique. The pump excitation energy was 2.54 eV. The measurement was done at low temperature, 80 K. Figure 4.2 (b) shows the PA spectrum of PTB7/$PC_{71}BM$ blend, in which the spectrum is comprised of two clear bands: one at low energy at ~ 0.3 eV and the other at ~1.2 eV. These bands are assigned P_1 and P_2, which are charged polarons. In the blend system, we do not observe the triplet exciton as in pristine polymer film. The polaron band observed at a low energy range is clearer in blend system than the pristine polymer film. Due to the contribution of $PC_{71}BM$ the PA spectrum of the blend is broad, and suggests that the blend captures more of the solar spectrum than the film if people make the solar cell device using these active layers. As in the pristine polymer PTB7 film, PADMR measurement was also done for the blend system, and the band is identified as a polaron band.

The PA measurement can only detect the long-lived photoexcitations in a pristine polymer PTB7 film and PTB7/ $PC_{71}BM$ blend. To detect the short-lived photogenerated species, we have to use different tools. Thus, we also used ultrafast pump-probe spectroscopy to identify the early photo-generated species in the same pristine polymer film and blends.

4.4.3 Transient Photoinduced Absorption (PA) of PTB7 Film

The transient ultrafast PA measurement of PTB7 film was performed using two types of laser systems: one with high repetition rate (80 MHz), low energy (0.1 nJ/pulse) and the other with low repetition rate (1 kHz), high energy (10 μJ/pulse) in different

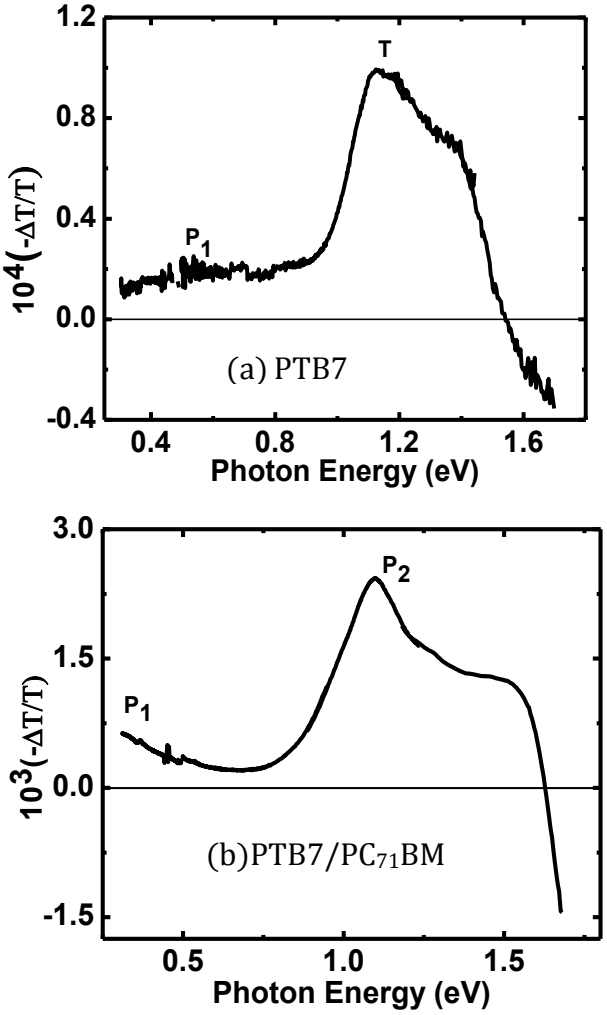

Figure 4.2: CW PA spectrum of (a) PTB7 film measured at 80 K, two bands triplet exciton (T) and polaron (P_1) are assigned. (b) PTB7/$PC_{71}BM$ blend measured at 80 K, two polaron bands P_1 and P_2 are assigned.

spectral regions from 0.25 -1.05 eV and 1.2 – 1.78 eV, respectively. Here, the transient PA spectra measured at different time delays of the probe beam in two different systems are presented separately. Figure 4.3 (a) shows the transient photomodulation (PM) spectra of PTB7 film measured at t = 0, 20 ps and 100 ps, respectively, in the spectral range from 0.25 – 1.05 eV. At t = 0 ps, the spectrum shows a PA band at ~ 0.95 eV, which is assigned as PA_1 and is related with the singlet exciton. Surprisingly, we see the formation of the other PA band starting at ~ 1 eV and keep increasing in high energy range. The limitation of a low intensity laser system is that it does not allow us to monitor this band in the spectral range from 0.25 – 1.05 eV. Thus, the same experiment was done in the high energy range to capture this band and to observe other possible bands in near – IR/ visible region. The transient PA spectra of the same sample PTB7 film measured at different time delays t = 0, 10 ps and 50 ps are shown in Figure 4.3 (b). At t = 0 ps a clear PA broad band peaked at ~1.35 eV is observed along with a stimulated emission (SE) band starting at 1.7 eV. The broad PA band observed at ~ 1.35 eV is the continuation of PA band that we observed in low intensity measurement. We see that the singlet exciton band splits into two bands peaking at energy difference of ~ 0.4 eV. The cause of the splitting is currently unknown, but it is recognized that similar splitting of the PA_1 band was observed in pristine RR-P3HT film in reference [104] and in RR-P3HT/PCBM blend in reference [105], respectively. The spectral decays show that the singlet exciton band observed at ~ 0.95 eV becomes broader in time 100 ps due to the diffusion of photogenerated excitons in nanodomains of the pristine polymer PTB7 film. Similar as in pristine RR-P3HT film, we see the decay of the singlet exciton in a pristine PTB7 film, but the build-up of polarons in expense of the singlet exciton is not observed in the entire spectral region in both measurements.

In addition to the transient PM spectra of a pristine PTB7 film, we also studied the transient decay kinetics of photogenerated species at different probe energies. Figure 4.4 (a) shows these decay dynamics at 0.95 eV, 0.65 eV and 0.3 eV probe energies, respectively.

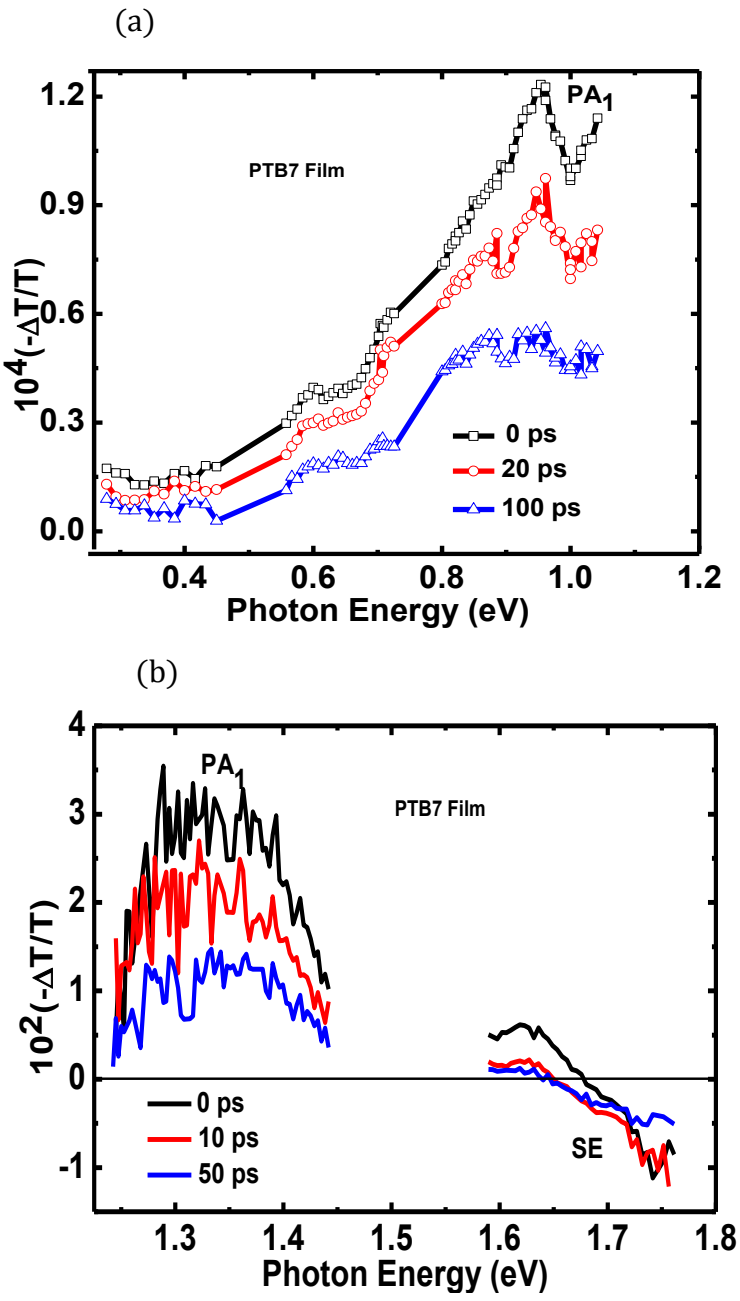

Figure 4.3: Transient PA spectra of PTB7 Film (a) at t = 0, 20 ps and 100 ps in the spectral arrange 0.25 – 1.05 eV, and (b) at t = 0, 10 ps and 50 ps in the spectral range from 1.2 – 1.78 eV.

(a)

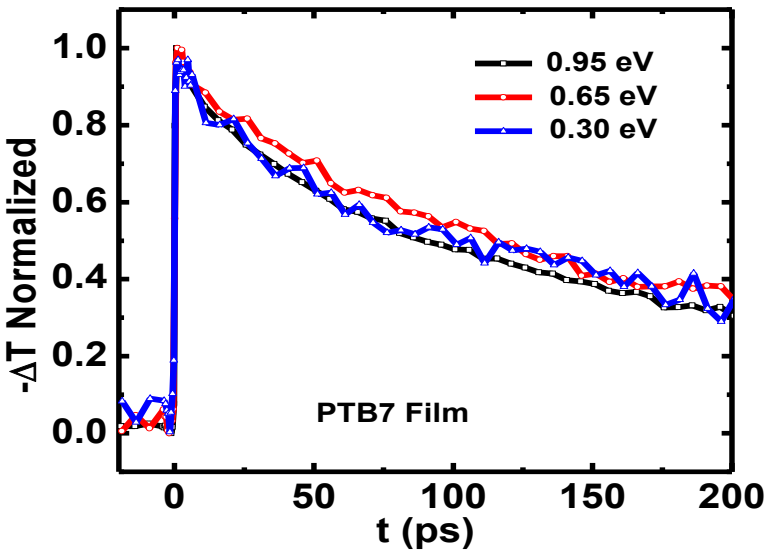

(b)

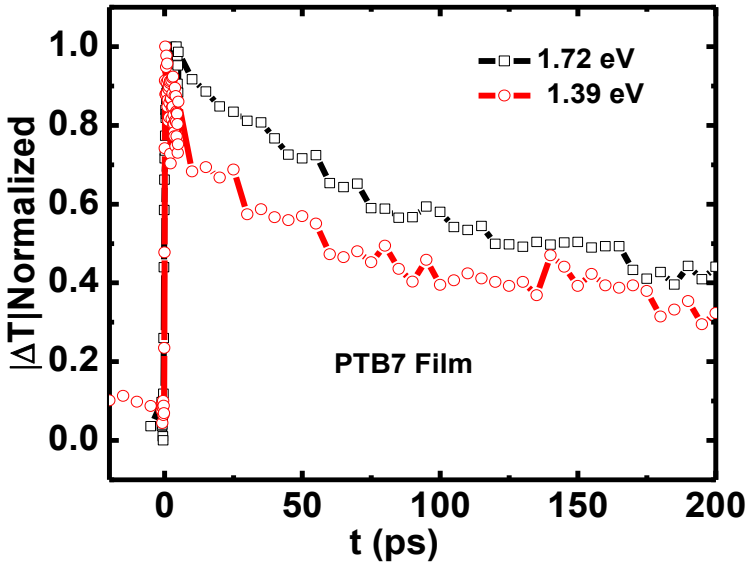

Figure 4.4: Transient decay kinetics of PTB7 Film (a) at 0.95 eV, 0.65 eV, and 0.3 eV in the spectral range 0.25 – 1.05eV, and (b) at 1.72 eV, and 1.39 eV in the spectral range 1.2 – 1.78 eV.

There is not much difference in decay mechanism for photogenerated species belonging to the spectral range from 0.25 – 1.05 eV so that all decay kinetics fit well with a single exponential with time constant ~ 90 ps. We thus assume that the spectrum is related with the singlet excitons throughout the spectral region. In contrast, the decay kinetics of the PA_1 band at 1.39 eV is faster than the SE band at 1.72 eV. SE bands fit well with the single exponential with time constant ~ 84 ps, whereas, the PA_1 band at 1.39 eV fits with biexponential with fast time component 4 ps and slow time component 61 ps. The decay of PA_1, SE and PB bands were almost the same in Pristine RR-P3HT film, as discussed in Chapter 3, and we were assuming that all these bands are somehow related to the singlet exciton. However, this is not the case in copolymer PTB7 film. The PA_1 band is different from the SE band. Thus, the spectrum shows the possibility of two types of photogenerated species in the entire spectral range. However, there is not much difference in decay dynamics which suggests that decay is affected by the spectral diffusion.

4.4.4 Transient Photoinduced Absorption (PA) of PTB7/$PC_{71}BM$ Blend

The transient ultrafast photoinduced absorption (PA) spectra of PTB7/$PC_{71}BM$ (1:1.5) blend measured using low energy (~ 0.1 nJ), high repetition rate (~ 80 MHz) ultrafast laser system in the spectral region 0.25 – 1.05 eV and high energy (10 μJ), low repetition rate (~ 1 kHz) ultrafast laser system in the range 1.25 – 1.9 eV are shown in Figures 4.5 (a) and (b), respectively. The spectrum at t = 0 ps in the spectral region 0.25 – 1.05 eV is comprised of three different bands, which are assigned PA_1, CT and P_1. The band PA_1 is the band of a singlet exciton, which is observed at the same probe energy as the PTB7 film and is completely associated with the singlet optical transition in a polymer network even though the polymer PTB7 is blended with $PC_{71}BM$.

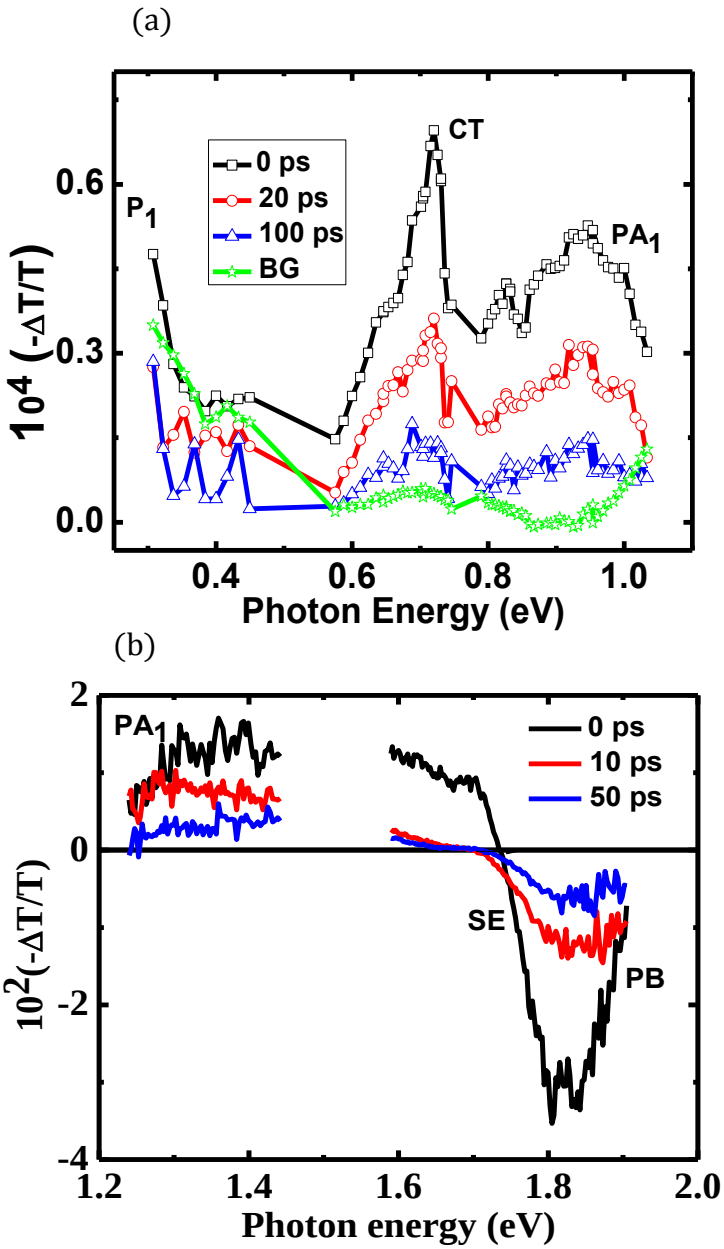

Figure 4.5: Transient PA spectra of PTB7/$PC_{71}BM$ blend film (a) at t = 0, 20 ps and 100 ps in the spectral arrange 0.25 – 1.05 eV, and (b) at t = 0, 10 ps and 50 ps in the spectral range from 1.25 – 1.9 eV.

The PA_1 band is broader in the PTB7/$PC_{71}BM$ blend than the PTB7 film. The broadening of the PA_1 band is due to the increase in the absorption of the blend. In ultrafast photophysics study of most of the polymer/ PCBM blends, we always observed the decay of excitons but not the buildup of polarons in expense of excitons. In contrast, we have clearly observed the buildup of polarons in the low energy range. However, the limitation of probe energy range in our system does not allow us to monitor the P_1 peak in our spectral range. If the spectral range can be extended down to 0.1 eV, there seems to be the possibility of getting P_1 band peak position.

We also observed a band between PA_1 and P_1, which we assigned as a charge transfer exciton (CT) band. The strength of CT band is stronger than other two bands observed in the spectral range from 0.25 – 1.05 eV. Surprisingly, this is the first time that we observed polaron, singlet exciton, and charge transfer exciton bands at the same time in the spectrum at t = 0 ps. The spectral dynamics measured at different time delays t = 20 ps and t = 100 ps of the probe beams show that the charge transfer exciton band decays faster than singlet exciton and polaron bands. The increase in the PA background below 0.5 eV also shows evidence of polaron formation at the expense of the singlet exciton.

The transient PA spectrum measured at t = 0 ps in the spectral range from 1.25 eV to 1.9 eV shows a PA_1 band followed by stimulated emission (SE) and photobleaching (PB) band above 1.84 eV. The spectral dynamics shows that the PA_1 band decays faster than other bands in this spectral range. In the blend system, we again observed the splitting of a singlet exciton band as in the film.

In order to clearly understand the decay mechanism of photo generated species, we studied the transient decay kinetics at different probe energy regions. Figure 4.6 (a) shows the comparison of decay dynamics at two probe energies 0.95 and 0.72 eV. The photogenerated species at 0.72 eV is a charge transfer exciton decaying faster than the species at 0.95 eV, which is a singlet exciton. Similarly, the decay dynamics at 1.58 eV related to a singlet exciton band is faster than the SE band at 1.72 eV.

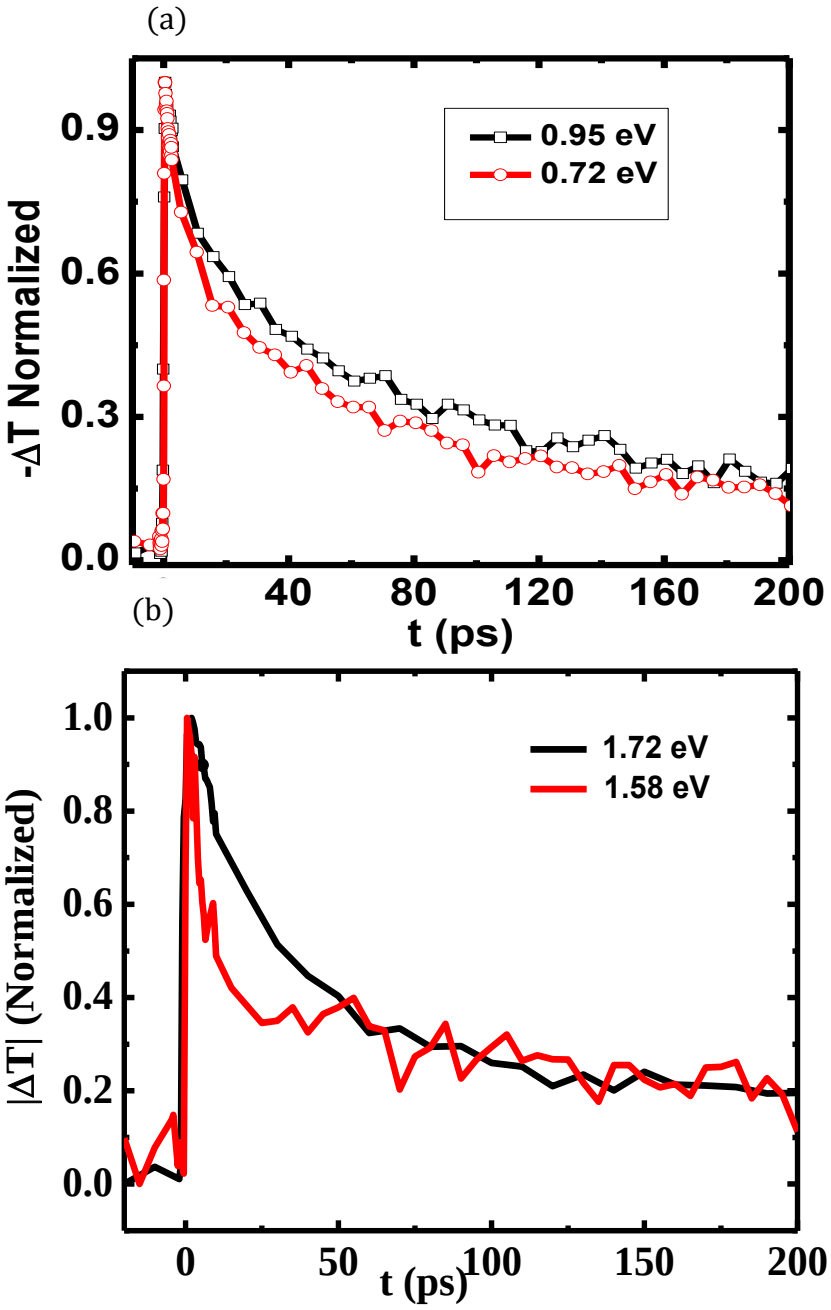

Figure 4.6: Transient decay kinetics of PTB7/PC71BM blend film (a) at 0.95 eV, 0.72 eV in the spectral range 0.25 – 1.05eV, and (b) at 1.72 eV, and 1.58 eV in the spectral range 1.25 – 1.9 eV.

When we compare the decay dynamics of all these bands, then we see that PA_1 and SE have almost the same decay, whereas, CT decays faster and P_1 slower.

4.5 Discussion

The power conversion efficiency (PCE) of an organic photovoltaic (OPV) solar cell fabricated using a RR-P3HT/PCBM active layer is reported ~ 6 % [13], which is not sufficient to compete with the inorganic solar cell PCE for industrial application. The low PCE of the OPV solar cell is due to the limited absorption of the active layer in the solar spectrum, a lack of understanding of charge recombination and dissociation processes following photoexcitation, and a limitation in the process of device fabrication. To resolve the first issue of limited absorption, Liang et al. [102] introduced the new concept of copolymer. They synthesized many low band gap polymers from the poly-thienophene-benzodithiophene (PTB) family, and showed the PTB7 copolymer to be the best among them with PCE 7.4 % when blended with $PC_{71}BM$ for solar cell application. After the invention of the copolymer, many researchers invested time and effort to study different phenomena such as hierarchical nanomorphologies to promote exciton dissociation in a polymer/fullerene bulk heterojunction solar cell [106], structure, dynamics, and PCE correlations in a new low band gap polymer/PCBM solar cell [107], etc. To the best of our knowledge, the photophysics of a low band polymer PTB7 film and its blend with $PC_{71}BM$ in the mid-IR range has not been studied. Thus, we focused our research on CW and transient photomodulation (PM) spectroscopy to understand the charge generation and recombination and/or dissociation processes in a PTB7 film and its blend with $PC_{71}BM$.

In Chapter 3, we studied the ultrafast phtophysics of a P3HT film and its blend with PCBM and observed that the singlet exciton diffuses at the interface in the blend system and forms a charge transfer exciton, which later dissociates into free polarons in long time scale. Due to the limitation of the experimental tool, we could not dictate the

separation of charge transfer excitons into free polarons in our time scale up to 2 ns. But we observed the clue of formation of free polarons from the background spectrum as it increases rapidly in the low energy range below 0.5 eV in our spectral range. The photophysics is not the same in all polymer/acceptor blend systems. We observed different photophysics in a PTB7/PC_{71}BM blend.

Surprisingly we observed the singlet exciton, charge transfer exciton and polaron band at the same time in the transient PA spectrum of PTB7/PC_{71}BM blend at t = 0 ps. This result suggests that many types of photoexcited species can be immediately photogenerated in a low band gap copolymer PTB7/PC_{71}BM blend following photoexcitation. The spectral and transient decay kinetics show that a charge transfer exciton dissociates into free polarons faster than the exciton decay, whereas, in the case of P3HT/PCBM, the charge transfer exciton was long-lived. This might be the one possible reason for getting high PCE 7.4 % in a PTB7/PC_{71}BM solar cell device. The increase in absorption of low band gap polymer in the near – IR region is the other reason for the improvement of PCE. From this ultrafast photophysics study of PTB7/ PC_{71}BM, we clearly see that the formation of polarons and charge transfer excitons at the early stage of photoexcitation is better than the formation of singlet excitons because these two early generated species can be harvested faster than a singlet exciton in OPV solar cell devices.

4.6 Conclusion

The main motivation of conducting optical density (O.D.), photoluminescence (PL), CW-photoinduced absorption, and transient ultrafast photoinduced absorption (PA) measurements of PTB7 film and PTB7/PC_{71}BM blend is to identify the reason for getting high power conversion efficiency (PCE) 7.4 % of a PTB7/PC_{71}BM active layer solar cell device [102] as compared to PCE 6 % in a P3HT/PCBM active layer solar cell device [13]. The other reason is to understand the charge generation, recombination, and

separation processes in film and blend systems after photoexcitation. We first studied the O.D. and PL of PTB7 film and PTB7/$PC_{71}BM$ blend, respectively. From O.D. measurement, we found that the absorption of the blend is enhanced in the visible spectral region due to the contribution of acceptor $PC_{71}BM$ as compared to the donor copolymer PTB7 film. In the PL spectra, there is not much difference in film and blend system, although the PL peak is sharper in blend than in the film. In contrast, the phonon side bands in the PL spectrum of a PTB7 film [Figure 4.1 (a)] are not clear as in P3HT film [Figure 3.3].

The CW PA spectrum of PTB7 film [Figure 4.2 (a)] clearly shows the triplet band at ~ 1.2 eV, and a very weak polaron flat band below 0.5 eV. Whether these two bands are in favor of OPV application or not, we could not decide by this measurement. Thus, we again did the same PA measurement in the PTB7/$PC_{71}BM$ blend. In the blended CW PA spectrum, we noticed two clear polaron bands, which are verified by photoinduced absorption detected magnetic resonance (PADMR) measurement. In photovoltaic applications, polarons move to the respective electrodes by an electric field created by the mismatch between anode and cathode and generates current. Thus, the formation of polaron bands in the PA spectrum should be better than the triplet exciton for an OPV application.

The CW PA monitors only long-lived photoexcited species. Thus, we also performed transient ultrafast PA measurement of both the PTB7 film and PTB7/$PC_{71}BM$ blend to identify the early photogenerated species. For the PTB7 film, a singlet exciton band is observed at ~ 0.95 eV [Figure 4.3 (a)] in the spectral region 0.25 – 1.05 eV and singlet excitons ~ 1.35 eV, as well as SE bands [Figure 4.3 (b)] are observed in the region 1.25 – 1.78 eV, respectively. Similarly, we also performed the same measurement for a PTB7/$PC_{71}BM$ blend and found that singlet excitons, polarons, and charge transfer excitons are generated immediately after photoexcitation. This is the first time we observed all types of photogenerated species at the same time t = 0 ps, even though we conducted several similar measurements in many polymer films and blends with PCBM.

In a RR-P3HT/PCBM blend transient ultrafast PA spectrum [Figure 3.7 (a)], we observed a singlet exciton band at t = 0 ps, charge transfer exciton band at t = 20 ps, and an increment of background below 0.5 eV due to the dissociation of a charge transfer exciton into free polarons at a later time. We did not observe the band of the polaron. In contrast, we observed a singlet exciton, charge transfer exciton, and polaron band at the same time in the PTB7/PC_{71}BM blend PA spectrum. The PCE of PTB7/PC_{71}BM solar cell device is reported higher than the P3HT/PCBM device, which is in agreement with the difference in ultrafast photophysics of these blends as we measured. The formation of polaron band immediately after photoexcitation is better for OPV solar cell application.

CHAPTER 5

PHOTOEXCITATIONS IN DOO-PPV ISOTOPES FILMS AND BLENDS WITH PCBM

5.1 Introduction

This chapter describes in detail the ultrafast photophysics of π – conjugated polymer poly(dioctyloxy) phenylenevinylene (DOO-PPV) isotopes' films and blends with [6,6]-phenyl C_{61} butyric acid methyl ester (PCBM). The isotopes of DOO-PPV are D-DOO-PPV, H-DOO-PPV, and C13-DOO-PPV which were synthesized in our laboratory by Mr. Leonard Wojcik. Synthetic reagents and solvents used in the preparation of the isotope-rich polymers were procured from Aldrich Chemical as reagent-grade and used as received. The detail synthesis process of D- Polymer and H-Polymer can be found in the supplementary information of a paper published by our group in *Nature materials, Tho et al.* [108]. For simplicity, D-DOO-PPV, H-DOO-PPV and C13-DOO-PPV are hereafter referred to as D- Polymer, H- Polymer and C- Polymer, respectively.

Transient photomodulation (PM) spectroscopy of π – conjugated polymer films and blends with PCBM is common in the polymer photophysics community. However, to the best of our knowledge the isotope effect on transient PM spectra has not been studied so far. Here we are interested to know the isotope effect on the photophysics of pristine polymer films and blends with the acceptor molecule PCBM.

The isotope effect observed in the spin response of π – conjugated polymer films and devices [108] added to our curiosity and encouraged us to perform a transient PM spectroscopy measurement to determine how the PM spectra differ from one isotope to the other, what types of photoexcitations are possibly generated, and how the photogenerated species dissociate or recombine in the three isotopes of DOO-PPV polymer films and blends with PCBM. In order to study the photophysics of isotopes we first measured the linear absorption and PL measurement, and subsequently performed transient PM measurement using low-intensity and high-intensity ultrafast laser systems. Using these two different ultrafast laser systems, the transient photomodulation (PM) spectrum spans a broad probe energy range from 0.25 – 2.5 eV; this allows us to monitor the transient behavior of the various photoinduced absorption (PA) bands of singlet excitons, stimulated emission (SE), and photobleaching (PB) bands.

5.2 Materials

5.2.1 Donor Materials (H-, D- and C- Polymers)

The donor materials that we used are H-, D- and C- Polymers; their chemical structures are shown in Figures. 2.1[(a), (b), and (c), respectively (Chapter 2)]. The side groups attached on each benzene ring are two 4-phenyl-2-propyl-indene (C_8H_{17}) through oxygen and two protonated hydrogen for H- Polymer. When solutions based on aromatic solvents are cooled, the polymer forms gels that precipitate in clumps, making unsmooth films. However, short polymer chain length (or oligomers) tend to be more soluble in solvents such as toluene, orthodichlorobenzene (ODCB) and do not gel out easily. This was addressed by *Hsieh* [109] and *Jiang-quing pan* [110], where they used a benzyl bromide end cap to shorten the polymer length. The synthesis of H- Polymer was performed using polymerization of 2,5-bis(chloromethyl)-1,-4-dictyloxybenzene with potassium t-butoxide in refluxing p-xylene. This route allowed some control of the polymer chain length and it is denoted by R^1 in the chemical structure. D- Polymer

contains deuterated hydrogen in place of protonated hydrogen. Similarly, some backbone C-12 carbon atoms are replaced by C-13 to make the C- Polymer. C-13 carbon isotope rich are denoted by red in Figure 2.1(c).

5.2.2 Acceptor Material (PCBM)

The chemical structure of PCBM is shown in Figure 2.1(g). It is the derivative of C_{60} or a fullerene molecule with one side group attached on it. The side group helps to improve solubility. The electro negativity of the fullerene molecule is high, so this material is considered a suitable candidate for the acceptor material in organic photovoltaic solar cell systems.

5.3 Linear Absorption and Photoluminescence Spectra

The DOO-PPV isotopes (D- Polymer, H- Polymer, and C- Polymer) films were prepared under similar conditions and linear absorption in terms of optical density (O.D.), and photoluminescence (PL) were measured using Cary -17 spectrometer and PL set up (Figure 2.4), respectively (these measurements were done by Mr. Tek Basel in our research group). Figure 5.1 shows a normalized O.D. and PL spectra. A broad featureless optical absorption is observed with its lower-energy edge lying at ~ 2.2 eV in all three isotopes. The absorption band above the optical band gap is due to π-π^* transitions that lead to the formation of singlet exciton [111-113], whereas below the gap the absorption is due to the presence of impurities and/or defects in the samples. The energy of the π-π^* transition is dependent on the extent of the π- electron delocalization. In relatively disordered polymers such as isotopes of DOO-PPV, the extent of delocalization tends to be limited by kinks and defects in the polymer chain leading to a range of π-π^* energies for a given sample. The lack of vibronic structure in the absorption spectra is thus attributed to inhomogeneous broadening due to a range of conjugated lengths within the sample [114].

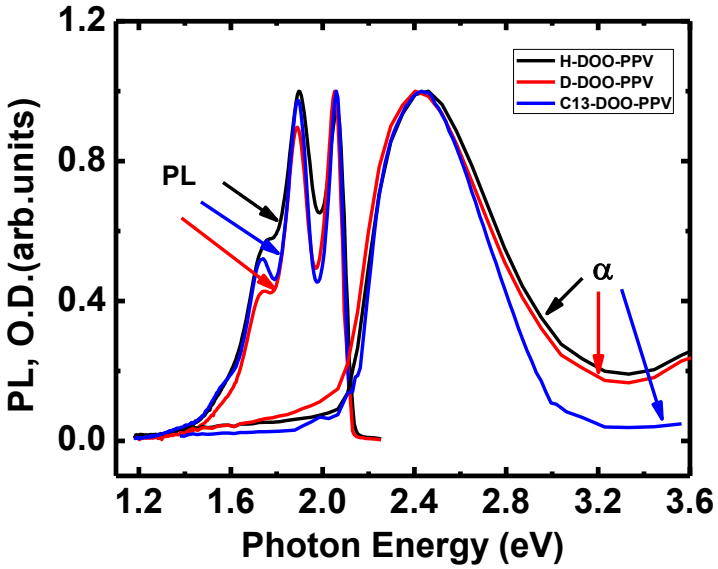

Figure 5.1: Normalized absorption and PL spectra of DOO-PPV isotopes. The absorption was measured at 300 K and PL at 80 K.

In the absorption spectra, we see that the absorption of C- Polymer is red-shifted compared to the other two isotopes D- and H- Polymers. However, the absorption spectra are very similar overall. Similarly, the PL spectra of all three isotopes show the same emission band with two clear phonon sidebands replica, thus verifying the polymer electronic structure and that the photoexcitation species such as excitons and polarons, are the same in the D-, H-, and C- Polymers [108]. The PL spectra of all isotopes are Stokes–shifted from the absorption spectra and have clearly resolved vibronic structures. These observations have been explained by migration of the photogenerated excitons to the lower energy (longer conjugation length) chain segments before radiative decay has time to occur [114-116]. Thus, the observed emission originates mainly from the lowest energy segments leading to the observed Stokes shift and reduced inhomogeneous broadening when compared to the absorption spectra. The relative strength of PL intensity of C- Polymer is the highest among all isotopes, which is also consistent with

the PL quantum efficiency (PLQE) results: we measured PLQE of 5 % for H-, 4.5 % for D-, and 12 % for C- Polymers, respectively.

5.4 Transient Photoinduced Absorption of Isotope Rich DOO-PPV Films

5.4.1 D-DOO-PPV (D- Polymer) Film

The transient ultrafast photomodulation (PM) spectra of D- Polymer film in a broad probe spectral range from 0.25 – 2.4 eV that we measured at t = 0 ps and t = 100 ps are shown in Figure 5.2 (a). These spectra were measured using low-intensity and high-intensity ultrafast laser systems. The PA signal that we obtained using high-intensity laser system is always higher than that of the low-intensity laser system. Therefore the PM spectra measured using two different laser systems are combined together with proper normalization to span the spectral range from mid-IR (0.25 eV) to near-IR/visible (2.4 eV). For further analysis the PM spectrum is divided into two different spectral regions: one region is below 1.7 eV, which has $-\Delta T/T > 0$ and the other region above 1.7 eV with $-\Delta T/T < 0$. The PM spectrum at t = 0 ps contains prominent PA band; peaked at 0.97 eV (PA_1) and two other bands, namely stimulated emission (SE) and photobleaching (PB) above 1.7 eV. The band below the absorption of the D-DOO-PPV film must be due to SE rather than PB of the absorption [117]. The SE band contains some phonon replicas, which are similar to those in CW PL spectrum (see Figure 5.1). Similarly, the band above SE is assigned a PB band. When the probe photon energy is above 1.7 eV, the probe beam experiences gain due to SE from photoexcited states and the signal is negative. In contrast, if the probe photon energy is below 1.7 eV, the probe beam is absorbed due to photoinduced absorption (PA) from excitons to higher excited states, and shows an opposite signal as compared to the SE signal. From these results, we see that SE and PA do not overlap and, therefore, there is no internal competition. This, however, is not the case for many other luminescent polymers, e.g., P3BT, PPE [118], and PPV [117].

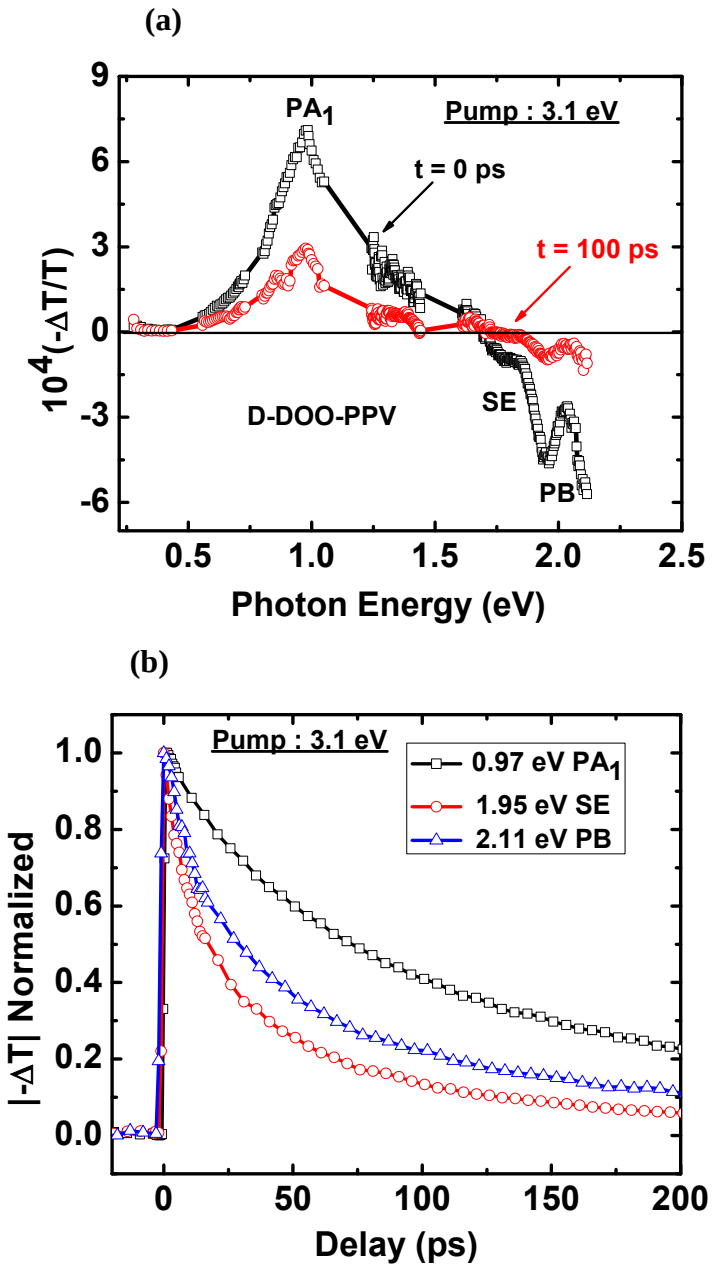

Figure 5.2: D-DOO-PPV Film: (a) the transient PA spectra at t = 0 ps and 100 ps. Various bands PA_1, SE, and PB (b) Decay dynamics at various probe energies.

At t > 0, the PM spectrum decays with the time t, most probably due to recombination of the photoexcited species.

The spectrum at t = 100 ps is the manifestation of such photoexcitation density decrease. But even after 100 ps the PM spectrum still consists of a clear singlet exciton band peaked at ~ 0.97 eV along with SE and PB bands. To understand how these different photo–excited species decay with time, we also measured the decay dynamics of PA_1, SE, and PB bands. Figure 5.2 (b) shows the transient decay behavior of various bands PA_1, SE and PB; the respective fitted time constants are presented in Table 5.1. Here PA_1 decay dynamics fits well with a single exponential with time constants of 88 ps. In contrast, SE and PB do not decay in a similar manner as PA_1. The SE band decays somewhat faster than the PB band, with a shorter time constant of 9 ps and a longer time constant of 55 ps, as compared to a 11 ps shorter time constant and a 67 ps longer time constant of PB as obtained in biexponential fitting. The small difference in the decay time constant may be due to the disorder and inhomogeneity that exists in the film, where different polymer chains have different exciton time constants.

Table 5.1: Time constants of various bands observed in the PM spectrum of the D-DOO-PPV Film.

Band	**Time constants (τ)**
PA_1	88 ps
SE	9 ps (24%), 55 ps (76 %)
PB	11 ps (24%), 67 ps (76%)

5.4.2 H-DOO-PPV (H- Polymer) Film

Figure 5.3 (a) shows the ultrafast PM spectra of H- Polymer film at t = 0 ps, 50 ps and 200 ps in the mid-IR spectral range from 0.25 – 1.05 eV measured upon excitation at 3.1 eV, above the polymer band gap. The spectrum is dominated by a PA band peaking at 1.02 eV (PA_1). However, the tail of the PA_1 band extends down to 0.55 eV and then remains flat in the probe energy range 0.25 – 0.43 eV. The PA signal in the probe energy range 0.25 – 0.43 eV is more than one order of magnitude smaller, as compared to the signal of the higher energy range. Thus the S/N ratio here is small and the decay at these probe range should be taken with a grain of salt. This is the reason we clearly observe the spectral decay at 200 ps for probe energy range > 0.55 eV, but hardly below this energy.

One advantage of transient PM technique is that we can measure the background spectrum and the transient PM spectrum of polymer film at the same time. The green color in Figure 5.3 (a) is the background spectrum of the H- Polymer measured directly through the same system at the same time. The background spectrum is flat all over the spectral range, and suggests that the photogenerated species in this probe energy range are due to one species. To confirm whether all species in this spectral range belong to the same species, we also measured the transient decay dynamics at various probe energies. The decay dynamics at two different probe energies, namely 1.02 eV and 0.65 eV, are shown in Figure 5.3(b), and the time constants are tabulated in Table 5.2. The time constants are roughly the same for the two probe energy decay kinetics, and hold true throughout the whole spectral range. Therefore, the PM spectrum in mid-IR range comes from the same photogenerated species, which we identify to be *singlet excitons*.

Table 5.2: Time constants of H-Polymer films for two bands

Probe Energy (eV)	**Time constants (τ)**
1.02	102 ± 2 ps
0.65	120 ± 2 ps

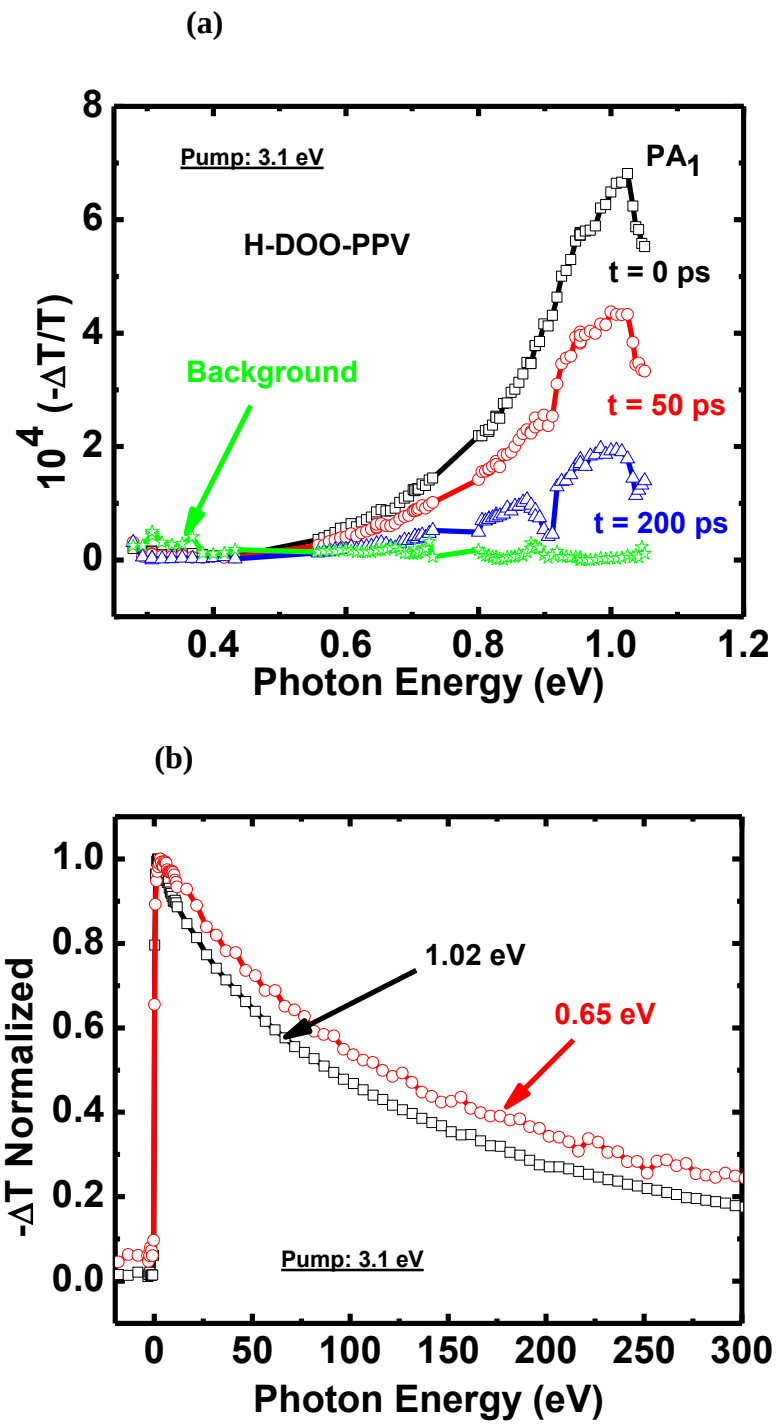

Figure 5.3: The transient PM spectrum of H-DOO-PPV film: (a) the transient PM spectra at t = 0 ps, 50 ps and 200 ps. A single PA_1 band is assigned. (b) Decay dynamics at various probe energies.

5.4.3 C13-DOO-PPV (C- Polymer) Film

The ultrafast PM spectra of C- Polymer film measured at t = 0 ps, 20 ps, 100 ps, and 300 ps with pump excitation energy 3.1 eV are shown in Figure 5.4 (a). In this measurement we have only used the low-intensity ultrafast laser system, which allows us to monitor the PM spectrum in the mid-IR range from 0.25 – 1.05 eV. Like the other two isotopes (D- Polymer and H- Polymer) films PM spectra, the PM spectrum of the C-Polymer film is also dominated by a single PA band that peaks at 1 eV with a long tail towards low energy spectral region. The spectrum at t = 300 ps still shows clear PA_1 peak with very little red-shift as compared to the spectrum observed at t = 0, which indicates that the spectral shift in the PM spectrum might influence the transient decay kinetics of the C- Polymer film.

In order to better understand the decay mechanism of photogenerated species in this spectral range, we measured the decay kinetics at various probe energies. Figure 5.4 (b) shows the decay dynamics at three probe energies 1 eV and 0.65 and 0.30 eV. The time constants of the decay dynamics that we obtained from single exponential fit are tabulated in Table 5.3. Here, we see that the PA observed from 0.55 – 1.05 eV have the same decay kinetics. The decay fits well with the single exponential and shows time constant ~106 ps. Assuming a radiative lifetime of the singlet exciton to be 1 ns [116], the PL quantum efficiency (PLQE) turns out to be ~ 11%, which is within the error bar with the 12 % PLQE using the integrated sphere. The decay is somehow slower in the probe range 0.25 – 0.43 eV as compared to the rest of the probe energy range. This may be due to transient spectral shift. In support for this we note that the time constants that we obtained after analyzing the decay are in the same order of magnitude. *We therefore conclude that the whole PM spectrum belongs to same photogenerated species, namely singlet excitons.* We also conclude that the singlet exciton diffuse in the film to lower energies and this explains the longer time constant at the low-probe energy range.

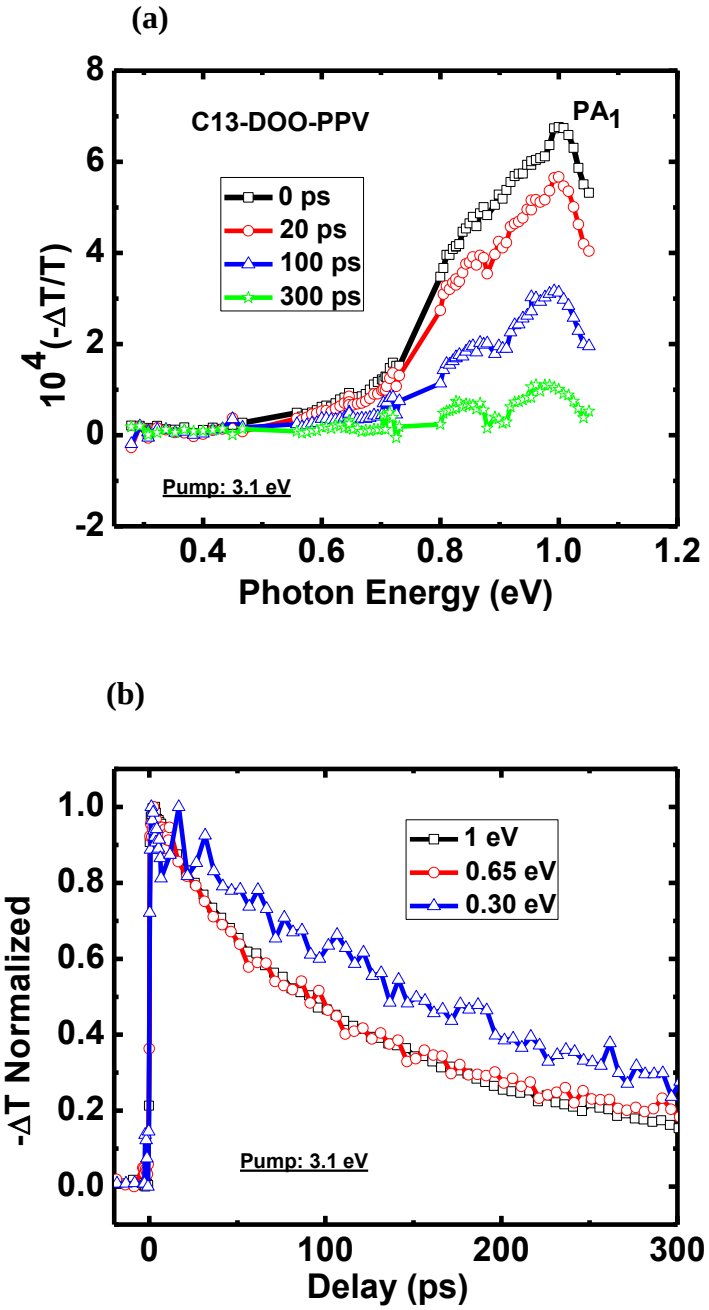

Figure 5.4: PM transient of C13-DOO-PPV film: (a) the transient PA spectra at t = 0 ps, 20 ps, 100 ps and 300 ps. A single PA_1 band is assigned. (b) Decay dynamics at various probe energies, as denoted.

Table 5.3: Time constants of C13-DOO-PPV films at various probe energies.

Probe Energy (eV)	Time Constants (τ)
1	106 ± 2 ps
0.65	97 ± 3 ps
0.30	261 ± 35 ps

5.4.4 Comparison of Pristine Isotopes Films Results

Figure 5.5 (a) shows the ultrafast PM spectra of the three isotopes (H-, D-, and C-Polymers) of DOO-PPV at t = 0 ps measured under similar conditions such as pump photon energy (3.1 eV), intensity, etc. In all three polymer isotopes we observed the same type of PM spectrum, in which the entire spectrum is dominated by a single PA band peaking at 1.02 eV (H- Polymer), 1 eV (C- Polymer), and 0.97 eV (D- Polymer). Here we can analyze the exciton PA_1 band in the three isotopes. The PA_1 band of D- Polymer is red-shifted with respect to that in C- Polymer and H- Polymer.

From NMR and Raman scattering measurement the replacement of protonated hydrogen by deuterated hydrogen, and C-12 atoms by C-13 atoms were confirmed. In the Raman scattering spectra [108] it is seen that the two main Raman-active vibrational modes at ~1300cm^{-1} (C-C stretching) and 1500 cm-1 (C=C stretching) are red-shifted by about 3 % upon deuteration of the polymer; this is in agreement with the expected isotope shift in CH (CD) units resulting from the square root of the mass ratio rule [119], namely $[m(CD)/m(CH)]^{1/2} \approx 1.037$. Change in molecular weight brings change in vibrational frequency of the molecules of the isotopes. The vibration of the molecules is associated with the electronic configuration of the material and affects the optical transitions. Therefore, the red-shift of PA_1 band of the D- Polymer with respect to the other two isotopes may be due to the smaller frequency of the C=C stretching vibration (see discussion section).

(a)

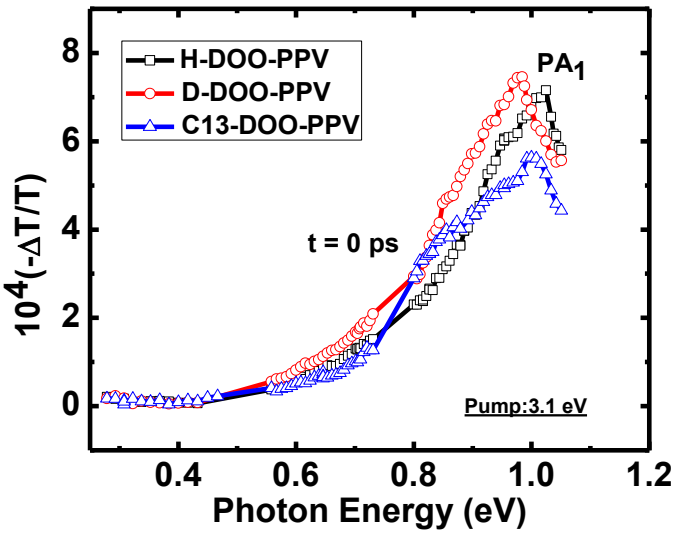

(b)

(c)

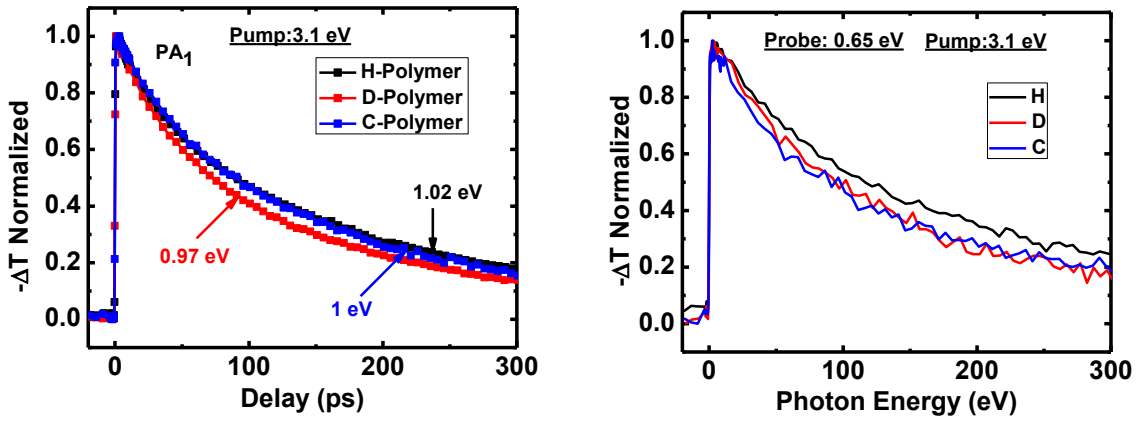

Figure 5.5: PA dynamics in the three DOO-PPV isotopes films (H-, D-, and C-Polymers): (a) Transient PA spectra at t = 0 ps, (b) Decay dynamics of PA_1; and (c) Decay dynamics at 0.65 eV.

We also compared the transient decay of the photogenerated species of all three isotopes over the entire spectral range at various probe energies. However, only two dynamics measured at the PA_1 band probe energy and at 0.65 eV are shown in Figure 5.5 (b) and (c), respectively. In Figure 5.5 (b), we clearly see that the PA_1 band decays in a similar way in all three isotopes even though the time constants (Table 5.4) obtained in single exponential fitting are a somewhat different. Similarly, we do not see much difference in the transient decay of all isotopes at probe energy 0.65 eV. The time constant obtained for all transient decay dynamics using a single exponential fitting are tabulated in Table 5.4. From these results, we assume that the entire transient PM spectrum mainly consists of only one kind of photogenerated species, of which decay changed due to the non–uniform effect of impurities at various probe spectral regions. We conclude that is impossible to rely on the time constants in this spectral range, since spectral diffusion would obscure the real decay lifetime.

Table 5.4: Time constants obtained using single exponential decay fitting of DOO-PPV isotopes transient decays.

Polymer	Probe energy	Time constant (τ)
H- DOO-PPV	PA_1 (1.02 eV)	102 ± 2 ps
D-DOO-PPV	PA_1 (0.97 eV)	88 ± 2 ps
C13-DOO-PPV	PA_1 (1.0 eV)	107 ± 2 ps
H- DOO-PPV	0.65 eV	120 ± 3 ps
D-DOO-PPV	0.65 eV	116 ± 3 ps
C13-DOO-PPV	0.65 eV	97 ± 3 ps

5.4.5 Discussion of Pristine Isotope Films Results

The main goal of studying transient photomodulation (PM) spectroscopy of DOO-PPV isotope-rich films is to figure out how the isotope effect comes into play in the PM spectrum, the formation of different types of photogenerated species within the spectral range of our interest, and whether or not the transient decay mechanism is affected by the change in the molecular isotopes. To get the concrete achievements of these goals, three isotope films (D- Polymer, H- Polymer, and C- Polymer) were prepared, and PM measurements were carried out under similar conditions. As stated earlier in individual isotope films' PM spectrum, we have found that the PM spectra are more or less similar in all three isotopes except for the position of the singlet exciton PA. From the beginning, we are claiming that a dominant band ~ 1 eV is the singlet exciton.

The PM spectrum of excitons in DOO-PPV is schematically explained in Figure 5.6 (a), which shows the ground and excited electronic levels and their associated transitions in a configuration coordinate (Q) diagram [120]. The pump beam induces the transitions from the ground state ($1A_g$) to the first allowed excitonic state ($1B_u$), which contains many vibrational states. Following a relatively small relaxation (~ 0.1 eV), SE (and PL) occurs between the relaxed $1B_u$ and $1A_g$. In addition to SE, PA from $1B_u$ to higher energy levels is induced for two even-parity states, namely mA_g and kA_g [Figure 5.6 (a)]. In a related study in our group, these two A_g states have been directly measured by two-photon absorption spectroscopy [121]. The theoretical calculations have identified mA_g and kA_g as the charge transfer exciton and biexciton (bound states of two excitons), respectively [122], but their exact index number cannot be inferred from our PM measurements.

The energy level diagram in Figure 5.6 (a) is substantiated by the EA spectrum on the same DOO-PPV film, as shown in Figure 5.6 (b). The EA spectrum is composed of a derivative - like feature with zero crossing at 2.25 eV, which is due to the quadratic Stark - shift of the $1B_u$ exciton at this energy [123], and two positive bands at 3.0 and 3.5 eV,

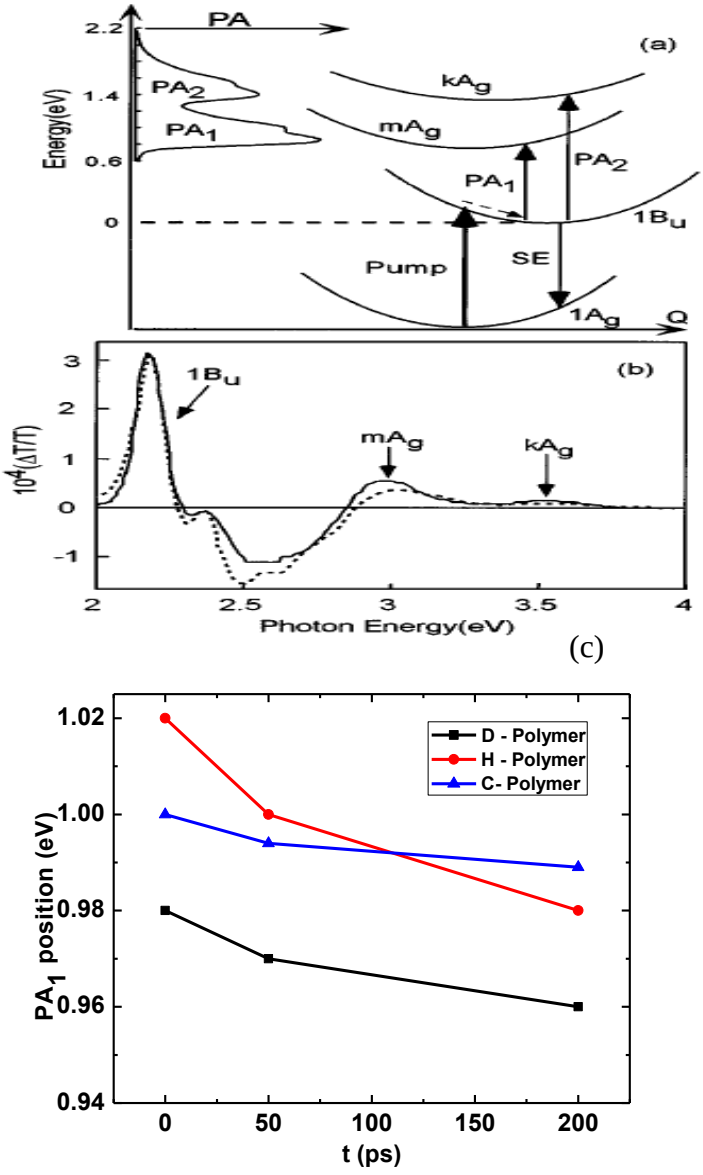

Figure 5.6: (a) Configuration coordinate diagram of the exciton model and optical transitions in DOO-PPV. (b) The EA spectrum (solid line) and its fit (broken line). (c) The spectral shift of PA_1 with time.

respectively. These two bands are due to even parity states (mA_g and kA_g), which become partially allowed in EA due to symmetry breaking caused by the strong applied electric field. The energy difference between $1B_u$ and mA_g is ~ 0.7 eV forms the EA spectrum; however, we have observed the PA_1 band at a higher energy range than this value in all three DOO-PPV isotopes (at 0.97 eV in D-, 1 eV in C-, and 1.02 eV in H- Polymer films).

The reason for the obtained blue shift of the singlet exciton band in our PM spectrum as compared to the singlet exciton band inferred from the EA measurement is unclear. However, we may speculate about the cause for it here. The $1B_u$ level is composed of many vibrational states, in which the lowest has index 0 and above it the index is 1, 2, 3, etc. in increments of ~ 0.18 eV. The exciton PA peak observed in our transient PM spectrum of isotopes might not be the 0-0 transition, but alternatively could be due to higher 0-n transition such as 0-1, 0-2, etc. When we compare the three isotopes of DOO-PPV PM spectra, the singlet exciton band is more red - shifted in the D- Polymer film as compared to H- and C- Polymer films, which indicates that the peak is sensitive to the vibration mode frequency, which changes according to the isotope molecular mass. The increase in molecular mass always reduces the C = C stretching vibrational frequency, and consequently the 0-n transition associated with the reduced vibrational frequency gets red-shifted. The red-shift in vibrational frequency of the D- Polymer is verified by Raman scattering spectroscopy [108]. We may conclude that the main reason for the red-shift in the DOO-PPV film PA_1 is the decrease in frequency of the C = C stretching vibration.

The other goal of this study on PM spectroscopy is to examine the isotope's effect on the transient decay kinetics. The comparison of decay dynamics of all three isotopes at the same probe energy [Figure 5.5 (b)] shows that there is no significant difference in their decay mechanism. All the decay dynamics fit well with a single - exponential, with parameters of the same order with an error of 10 %. If we take the PA_1 decay time

constants of all the isotopes and calculate PLQE = $\tau_{PA1}/\tau_{rad,}$ assuming a radiative lifetime of 1ns, it turns out to be 10 %, 9%, and 11 % in H-, D- and C- Polymers, respectively, which is not the same as the observed 5 %, 4 %, and 12 % for H-, D-, and C- polymers using an integrated sphere.

Interestingly, PLQE is almost the same in the C- Polymer in both measurements but these values are different in the H-, and D- Polymers. The difference in PLQE values obtained from decay time constants are related with *spectral shift*. The decay kinetics is affected by a transient spectral shift in the PA spectrum of all isotopes. The transient spectral shift [Figure 5.6 (c)] is less in the C- Polymer as compared to the D-, and H-Polymers. Thus, the decay dynamics at 0.65 and PA_1 are same in the C- Polymer; but they are different in the H-, and D- Polymers. We therefore conclude that the true decay dynamics are not observed in our mid-IR PA spectrum due to the effect of transient spectral shift.

5.5 Transient Photoinduced Absorption of DOO-PPV Isotopes/ PCBM Blends

5.5.1 D-DOO-PPV (D- Polymer)/PCBM Blend

The ultrafast PM spectra of the D-Polymer/PCBM blend (1:1.5) measured at t = 0 ps, 10 ps, and 20 ps using the low-intensity laser system upon excitation at 3.1 eV is shown in Figure 5.7 (a). The PM spectrum of the blend at t = 0 ps looks very similar to the spectrum of the D- Polymer film, except the appearance of a new weak band PA^* at ~ 0.6 eV. The spectrum is dominated by a single PA_1 band, which indicates that even in the blend of D- Polymer/PCBM most of the absorption occurs in the D- Polymer phase. However, the spectral decay here is not the same as in the pristine D- Polymer film. In Figure 5.7 (a) we clearly see that PA_1 disappears completely in 20 ps, whereas, a clear PA_1 band [Figure 5.2 (a)] is still observed in D- Polymer film after 100 ps. We also see that the spectral decay is not uniform over the entire spectral region. This result suggests

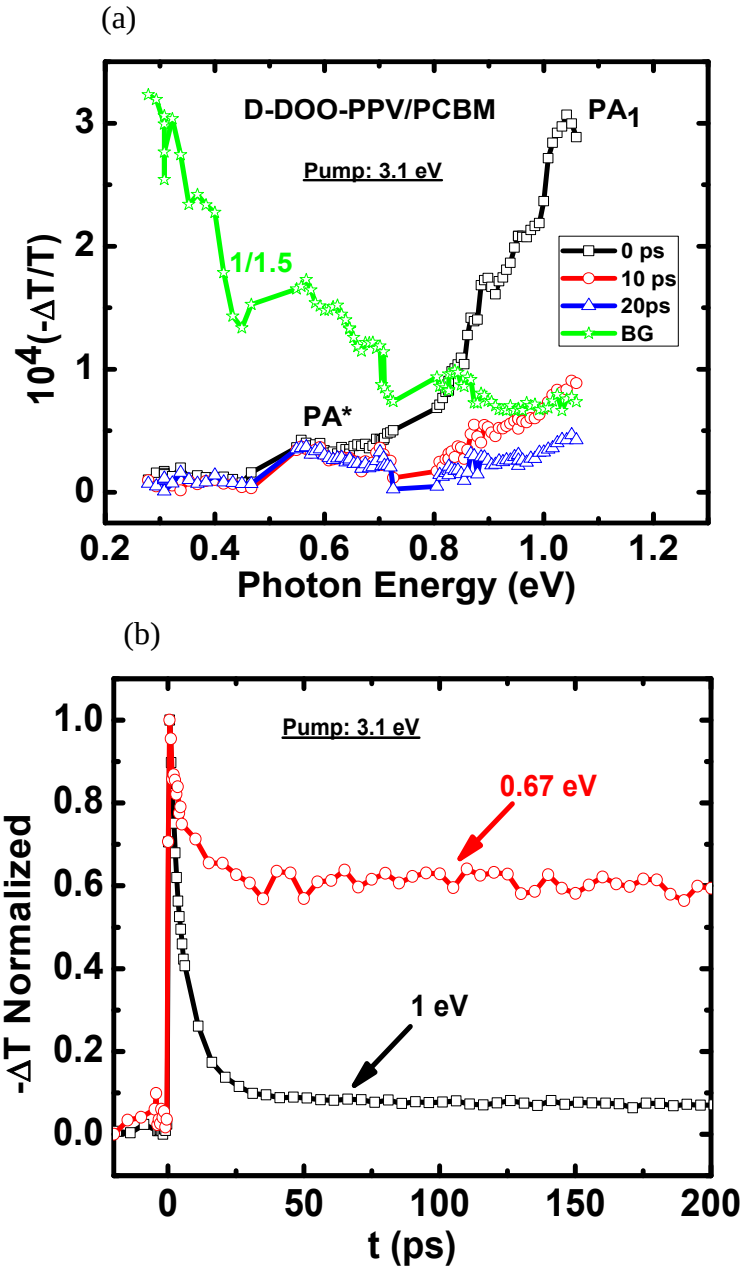

Figure 5.7: Transient PM in D-DOO-PPV/PCBM blend: (a) the transient PA spectra at t = 0 ps, 10 ps, and 20 ps. PA_1 and PA^* bands are assigned. (b) Decay dynamics at 0.67 eV and 1 eV probe energies.

that when a D- Polymer is blended with an acceptor such as PCBM, the decay dynamics is different from that in pristine polymer.

The background spectrum clearly shows that long-lived species are generated in the low probe energy region. In order to clearly understand the recombination process of photogenerated species, we have also measured the decay kinetics at various probe energies. The transient decay kinetics measured at two probe energies, 1 eV and 0.67 eV, are shown in Figure 5.7 (b), and their corresponding time constants obtained through double exponential fitting are 3.1 ps (34 %) and 10.2 ps (78 %), and 2 ps (16 %) and 10.5 ps (31 %), respectively. We see that PA_1 band decays faster than the PA^* band. In fact, the decay of the exciton band PA_1 should be mirrored by a build-up of a polaron band somewhere in the spectrum. Unfortunately, this type of build-up is not observed in our spectral range.

5.5.2 H-DOO-PPV (H-Polymer)/PCBM Blend

Figure 5.8 (a) shows the transient PM spectra of H- Polymer/PCBM blend (1:1.5) measured at different time delays; t = 0 ps, 10 ps, and 20 ps of the probe beam using pump excitation energy 3.1 eV in an ultrafast low-intensity laser system. The PM spectrum at t = 0 ps again looks very similar to the transient PM spectrum of the pristine H- Polymer film [Figure 5.3 (a)] in the entire spectral range except the position of the PA_1 band peak. In the H- Polymer film, the PA_1 band peak was clearly observed at 1.02 eV. In contrast, we do not see the PA band peak in the H- Polymer/ PCBM blend spectrum. The PA_1 peak is blue-shifted in the blend as compared to the film, and our system does not allow us to monitor the PA_1 peak in our spectral region. The spectrum of the H- Polymer/PCBM blend almost looks flat after ~ 20 ps, whereas, the PA_1 band is still clearly observed after 200 ps in the pristine H- Polymer film. This means the spectral decay is completely different when comparing pristine and PCBM blend H- Polymer.

The similarity in the PM spectra of blend and pristine film at t = 0 shows that most of the absorption occurs in the polymer phase, and then the decay is affected by the presence of the PCBM. In a blend system, it is generally expected to see the buildup of

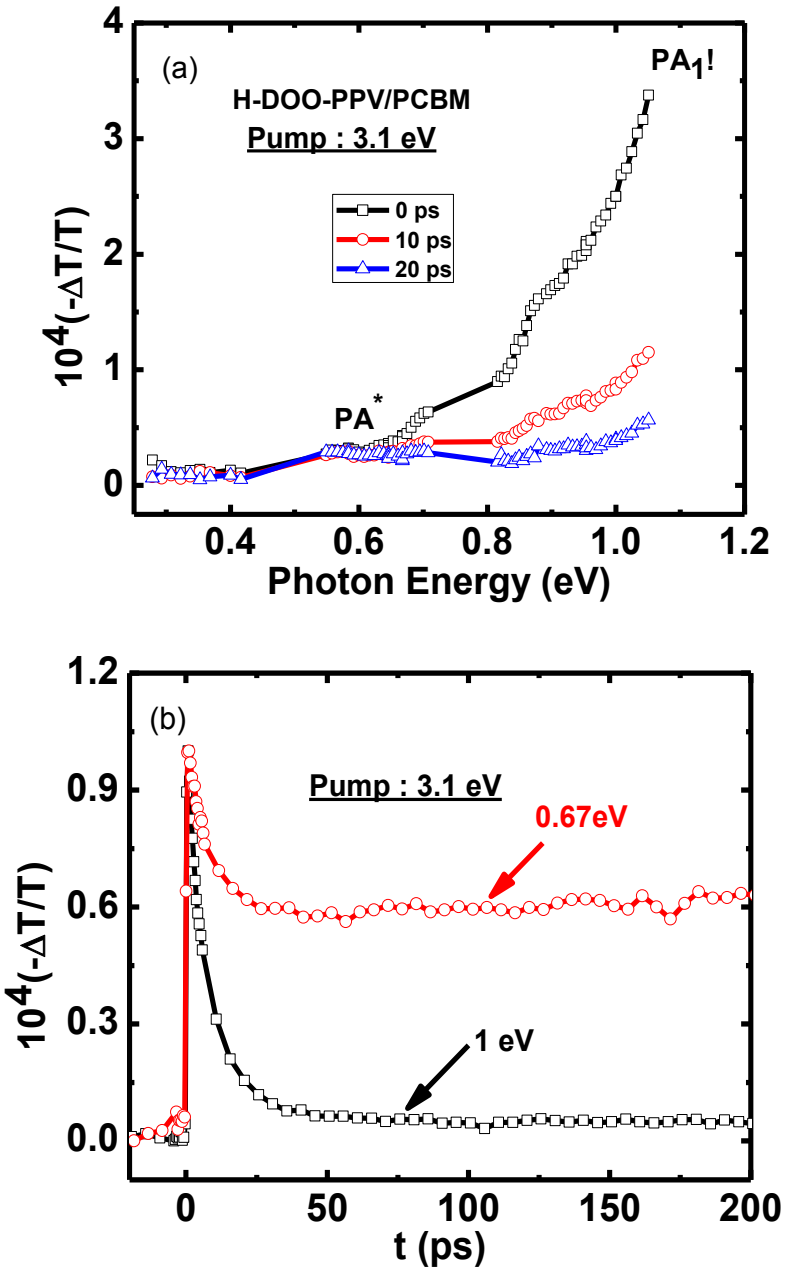

Figure 5.8: Transient PM in H-DOO-PPV/PCBM blend: (a) the transient PA spectra at t = 0 ps, 10 ps, and 20 ps. (b) Decay dynamics at 0.67 eV and 1 eV probe energies.

polarons at the expense of the exciton decay, but the expected buildup is not achieved in the entire PM spectrum. Instead, the spectrum is almost flat within a few ps. That means almost all photogenerated excitons decay to the ground state by radiative and non-radiative processes. We note that the decay is faster in the blend system for spectral region > 0.55 eV and slower below this energy range as compared to the decay observed in the same polymer film. Thus, we confirm that the spectrum is coming from the contribution of two different photogenerated species. The transient decay kinetics measured at two probe energies at 1 eV and 0.67 eV are shown in Figure 5.8 (b). Like the transient decay kinetics of the D- Polymer/ PCBM blend, the transient decay of the H-Polymer/PCBM is faster at 1 eV than at 0.67 eV. Both of these results show that two kinds of species are possible in a blend system. They may be due to photogenerated free excitons and trapped excitons at the polymer/PCBM interfaces, respectively.

5.5.3 C13-DOO-PPV (C- Polymer)/ PCBM Blend

Like the H- Polymer/ PCBM blend and the D- Polymer/ PCBM blend, we prepared the C-Polymer/PCBM blend (1:1.5) and measured the transient PM spectra at different time delays of the probe beam in the spectral range from 0.25 – 1.05 eV using a low-intensity ultrafast laser system at pump excitation energy 3.1 eV. Figure 5.9 (a) shows the transient PM spectra of the C- Polymer/ PCBM blend at t = 0 ps, 10 ps, and 20 ps, respectively. The spectrum of the C- Polymer/PCBM blend at t = 0 ps is very similar with the spectrum of the C- Polymer film alone measured at t = 0 ps under similar conditions. From these two measurements, we clearly see that even if we mix the PCBM in the C- Polymer, it does not affect the absorption, as most of the absorption happens in the polymer phase. Like the other isotopes (H- Polymer and D- Polymer) blend spectra, the spectrum of the C- Polymer/ PCBM blend is dominated by a PA band peaked at ~1 eV.

The singlet exciton band (PA_1) is observed in the same probe energy in both the film and blend systems, whereas a small shift of this band was observed in other isotope

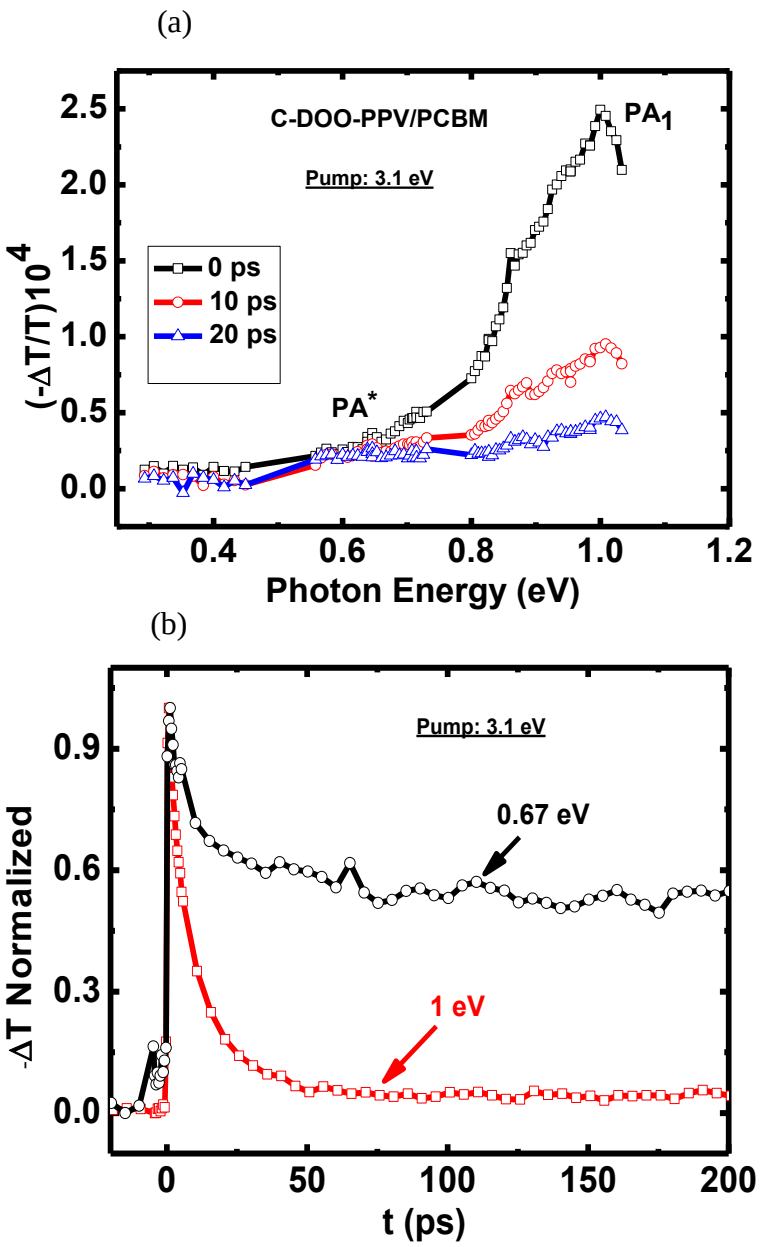

Figure 5.9: PM transient in C-DOO-PPV/PCBM blend: (a) the transient PA spectra at t = 0 ps, 10 ps, and 20 ps. PA_1 and PA* bands are assigned. (b) Decay dynamics at 0.67 eV and 1 eV probe energies.

films and blends. Here, we also want to know whether we are creating the same kind of species in the entire spectrum or not. To resolve this issue, we also measured the transient spectra of the C- Polymer/ PCBM at t = 10 ps and 20 ps, and transient decay kinetics at various probe energies. In the spectral dynamics, we see that the singlet exciton band peak PA_1 completely disappears in 20 ps, but this is not the case in the C- Polymer film; even after 300 ps, a clear PA_1 peak is left over. From these two results, we clearly see that PCBM is taking the crucial role in the dissociation of the singlet exciton in the blend. The transient decay behavior of the photoexcited species at two probe energies 1eV and 0.67 eV is shown in Figure 5.9 (b). Both the decays fit well with the double exponential with the following parameters: fast decay time constants 2 ps (18 %), 2.5 ps (11 %) and slow decay time constants 11.4 ps (76 %) and 10.6 ps (31 %) at 1 eV and 0.67 eV, respectively. These results show that two types of species are generated in our spectral region. The decay kinetics are checked in the entire spectrum, and we found that below and above 0.76 eV, the relaxation process is different because of the difference in photogenerated species. Therefore, we claim that free excitons and trapped excitons are created simultaneously in the blend. The free exciton decays faster than the trapped excitons.

5.5.4 Comparison of DOO-PPV Isotopes/ PCBM Blends

The transient ultrafast spectra of DOO-PPV isotopes/ PCBM blends measured at t = 0 ps are compared in Figure 5.10 (a). The spectra are very similar to each other except in the PA_1 peak position. The entire spectrum is dominated by a clear PA band peak (PA_1) at 1 eV and 1.04 eV in the C- Polymer/PCBM and D- Polymer/PCBM blends, respectively. In contrast, the PA_1 peak position is not in our spectral range for the H-Polymer/PCBM blend. The position of the PA_1 peak is not exactly at the same probe photon energy as observed in the transient PA spectra of the pristine DOO-PPV isotope films. The PA spectrum of D- Polymer/PCBM and C- Polymer/PCBM blend spectra are

red-shifted as compared to the PA spectrum of the H- Polymer/PCBM blend. The spectral red-shift in the blends is also consistent with the red-shift in the PA of pristine films.

The transient decay kinetics of DOO-PPV isotopes/PCBM blends at various probe energies were measured in the entire spectrum. However, only two decay kinetics at 1 eV and 0.67 eV are shown in Figure 5.10 (b) and (c) for better comparison. The transient decay of the D- Polymer/ PCBM blend is somewhat faster than the H-Polymer/PCBM and C- Polymer/PCBM blends at 1 eV; however, it is almost the same at 0.67 eV for all isotopes/PCBM blend systems. When we compared the decays at 1 eV and 0.67 eV, we clearly see that the PA does not originate from a sole photoexcitation. The photoexcitation species that dominates the PA at 0.67 eV is long-lived as compared to the species at 1 eV. The time constants obtained through the double exponential fitting of all transient decay kinetics are presented in Table 5.5. The background is also increasing in all isotopes/PCBM blend systems below 0.75 eV (only shown for the D-Polymer/PCBM blend), and this indicates that free polarons are indeed generated, but at a longer time. We recollect that the build-up of polarons in the ps domain is not seen in the entire spectral region for all isotopes/PCBM blends, although the singlet exciton decay is observed. This mystery in the photophysics measurement of polymer/fullerene blends remains unsolved so far.

Table 5.5: Time constants of transient decay kinetics at 1 eV and 0.67 eV for all DOO-PPV isotopes/PCBM blends.

Polymer	Probe energy	Time constants (τ_1, τ_2)
H- DOO-PPV/PCBM	1 eV	2.2 ps (24 %), 10.3 ps (77 %)
D-DOO-PPV/PCBM	1 eV	3.1 ps (34 %), 10.2 ps (78 %)
C13-DOO-PPV/PCBM	1 eV	2 .0 ps (18 %), 11.4 ps (76 %)
H- DOO-PPV/PCBM	0.67 eV	4.7 ps (17 %), 14.3 ps (35 %)
D-DOO-PPV/PCBM	0.67 eV	2.0 ps (16 %), 10.5 ps (31 %)
C13-DOO-PPV/PCBM	0.67 eV	2.5 ps (11 %), 10.6 ps (31 %)

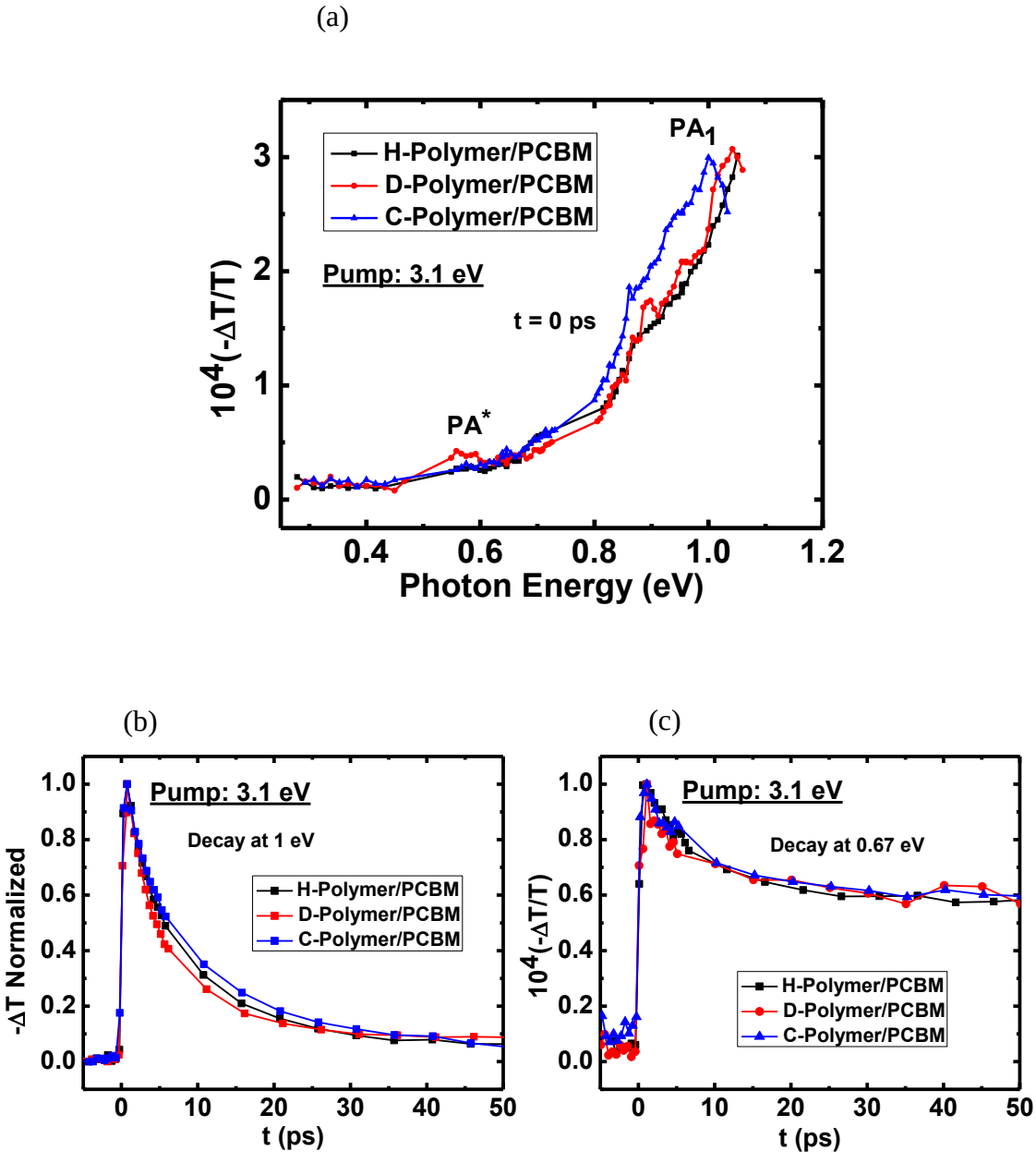

Figure 5.10: DOO-PPV Isotopes (H-, D-, and C- Polymers) /PCBM blends: (a) transient spectra at t = 0 ps, and (b) decay dynamics at 1 eV, and (c) decay dynamics at 0.67 eV.

5.5.5 Discussion of Isotopes/PCBM Results

The similarities in the transient PM spectra of DOO-PPV isotope films [Figure 5.5 (a)] and their blends with PCBM [Figure 5.10 (a)] clearly show that most of the absorption occurs in polymer phase domains even though the polymer is blended with PCBM. Here, we want to investigate whether or not the exciton band peak in all three isotopes is affected by the presence of acceptor PCBM. From the transient decay dynamics study in isotope polymer films [Figures 5.5 (b) and (c)] and blends with PCBM [Figures 5.10 (b) and (c)], it is noticeable that the role of PCBM is on the recombination and dissociation processes of photogenerated species created in the polymer networks, indicating that decay is completely different in blends as compared to films in all isotopes. Thus, the main reason for focusing our research on ultrafast photophysics of DOO-PPV isotope/PCBM blends is to understand the role of PCBM in isotopes of this polymer for photogenerated species' recombination and dissociation processes.

First we try to explain the shift of the PA_1 band in isotopes/PCBM blend as compared to each other and then with isotope films. In the blend systems, the singlet exciton peaks (PA_1) of C- and D- Polymer/PCBM blends are red-shifted as compared to the H- Polymer/PCBM blends. As explained earlier, the vibrational frequency associated with C = C of isotopes is smaller for which molecular mass is bigger. Thus the red-shift of PA_1 is observed in the C- and D- Polymer/PCBM blends as compared to the H-Polymer/PCBM blend. However, the shift in the D- Polymer/PCBM blend PA_1 is less than the C- Polymer/ PCBM blend, which is not understood so far.

When we compare the singlet exciton position in film and blend spectra of isotopes one by one, it is clearly noticeable that there is no shift of PA_1 in C- Polymer films and blends with PCBM, which is not understood so far. However, the PA_1 is blue-shifted in D- and H- Polymer/PCBM blend spectra as compared to their films spectra. One possible reason of the blue shift is related with short conjugation length in the polymer domains when the blends with PCBM are formed. The mixture increases the

density of natural defects and impurities in the polymer chains, which may cause short conjugation length. Although it is not known whether the PA_1 blue- or red-shifts in polymers having short conjugation length, we speculate that PA_1 blue-shifts in short oligomers, since it is known that all electronic levels in such oligomers blue-shift [124].

As stated earlier, the transient decay is not the same in an isotope/PCBM blend system and pristine isotope films, which is due to the proximity of PCBM to the polymer chains. Even in the entire spectral region of the blends, the decay is not the same. Two types of decay dynamics are observed as shown in Figures 5.10 (a) and (b), respectively. This result suggests that two types of photoexcitation species are generated, which dominate separately in two different spectral regions: 0.55 to 0.78 eV and 0.8 to 1.05 eV. The background PA spectrum [Figure 5.7 (a), green color] also shows the possibility of another type of species below 0.55 eV because of a huge increase in background. From these results we propose that three types of species are possible in the entire spectral region from 0.25 to 1.05 eV, as discussed below.

To verify the possibilities of three different types of photogenerated species in three different spectral regions, we created a new idea from our observed spectra at different time delays of the probe beam. We normalized the t = 20 ps spectrum with the t = 0 spectrum at 1 eV in all isotopes/PCBM blend, and then took the difference between the normalized spectra. Interestingly, two new bands are found at ~ 0.35 and ~ 0.62 eV in all isotopes/PCBM blends. Figures 5.11 (a), (b), and (c) show the new spectrum of D-, H- and C- Polymer/PCBM blends, respectively, obtained after manipulating the observed spectrum at t = 20 ps. The new spectrum clearly shows the polaron band P_1 and the charge transfer exciton band CT_1 band in all isotopes/PCBM blends. The CT_1 lives longer than the singlet exciton PA_1 but less long than the polaron P_1. The background PM spectrum also manifests huge BG below 0.55 eV, which is due to the formation of free polaron, whereas the 0.55 to 0.78 eV BG is due to charge transfer excitons, and 0.8 to 1.05 eV is due to singlet exciton. Thus, the transient PM spectra of all three DOO-PPV

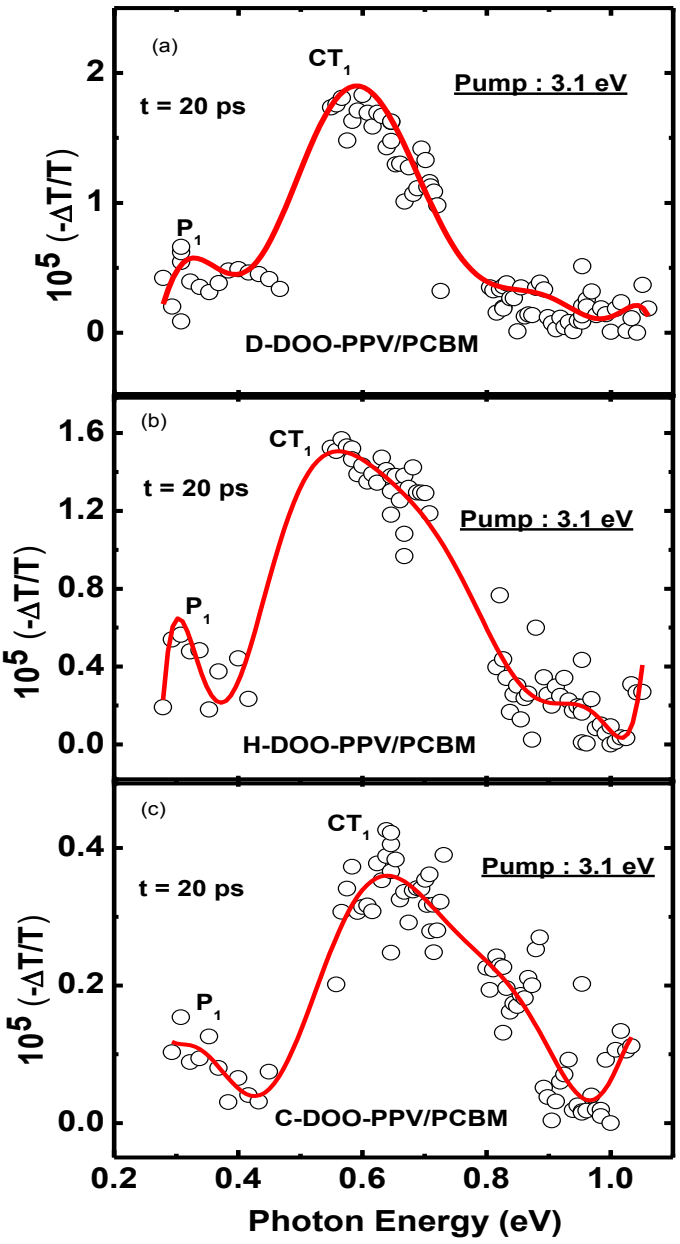

Figure 5.11: The transient PM spectra of DOO-PPV isotopes / PCBM blends at t = 20 ps, normalized and subtracted from the PM spectrum at t = 0. (a) D-DOO-PPV/PCBM, (b) H-DOO-PPV/PCBM, and (c) C-DOO-PPV/PCBM.

isotopes/PCBM blends consist of three different bands, namely, singlet exciton, charge transfer exciton, and polaron.

The CT_1 PA band does not show a significant isotope effect. This is in contrast to the PA_1 of excitons (see above). We thus conclude that the CT exciton transition does not show phonon replicas, as is the case for the exciton PA.

5.6 Conclusion

In this chapter, the transient ultrafast photophysics of pristine films of three DOO-PPV isotopes (D- Polymer, H- Polymer and C- Polymer) and their blends with PCBM have been studied using the pump-probe spectroscopy technique. Linear absorption spectra, PL spectra, and PLQE measurements were also performed on films of all isotopes. The transient spectra of all three pristine isotope films at t = 0 ps were found to be similar to each other, except the PA_1 band peak position. The PA_1 band is red-shifted in the D- Polymer and C- Polymer films as compared to the H- Polymer film. The reason for the PA_1 red-shift in the D- and C- Polymer films in comparison with the H- Polymer is attributed to the increase in molecular mass, which ultimately changes the vibrational frequency coupled to the electronic transitions (phonon replica). The red-shift in the vibrational frequency is confirmed using Raman spectroscopy.

We also studied the transient PM spectra of DOO-PPV isotopes/PCBM blends at different time delays using the same set-up as in the pristine DOO-PPV isotope films measurements. The PA spectra of all three isotopes/PCBM blends were found to be very similar to the isotope films' spectra at t = 0 ps, except the PA_1 band position. The PA_1 peak in the blends is clearly observed in the D- Polymer/ PCBM and C- Polymer/ PCBM blends, but we could not resolve the PA_1 peak position for the H- Polymer/PCBM blend in our probe spectral range. The PA_1 band is red-shifted in the D- and C- Polymer/ PCBM blends as compared to the H- Polymer/PCBM blend. However, the shift is greater in the C- Polymer/PCBM blend than in the D- Polymer/PCBM blend, which is just the

opposite in the pristine D- and C- Polymer films. The reason for this might be the difference in the intermixing property of isotopes with PCBM.

In order to better understand the recombination and dissociation process of photogenerated species, we also measured the transient decay kinetics in the entire probe spectral range. In all three pristine isotope films, there is not much difference in transient decay from the 0.25 – 1.05 eV spectral region. The decay is somewhat slower in the lower probe photon energy range, which might be due to trapping of singlet excitons and/or spectral diffusion. Therefore, we have identified two different regions of the spectrum: one below 0.75 eV and one above due to more trapped and less trapped singlet excitons, respectively.

We also monitored the transient decay kinetics of the DOO-PPV isotopes/PCBM blends in the energy range 0.25 – 1.05 eV. The decay dynamics is fast above 0.75 eV and slow below this probe energy range. This result suggests that two different species are photogenerated in the blends. The species that dominate the PA above 0.75 eV is the singlet exciton, which decays faster in the blend due to the proximity of the PCBM molecules to the polymer chains, whereas the species that dominates the PA spectrum below 0.75 eV is long-lived and is probably either a trapped exciton, or a charge-transfer exciton. Polaron photogeneration in the blend which dominate the PA spectrum at low photon energy can be identified only in the background PA spectrum. After analyzing the spectra of all three isotopes/PCBM blends (see discussion), we have proved that the spectrum consists of three completely different photoexcitation bands: singlet exciton, charge transfer exciton, and polarons, but a clear formation of a free polaron PA band is not observed in the ps time domain.

CHAPTER 6

SUMMARY

In this chapter, we summarize what we have presented in chapters 1 through 5 and expose the conclusions drawn from various experimental tools in brief in order to provide a clearer picture of the thesis to the casual reader. In Chapter 1, we explained in detail the basic phenomena that might happen in π – conjugated polymers during photoexcitation. The neutral and charged photoexcitation energy level diagrams and the allowed optical transitions in dipole-moment approximation are clearly presented. The theoretical models used to describe the photoexcitations in π – conjugated polymers are presented in a simple way for better understanding. At the end of the first chapter, organic photovoltaic solar cells are also introduced.

In Chapter 2, first we introduced the chemical structures of all donor and acceptor materials that we used in this thesis for studying various phenomena presented in Chapters 3 to 5. In addition we also presented the experimental techniques that we used to measure linear absorption in terms of optical density (O.D.), photoluminescence (PL), doping induced absorption (DIA), electroabsorption (EA), continuous wave (CW) photoinduced absorption (PA), and transient PA, X-ray diffraction and OPV device characterization.

Chapter 3 is focused on the ultrafast photophysics studies of pristine P3HT films and blends with the acceptor PCBM. In addition to these measurements we also presented linear absorption, PL, intensity-dependent PA measurement, XRD and solar cell device

characterization results. From all these measurements our goal was to understand charge photogeneration process and choose which material is better for OPV application. We used RR-P3HT and RRa-P3HT as donor materials and PCBM as acceptor material.

We received as gifts high molecular weight (HMW) and low molecular weight (LMW) RR-P3HT from Plextronics Ltd Company and other two from Rieke and ADS companies for comparison. From the ultrafast photophysics studies of the RR-P3HT films we proposed that HMW RR-P3HT is better for OPV application. We also compared the transient PA of HMW RR-P3HT with RRa- P3HT in films and blends with PCBM separately, and found that RR-P3HT is far better than RRa-P3HT for OPV application. We introduced the concept of charge transfer exciton formation at the interface of donor-acceptor in the blend system. We demonstrate that the singlet exciton that is photogenerated in the RRa-P3HT polymer domain diffuses ~ 0.5 ps to the D-A interface, where it forms charge transfer excitons, which live much longer without dissociation into free polarons. In contrast, the singlet exciton formed in the RR-P3HT domains of RR-P3HT/PCBM blend takes ~ 10 ps to diffuse to the D-A interface where it forms charge transfer exciton. We do not observe the direct dissociation of these charge transfer excitons into free polarons in our transient decay kinetics time range up to 2 ns. However the increase in the background PA below 0.55 eV suggests that the charge transfer excitons dissociate into free polarons at a later time.

In Chapter 4, we used PTB7 polymer, which is a low band gap (~ 1.84 eV) copolymer synthesized by the Chicago group. We studied O.D., PL, CW PA and transient ultrafast PA of PTB7 film and its blend with $PC_{71}BM$. From these measurements, we concluded that the photophysics of this polymer film and blend with $PC_{71}BM$ is different from that of other polymers such as P3HT and P3HT/PCBM blend. The O.D is enhanced in the blend due to $PC_{71}BM$. PL does not show clear phonon side bands. The CW PA of the film shows clear triplet and weak flat polaron bands, whereas only polaron bands are observed in the CW PA of PTB7/$PC_{71}BM$ blend. In transient ultrafast PA measurement of the PTB7 film the singlet exciton band dominates the entire spectrum, but in the

PTB7/$PC_{71}BM$ blend *three types* of photogenerated species-singlet exciton, charge transfer exciton, and polaron-are clearly identified.

In Chapter 5, we compared the linear absorption, PL, and transient ultrafast PA spectra of three isotopes of DOO-PPV films. In addition we also studied the isotope effect on transient ultrafast PA of isotope/PCBM blends. In linear absorption and PL spectra we did not see much difference in the three isotope films. Similarly, the transient ultrafast PA spectra of isotope films were also found to be similar, except for the shifting of the singlet exciton peak position. In the blend system, we also noticed similar spectra as in pristine films with little shift in the singlet exciton peak position. However, the analysis of all isotope blends' PA spectra showed that three types of species-singlet exciton, charge transfer exciton, and polaron-are generated after few ps but not immediately after photoexcitation. In the transient decay dynamics study, we found that there is not much difference in decay mechanism in all isotope films in the spectral range 0.25 -1.05 eV. In contrast, slow and fast decay dynamics are observed below and above 0.75 eV in isotopes' blend system in the spectral range from 0.25 – 1.05 eV, showing the possibility of two different photogenerated species.

APPENDIX A

DERIVATION OF FÖRSTER ENERGY TRANSFER DYNAMICS FOR EXCITONS IN THE POLYMER GRAINS

The detail derivation of Förster energy transfer dynamics for excitons in the polymer grains is written below. Here, we assume that the polymer grain is in spherical shape of radius R, as shown in Figure A.1. We also hypothesize that the Förster energy transfer (FRET) kinetics from a point 'r' inside the polymer grain to its surface is exponential in nature. Therefore, the surviving exciton density inside the polymer grain at point 'r' can be written as follows:

$$n(t) = n(0)\exp(-\nu(R)t) \tag{A.1}$$

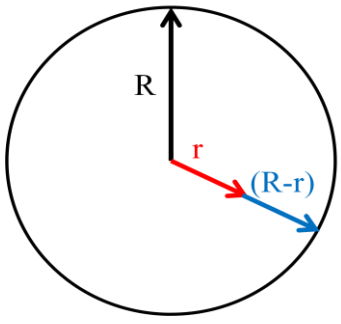

Polymer grain

Figure A.1 : Schematic diagram of the polymer grain of radius of R, where r is the exciton distance from the grain's center.

where $v(R) = v_0 \frac{R_0^6}{(R-r)^6}$ and R_0 is the FRET radius [76]. In order to calculate the total surviving exciton density, N(t) inside the polymer grain we integrate over the distance, r, normalized by the volume:

$$N(t) = N(0) \frac{\int_0^{R_{min}} \exp(-v(R)t) 4\pi r^2 \, dr}{4\pi R^3/3} \qquad (A.2)$$

where, R_{min} is the distance from the center where $v(R)$ reaches its maximum rate, v_{max}, and thus does not change with r anymore. Equation (A.2) can also be written in terms of the exciton life time, τ

$$N(t) = N(0) \frac{\int_{\tau_{max}}^{\tau_{min}} \exp\left(-\frac{t}{\tau}\right) g(\tau) d\tau}{4\pi R^3/3} \qquad (A.3)$$

where $\frac{1}{\tau} = \frac{1}{\tau_0} \frac{R_0^6}{(R-r)^6}$ and τ_0 is the polymer exciton natural decay life time in the bulk polymer. Writing for simplicity $R = \mu R_0$, where μ is a constant (<1), we can substitute distance 'r' and life time 'τ': $r = R_0(\mu - (\frac{\tau}{\tau_0})^{\frac{1}{6}})$ and $dr = -\frac{R_0}{6\tau_0^{\frac{1}{6}}} \tau^{-5/6} d\tau$. Substituting these relations in Equation (A.2), we get:

$$\frac{N(t)}{N(0)} = \frac{\exp(-t/\tau_0)}{\frac{4}{3}\pi\mu^3 {R_0}^3} \int_{\tau_{min}}^{\tau_{max}} \exp(-t/\tau)\, 4\pi R_0^2 \left(\mu - (\tau/\tau_0)^{1/6}\right)^2 \frac{R_0}{6\tau_0^{1/6}} \tau^{-5/6} d\tau$$

$$= \frac{\exp(-t/\tau_0)}{2\mu^3 \tau_0^{\frac{1}{6}}} \int_{\tau_{min}}^{\tau_{max}} \frac{\exp(-t/\tau)}{\tau^{5/6}} \left(\mu - (\tau/\tau_0)^{1/6}\right)^2 d\tau$$

$$= \frac{\exp(-t/\tau_0)}{2\mu^3 \tau_0^{\frac{1}{6}}} \int_{\tau_{min}}^{\tau_{max}} \frac{\exp(-t/\tau)}{\tau^{5/6}} [\mu^2 + (\tau/\tau_0)^{1/3} - 2\mu(\tau/\tau_0)^{1/6}] d\tau$$

$$= \frac{\exp(-t/\tau_0)}{2\mu^3 \tau_0^{\frac{1}{6}}} [I + II + III] \qquad (A.4)$$

where, $I = \int_{\tau_{min}}^{\tau_{max}} \frac{\exp(-t/\tau)}{\tau^{5/6}} \mu^2 d\tau \qquad (A.5)$

$$II = \int_{\tau_{min}}^{\tau_{max}} \frac{\exp(-t/\tau)}{(\tau_0)^{1/3}} \tau^{-\frac{1}{2}} d\tau \qquad (A.6)$$

$$III = \int_{\tau_{min}}^{\tau_{max}} \frac{\exp(-t/\tau)}{(\tau_0)^{\frac{1}{6}}} \tau^{-2/3} d\tau \qquad (A.7)$$

Now, replacing $\frac{t}{\tau} = X$ and $d\tau = -\frac{t}{X^2} dX$, $X_{min} = 0.1$ and $X_{max} = \infty$ I, II and III can be solved separately and the integral can be written in the following forms:

$$I = \mu^2 t^{\frac{1}{6}} \int_{0.1}^{\infty} \exp(-X) X^{-7/6} dX \qquad (A.8)$$

$$II = \frac{t^{\frac{1}{2}}}{(\tau_0)^{1/3}} \int_{0.1}^{\infty} \exp(-X) X^{-3/2} dX \qquad (A.9)$$

$$III = \frac{2\mu}{(\tau_0)^{\frac{1}{6}}} t^{\frac{1}{3}} \int_{0.1}^{\infty} \exp(-X) X^{-4/3} dX \qquad (A.10)$$

Putting the integrated values of I, II, and III in Equation (A.4) and arranging the terms, the final expression takes the form,

$$\frac{N(t)}{N(0)} = \exp\left(-\frac{t}{\tau_0}\right)\left[m_1 + m_2\left[\left(\frac{0.542}{\mu}\right) t^{\frac{1}{6}} + \left(\frac{0.203}{\mu^3}\right) t^{\frac{1}{2}} - \left(\frac{0.66}{\mu^2}\right) t^{\frac{1}{3}}\right]\right. \qquad (A.11)$$

The above expression is derived for a single grain size R. For simplicity, we assume that most polymer grains are of size R_{avg} where $R_{avg} = \mu_{avg} R_0$. Including μ_{ava} into Equation (A.11), we get the final Equation (A.12) for the decay of excitons in the polymer/PCBM blend.

$$\frac{N(t)}{N(0)} = \exp\left(-\frac{t}{\tau_0}\right)\left[m_1 + m_2\left[\left(\frac{0.542}{\mu_{avg}}\right) t^{\frac{1}{6}} + \left(\frac{0.203}{\mu_{avg}^3}\right) t^{\frac{1}{2}} - \left(\frac{0.66}{\mu_{avg}^2}\right) t^{\frac{1}{3}}\right]\right. \qquad (A.12)$$

We found that the best fit to PA_1 decay was obtained using $m_2 = 7$ and $\mu_{avg} = 1.3$ as shown in Figure (A.2). Using this μ_{avg} and $R_0 = 6$ nm, the average grain size of the polymer will be ~ 8 nm which is in good agreement with our XRD measurement.

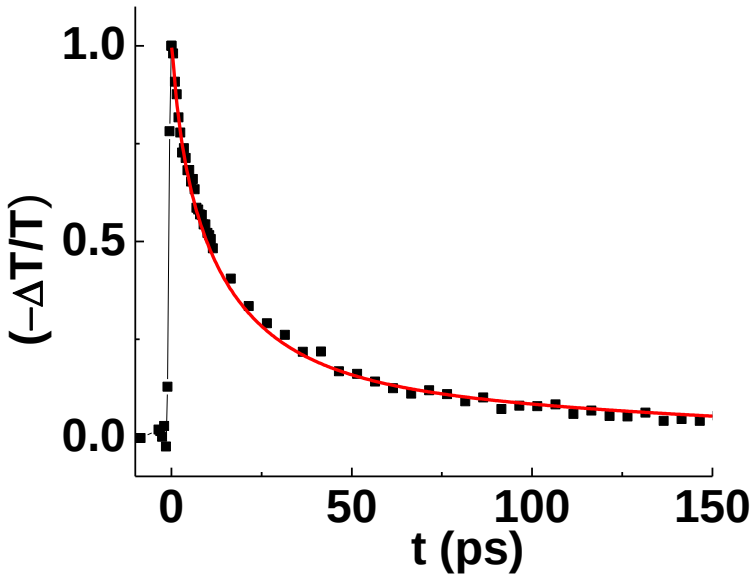

Figure A.2: The decay of PA_1 band in the polymer blends at 1eV. It is fitted with Equation (A.11)

REFERENCES

[1] R. J. Young and P. A. Lovell, Introduction to Polymers. 2nd edition (1991).

[2] G. Inzelt, in Conducting Polymers, Springer Berlin Heidelberg, p.265 (2008).

[3] B. G. Levi. Physics Today **53**, 19 (2000).

[4] H. Shirakawa, E. J. Louis, A. G. MacDiarmid, C. K. Chiang and A.J. Heeger. J. Chem. Soc., Chem. Commun**. 578** (1977).

[5] N.S.S. Harald Hoppe, Journal of Materials Research Society, **19** (2004).

[6] C.J. Brabec, S. Gowrisanker, J. J. M. Halls, D. Laird, S. Jia, and S.P. Williams, Adv. Mater. **22**, 3839 (2010).

[7] H. Spanggaard and F.C. Krebs, Solar Energy Materials and Solar Cells, **83**, 125 (2004).

[8] C. J. Brabec, N. S. Sariciftci, and J. C. Hummelen, Adv. Funct. Mater. **11**, 15 (2001).

[9] S. Günes, H. Neugebauer, and N. S. Sariciftci, Chem. Rev. **107,** 1324 (2007).

[10] Yam, WOLEDs, Organic Photovoltaic: Recent Advances and Applications, Green Energy and Technology (2010).

[11] Z. Bao, Organic Field-Effect Transistors, CRC Press, Boca Raton (2007).

[12] S. Sanvito, Nature Mater. **6**, 803 (2007).

[13] J. Y. Kim, K. Lee, N. E. Coates, D. Moses, T. Q. Nguyen, M. Dante, and A. J. Heeger. Science, **317**, 222 (2007).

[14] M. A. Green, K. Emery, D. L. King, Y. Hishikawa, and W. Warta. Prog. Photo Volt: Res. Appl. **14,** 455 (2006).

[15] J. Clark, Ph. D. thesis, University of Cambridge, 2007.

[16] N. Ashcroft and N. Mermin. Solid State Physics, 1976.

[17] W. Barford, Electronic and Optical Properties of Conjugated Polymers, Oxford: Clarendon Press (2005).

[18] K. Gottfried and T. Yan. Quantum Mechanics Fundamentals, Spring Science & Business (2003).

[19] A. M. Ellis. J. Chem. Ed **76,** 1291 (1999).

[20] O. Laporte and W. F. Meggers. J. Opt. Soc. of America **11,** 459 (1925).

[21] R. E. Peierls. Quantum Theory of Solids, Oxford: At the Clarendon Press (1995).

[22] S. Singh. Ph.D thesis, University of Utah, 2010.

[23] W. P. Su, J. R. Schrieffer, and A. J. Heeger, Phys. Rev. B **22**, 4, 2099 (1980).

[24] S. Mazumdar and S. N. Dixit, Synth. Metals **28**, 463-8 (1989).

[25] S. Mazumdar and S. N. Dixit, Phys. Rev. Lett. **51**, 4, 292 (1983).

[26] S. F. Alvarado, P. F. Seidler, D. G. Lidzey, and D. D. C. Bradley, Phys. Rev. Lett. **81**, 1082 (1998).

[27] D. K. Campbell and A. R. Bishop, Nuclear Phys. B **200**, 297 (1982).

[28] J. S. Wilson, A. Kohler, R. H. Friend, M. K. Al - Suti, M. R. A. Al - Mandhary, M. S. Khan, and P. R. Raithby, J. Chem. Phys. **113**, 17, 7627-34 (2000).

[29] X. Wei, Z. V. Vardeny, N. S. Sariciftci, and A. J. Heeger, Phys. Rev. B **53**, 5, 2187 (1996).

[30] S. A. Jenekhe and J. A. Osaheni, Science **265**, 5173, 765-768 (1994).

[31] R. Farchioni and G. Grosso, Organic Electronic Materials: Conjugated Polymers and Low Molecular Weight Organic Solids, Berlin; New York: Springer (2001).

[32] D. D. Gebler, Y. Z. Wang, D. K. Fu, T. M. Swager, and A. J. Epstein, J. Chem. Phys. **108**, 18, 7842-7848 (1998).

[33] I. D. W. Samuel, G. Rumbles, and C. J. Collison, Phys. Rev. B **52** 16, R11573 (1995).

[34] M. Pope and C. E. Swenberg, Elecronic Processes in Organic Crystals and Polymers, 2nd ed., New York: Oxford University Press (1999).

[35] J. W. Blatchford, S. W. Jessen, L.B. Lin, J. J. Lih, T. L. Gustafson, A. J. Epstein, D. K. Fu, M. J. Marsella, T. M. Swager, A. G. MacDiarmid, S. Yamaguchi, and H. Hamaguchi, Phys. Rev. Lett. **76,** 9, 1513 (1996).

[36] J. M. Lupton, Chem. Phys. Lett. **365**, 3-4, 366-368 (2002).

[37] U. Lemmer, S. Heun, R. F. Mahrt, U. Scherf, M. Hopmeier, U. Siegner, E.O. Gobel, K. Mullen, and H. Bassler, Chem. Phys. Lett. **240**, 4, 373-378 (1995).

[38] Y. J. Cheng, S. H. Yang, and C.S. Hsu, Synthesis of Conjugated Polymers for Organic Solar Cell Applications, Chem. Rev. **109,** 5868-5923 (2009).

[39] C. J. Brabec, N. S. Sariciftci, and J. C. Hummelen, Adv. Funct. Mater. **11,** 15 (2001).

[40] S. Günes, H. Neugebauer, and N. S. Sariciftci, Chem. Rev. **107**, 1324 (2007).

[41] D. Wöhrle, and D. Meissner, Adv. Mater. **3**, 129 (1991).

[42] J. J. Halls, K. Pichler, R. H. Friend, S. C. Moratti, and A. B. Holmes, Appl. Phys. Lett. **68**, 3120 (1996).

[43] D. E. Markov, E. Amsterdam, P.W. Blom, A. B. Sieval, and J. C. Hummelen, J. Phys. Chem. A **109,** 5266 (2005).

[44] G. Yu, J. Gao, J. C. Hummelen, F. Wudl, and A. J. Heeger, Science **270**, 1789 (1995).

[45] N. S. Sariciftci, L. Smilowitz, A. J. Heeger, and F. Wudl, Science **258,** 1474 (1992).

[46] Y. Zhang, Ph.D thesis, University of Utah, 2010.

[47] A. Lohner, P. Kruck, and W. W. Rühle. Appl. Phys. B **59**, 211 (1994) [DFG Crystal (A_gGaS_2).]

[48] M. T. Asaki, C. P. Huang, D. Garvey, J. Zhou, H. Kapteyn, and M. M. Murane. Optics Lett. (1997).

[49] O. J. Korovyanko, Ph.D thesis, University of Utah, 2002.

[50] M. Chandross, S. Mazumdar, M. Liess, P. A. Lane, Z. V. Vardeny, M. Hamaguchi, and K. Yoshino, Phys. Rev. B **55**, 1486, (1997); M. Chandros and S. Mazumdar, Phys. Rev. B **55**, 1497 (1997.)

[51] M. J. Rice and Y. N. Garstein, Phys. Rev. Lett. **73**, 2504 (1994).

[52] J. Cornil, D. Beljone, R. H. Friend, and J. -L. Bredas, Chem. Phys. Lett. **223**, 82 (1994).

[53] T. Drori, J. Holt, and Z. V. Vardeny, Phys. Rev. B **82**, 075207 (2010).

[54] R. Österbacka, C. P. An, X. M. Jiang, and Z. V. Vardeny, Science **287,** 831-842 (2000).

[55] C. X. Sheng, Ph.D thesis, University of Utah, 2005.

[56] G. Li, V. Shrotriya, J. Huang, Y. Yao, T. Moriarty, K. Emery and Y. Yang, Nature Mater. **4,** 864 (2005).

[57] Y. Kim, S. Cook, S. M. Tuladhar, S. A. Choulis, J. Nelson, J. R. Durrant, D. D. C. Bradley, M. Giles, I. McCulloch, C. S. Ha, and M. Ree, Nature Mater. **5**, 197 (2006).

[58] M. D. Irwin, D. B. Buchholz, A. W. Hains, R. P. H. Chang, and T. J. Marks, Proceedings of the National Academy of Sciences **105,** 2783 (2008).

[59] R. Osterbacka, C. P. An, X. M. Jiang, and Z. V. Vardeny, Science **287**, 5454, 839-842 (2000).

[60] J. XiaoMei, R. Osterbacka, O. Korovyanko, C. P. An, B. Horovitz, R. A. J. Janssen, and Z. V. Vardeny, Adv. Funct. Mater. **12,** 9, 587-97 (2002).

[61] O. J. Korovyanko, R. Osterbacka, X. M. Jiang, Z. V. Vardeny, and R. A. J. Janssen, Cond. Matt. and Mater. Phys. **64**, 23, 235122-1 (2001).

[62] M. Furukawa, K. Mizuno, A. Matsui, S.D.D.V. Ruhoopth, and W. C. Walker. J. Phys. Soc. Japan **58**, 2976 (1989).

[63] U. Rauscher, H. Bassler, D. D. C. Bradley and M. Hennecke. Phys. Rev. B **42**, 9830 (1990).

[64] H. Bassler, M. Gailberger, R. F. Mahrt, J. M. Oberski, and G. Weiser. Synth. Metal **49-50**, 341 (1992).

[65] H. Sirringhaus, P.J. Brown, R. H. Friend, M. M. Nielsen, K. Bechgaard, B. M. W. Langeveld-Voss, A. J. H. Spiering, R. A. J. Janssen, E. W. Meijer, P. Herwig, and D. M. de Leeuw, Nature **401**, 685 (1999).

[66] O. J. Korovyanko, Ouml, R. Sterbacka, X. M. Jiang, Z. V. Vardeny, and R. A. J. Janssen, Phys. Rev. B **64,** 235122 (2001).

[67] J. Clark, C. Silva, R. H. Friend, and F. C. Spano, Phys. Rev. Lett. **98**, 206406 (2007).

[68] F. C. Spano, J. Clark, C. Silva, and R. H. Friend, J. Chem. Phys. **130,** 074904 (2009).

[69] T. Drori, J. M. Holt, and Z. V. Vardeny, Phys. Rev. B **82**, 075207 (2010).

[70] S. V. Frolov, Z. Bao, M. Wohlgenannt, and Z. V. Vardeny, Phys. Rev. B **65**, 205209 (2002).

[71] C. X. Sheng, M. Tong, S. Singh and Z. V. Vardeny, Phys. Rev. B **75**, 085206 (2007).

[72] S. Yamamoto et al. Adv. Funct. Mater. **18,** 2555 (2008).

[73] J. M. Guo et al. Jour. Chem. Soc. **132**, 6154 (2010).

[74] R. A. Marsh, J. M. Hodgkiss, S. A. Seifried, and R. H. Friend, Nano Lett. **10,** 923 (2010).

[75] A. A. Bakulin et al. Chem. Phys. Lett. **482**, 99 (2009).

[76] T. Förster, Discuss. Faraday Soc. **27**, 7 (1959).

[77] D. C. Coffey et al. ACS Nano **4**, 5437 (2010).

[78] I. W. Hwang, D. Moses, and A. J. Heeger, J. Phys. Chem. C. **112,** 4350 (2008).

[79] X.- Y Zhu, Q.Yang, and M. Muntwiler, Acc. Chem. Res. **42,** 1779 (2009).

[80] S. Singh, Ph.D. thesis, University of Utah, 2010.

[81] D. W. McBranch, M. B. Sinclair, in: N. S. Sariciftci (Ed.), World Scientific, Singapore, 587 and reference therein (1997).

[82] H. Sirringhaus et al. Nature **401**, 685 (1999).

[83] P. H. Heiney et al. Phys. Rev. Lett. **66**, 2911 (1991).

[84] C. H. Woo, B. C. Thompson, B. J. Kim, M. F. Toney, and J. M. J. Frechet, JACS, **130**, 48 (2008).

[85] P. Schilinsky, U. Asawapirom, U. Scherf, M. Biele, C. J. Brabec, Chem. Matter **17,** 2175-2180 (2005).

[86] M. Ma, J. Y. Kim, K. Lee, A. J. Heeger, Macromol. Rap. Commun. **28**, 1776-1780 (2007).

[87] M. Urien, L. Bailly, L. Vignau, E. Cloutet, de Cuendias, A. Wantz, G. Cramail, H Hirsch, and L. Parneix, J. Polym. Int. **57**, 764-769 (2008).

[88] M. Brinkmann, P. Rannou, Adv. Funct. Mater. **17**, 101-108 (2007).

[89] A. Zen, J. Pflaum, S. Hirschmann, W. Zhuang, F. Jaiser, U. Asawapirom, J. P. Rabe, U. Scherf, and D. Neher, Adv. Funct. Mater. **148,** 757-764 (2004).

[90] M. Koppe and C. J. Brabec, Macromolecule **42**, 4661-4666 (2009).

[91] K. Vakhshouri, D. R. Kozub, C. Wang, A. Salleo, and E. D. Gomez, Phys. Rev. Lett. **108**, 026601 (2012).

[92] J. M. Szarko, J. Guo, B. S. Rolczynski, and L. X. Chen, J. Mater. Chem. **21**, 7849 (2011).

[93] E. Bundgaard and F. Krebs, Sol. Energy Mater. Sol. Cells **91**, 954 (2007).

[94] Y. Y. Liang and L. P. Yu, Acc. Chem. Res., **43**, 1227 (2010).

[95] Y. Liang, Z. Xu, J. Xia, S.T. Tsai, Y. Wu, G. Li, C. Ray and L. Yu, Adv. Mater. **22**, E135 (2010).

[96] Y. Y. Liang, D. Q. Feng, J.C. Guo, J. M. Szarko, C. Ray, L. X. Chen and L. P. Yu, Macromolecules **42**, 1091 (2009).

[97] Y. Liang, S. Xiao, D. Feng and L. Yu, J. Phys. Chem. C. **112**, 7866 (2008).

[98] Y. Y. Liang, Y. Wu, D. Q. Feng, S.T. Tsai, H. J. Son, G. Li, C. Ray and L. P. Yu, J. American Chem. Soc. **131**, 56 (2009).

[99] Y. Y. Liang, D. Q. Feng, Y. Wu, S.T. Tsai, G. Li, C. Ray and L. P. Yu, J. American Chem. Soc. **131**, 7792 (2009).

[100] Y. Yao, Y. Liang, V. Shrotriya, S. Xiao, L. Yu and Y. Yang, Adv. Mater. **19**, 3979 (2007).

[101] Y. Y. Liang and L. P. Yu, Polym. Rev. **50**, 454 (2010).

[102] Y. Liang, Z. Xu, J. Xia, S. T. Tsai, Y. Wu, G. Li, C. Ray and L. Yu, Adv. Energy Mater. **22**, E 135- E 138 (2010).

[103] G.H. Markosian, Ph.D thesis, University of Utah, 2011.

[104] V. Perebeinos, J. Tersoff, and P. Avouris, Phys. Rev. Lett. **92**, 257402 (2004).

[105] J. M. Holt, Ph.D thesis, University of Utah, 2009.

[106] W. Chen, T. Xu, F. He, W. Wang. C. Wang, J. Strazalka, Y. Liu, J. Wen, D. J. Miller, J. Chen, K. Hong, L. Yu and S. B. Darling, Nano Lett. **11**, 3707-3713 (2011).

[107] J. Guo, Y. Liang, J. Szarko, B. Lee, H. J. Son, B. S. Rolczynski, L. Yu, and L. X. Chen, Jour. of Phys. Chem. B **114**, 742-748 (2010).

[108] T. D. Nguyen, G. H. Markosian, F. Wang, L. Wojcik, X. G. Li, E. Ehrenfreund and Z. V. Vardeny, Nature Mater. **14** (2010).

[109] B. R. Hsieh, Y. Yu, A. C. Vanlaeken, and H. Lee, Macromolecules **30,** 8094 (1997).

[110] J. Q. Pan, Z. K. Chen, Y. Xiao, and W. Huang, Chinese J. Poly. Sci. 1**8**, 541 (2000).

[111] M. Furukawa, K. Mizuno, A. Matsui, S.D.D.V. Ruhoopth, and W. C. Walker. J. Phys. Soc. Japan **58**, 2976 (1989).

[112] U. Rauscher, H. Bassler, D. D. C. Bradley and M. Hennecke, Phys. Rev. B **42**, 9830 (1990).

[113] H. Bassler, M. Gailberger, R. F. Mahrt, J. M. Oberski, and G. Weiser. Synth. Metals **49-50**, 341 (1992).

[114] S. Webster and D. N. Batchelder, Polymer, vol 37, n., 22 **4961-4968** (1996).

[115] R. Mahrt, J. Yang, A. Greiner, H. Bessler and D.D.C. Bradley, Macromol. Chem. Rapid Commun. **11**, 415 (1990).

[116] I. D.W. Samuel, B. Crystall, G. Rumbles, P.L. Burn, A. B. Holmes, and R.H. Friend, Synth. Metals **54**, 281 (1993).

[117] M .Yan, L. J. Rothberg, F. Papadimitrakopoulos, M. E. Galvin, and T. M. Miller, Phys. Rev. Lett. **72**, 1104-1107 (1994).

[118] S. V. Frolov, Ph.D thesis, University of Utah, 1996.

[119] Z. V. Vardeny, O. Brafman, E. Ehrenfreund, Solid State Commun. **53**, 615 (1985).

[120] M. Liess, S. Jeglinski, P.A. Lane and Z. V. Vardeny. Synth. Metals **84**, 891 (1997).

[121] S. Yamaguchi, and T. Tahara, Chem. Phys. Lett. **376**, 237-243 (2003).

[122] M. Chandross, S. Mazumdar, S. Jeglinski, X. Wei, Z. V. Vardeny, E. W. Kwock, and T. M. Miller, Phys. Rev. B **50**, 14702 (1994).

[123] S. Guha, J. D. Rice, Y. T. Yau, C. M. Martin, M. Chandrasekhar, H. R. Chandrasekhar, R. Guentner, P. Scanduicci de Freitas, and U. Scherf, Phys. Rev. B **67**, 125204 (2003).

[124] J. M. Hancock, A. P. Gifford, R. D. Champion, and S. A. Jenekhe, Macromolecules **41,** 3588-3597 (2008).